DMSO-Free Cryopreservation of Therapeutic Cells by Agarose Hydrogel Encapsulation

A Dissertation

SUBMITTED TO THE FACULTY OF

UNIVERSITY OF MINNESOTA

BY

Mian Wang

IN PARTIAL FULFILLMENT OF THE REQUIREMENTS

FOR THE DEGREE OF

DOCTOR OF PHILOSOPHY

Advisor: Dr. Alptekin Aksan

July 2023

Acknowledgments

First of all, I would like to express my sincere gratitude to my advisor, Prof. Alptekin Aksan, whose consistent support, exceptional guidance, and profound insights in this field have made my research journey truly inspiring. His patience, encouragement, and dedication have fostered my growth as a scientist.

I would like to thank my dissertation committee, Prof. William Northrop, Prof. Michael McAlpine, Prof. David Wood, and Prof. Chun Wang for their insightful perspectives, constructive discussions, and contribution to the development of ideas throughout this study. I would also like to thank our collaborators: Prof. Jens O.M. Karlsson, Prof. David McKenna, and Prof. Jeffrey Miller for their valuable feedback and resources that have assisted in my research.

I would like to acknowledge all the present and past members of the Biostabilization and Bioencapsulation Lab for their support, collaboration, and friendship: Advitiya Mahajan, Beatriz De Souza, Andrew Frederickson, Dr. Anitha Simon, Dr. Jonathan Sakkos, Dr. Joseph Benson, Dr. Sampreeti Jena, Dr. Julian Preciado, Dr. Diego Escalante, and Dr. Morwena Solivio.

Last but not least, I would like to thank my family, for their unwavering support and encouragement all the time. This dissertation would not have been possible without their unconditional love.

Abstract

In recent decades, the rapid advancement of cell therapy and regenerative medicine has generated an urgent need for efficient and safe cell/tissue cryopreservation techniques on both laboratory and industrial scales. The current use of dimethyl sulfoxide (DMSO) as a cryoprotective agent (CPA) presents toxicity concerns, prompting the development of alternative methods. The primary objective of this research is to develop a novel cryopreservation method for therapeutic cells using hydrogel encapsulation, which aims to minimize cryoinjuries while eliminating the need for toxic penetrating CPAs such as DMSO.

The dissertation consists of three main parts. In the first part, molecular changes associated with warming injury in cryopreserved human white blood cells (WBCs) were analyzed. It was observed that slow warming led to irreversible dehydration of cell membrane lipids and denaturation of cellular proteins. Also, WBCs were found to be very susceptible to kinetic processes during warming, including eutectic crystallization/melting, devitrification, and ice recrystallization. The second part focuses on the development of an encapsulation cryopreservation method using the combination of agarose hydrogel and trehalose as an alternative to membrane-permeable CPAs. A comprehensive analysis of the kinetic and thermodynamic changes within the agarose-trehalose hydrogel during freeze/thaw was conducted. The combination of agarose and hydrogel was found to reduce ice phase volume with a less ordered structure, eliminate eutectic crystallization and melting, and inhibit ice recrystallization during warming. The third part of the

dissertation involves the validation of the DMSO-free hydrogel encapsulation method for the cryopreservation of natural killer (NK) cells. High post-thaw cell viability was achieved, while decreased viability with compromised cytotoxicity was observed after cells were extracted from the hydrogel. Ongoing efforts are focused on optimizing the cell extraction process from the hydrogel.

Table of Contents

List of Tables

List of Figures

Chapter 1: Introduction

1.1 Motivation

Driven by the rising number of clinical studies of cell therapies, the global cell-based products market size was valued at USD 8 billion in 2020 and is expected to grow at an average annual rate of 15% until 2030.[1] The manufacturing of cell-based products typically involves several steps, including cell isolation, engineering, and cryopreservation, before they can be shipped from a centralized facility to clinics for infusion, as shown in ***Figure 1.1***. In this process, cryopreservation is critical to sustaining the viability and functionality of cells during transportation and application in order to achieve desired clinical outcomes. Although the ultra-low temperature can reduce or suspend physiochemical and metabolic activities in cells, the process of cryopreservation, which involves freezing and thawing, can result in cell damage due to the formation of ice both inside and outside of the cells. Cell damage may occur through direct action by ice crystals, such as mechanical damage,[2, 3] or indirect effects resulting from changes in the composition of the liquid phase after ice formation, including dehydration, oxidation, and elevated levels of toxic solutes.[2-5] To attenuate the adverse effects of cryopreservation, certain approaches are necessary, which include precisely controlling the cooling and warming rates, as well as cryopreserving the cells with cryoprotectant agents (CPAs).

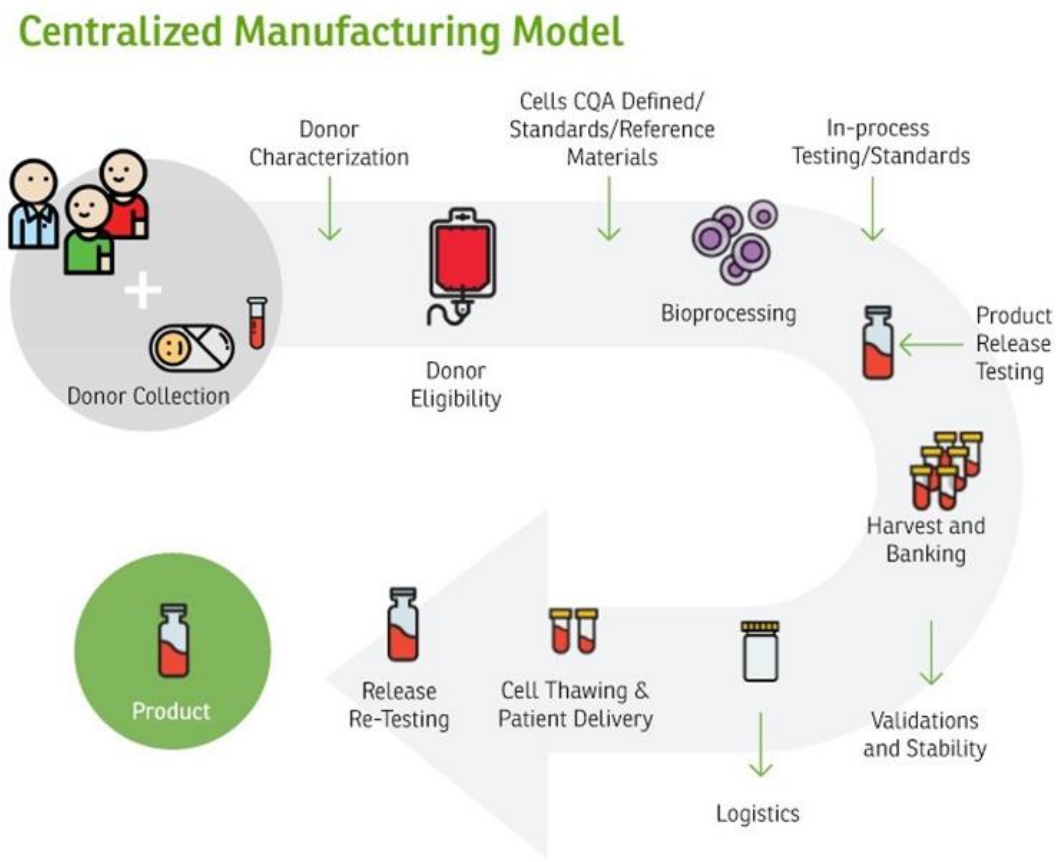

Figure 1.1 Diagram of Centralized Manufacturing Model [6]

Cooling and warming rates are crucial factors to post-thaw cell survival.[5, 7, 8] According to Mazur's two-factor hypothesis (explained in more detail in **Section 2.1**),[9] slow cooling rates are associated with osmotic dehydration due to solute rejection during extracellular ice growth, whereas rapid cooling is associated with deleterious intracellular ice formation (IIF). Therefore, cell survival is maximized at some optimal intermediate rate of cooling, and the magnitude of this optimum cooling rate is dependent on the cell type.[9] In contrast to the cooling process, literature regarding the warming of cryopreserved human cell samples is limited, and the mechanisms of cryoinjury dominant during the warming of cryopreserved

cells are poorly understood. Typically, rapid warming is preferred to prevent the growth of ice crystals, and it is simply done by immersing the cryovial with samples in a water bath at 37°C. However, theoretical and experimental results suggest that in certain situations, slow warming can also improve post-thaw viability.[10-12] Slow-warming injury is commonly attributed to nonequilibrium ice crystal growth mechanisms, including devitrification[5, 12-15] (the vitrified sample devitrifies to supercooled liquid) and recrystallization[12, 13, 15] (the growth of smaller ice crystals into larger ones) (explained in more detail in **Section 2.3**). However, evidence to support these two hypotheses is largely circumstantial, and the specific ways in which cellular components (such as proteins and membrane lipids) may be affected during slow warming remain largely unexplored.

The addition of CPAs to cells before cryopreservation is another approach to improve the outcome of cryopreservation. A detailed introduction to CPAs can be found in **Section 2.2**. Currently, the most widely used CPA is dimethyl sulfoxide (DMSO), which is a cell membrane-permeable molecule with a strong affinity for water.[16] It's found that DMSO with a concentration of as low as 10% can effectively inhibit ice formation both inside and outside cells during cryopreservation,[17, 18] and thus now it has become an indispensable component in many commercially available freezing media, including those for therapeutic cells (such as CryoStor CS10 from STEMCELL and Recovery from Gibco). Despite its effectiveness, however, lots of studies have revealed that DMSO can be toxic to cells, especially at room temperature and higher concentrations. Exposure of cells to DMSO can

result in changes in gene expression, reduction in cell function, and lower viability.[19-23] Furthermore, incomplete removal of DMSO from cryopreserved therapeutic cells before infusion can lead to adverse side effects in patients, including nausea, chills, hypotension, heart arrhythmias, and stroke .[24-26] Detailed information on the toxicity of DMSO can be found in **Section 2.2**. Given these concerns, much effort has been paid to find alternative CPAs that are nontoxic for therapeutic cells to minimize the adverse effects on patients.

Recently, studies have shown that encapsulating cells in hydrogels before cryopreservation can reduce the need for higher concentrations of membrane-permeable CPAs, without compromising the function and viability of the cryopreserved cells.[27-31] For example, Huang et al. reported that alginate encapsulation enables the vitrification of pluripotent and multipotent stem cells using 4 times lower concentrations of penetrating CPAs (as low as 2 M), in sample volumes up to 100 times larger (up to 250 μL), and at a slower cooling rate, compared to the conventional vitrification method.[31] Another study by Cao and colleagues utilized an alginate hydrogel microfiber approach to cryopreserve human red blood cells (RBCs) in the presence of very low concentrations of glycerol (2.5% to 5% v/v).[30] More recently, a study demonstrated that even in the absence of DMSO or any other penetrating CPAs, encapsulated cells can be well-protected during cryopreservation. In this study, Yao and colleagues developed a method to cryopreserve RBCs in alginate microcapsules while using trehalose (in the range of 0.3M to 1M) as the sole CPA. After freeze/thaw and removal from the alginate microcapsules, these cryopreserved RBCs demonstrated high survival

rates (>85%), preserved morphology, and normal ATP levels comparable to those of fresh cells.[32]

Despite the promising results of using hydrogel encapsulation for cell cryopreservation, there are still some limitations that must be addressed. First, although these methods reduce the amount of penetrating cryoprotectants needed for cell cryopreservation, the potential risk still exists for patients receiving these cryopreserved cells, due to the incomplete elimination of toxic CPAs. Even if Yao et al. demonstrated the feasibility of cryopreserving encapsulated RBCs using trehalose as the sole CPA, it should be noted that this method is not necessarily suitable for other therapeutic cell types (such as T cells, NK cells, and stem cells) since RBCs possess a simpler structure, smaller size, and higher water permeability.[33, 34] Additionally, the protection mechanism offered by hydrogel during cryopreservation is not yet fully understood, although some hypotheses have been proposed to explain the mechanism. One hypothesis suggests that the hydrogel network could restrict the growth of ice crystals during cooling and warming (a phenomenon known as ice recrystallization).[35] Another hypothesis suggests that the hydrogel matrix facilitates the vitrification of confined water in the presence of CPAs during cooling while minimizing their devitrification during warming.[29, 30, 36] Even though these hypotheses are reasonable, they are mainly concluded from the observations from light-transmitted microscopes, and as such, their validity requires further confirmation through kinetic and thermodynamic analyses.

In summary, there exists an urgent need to improve the current cryopreservation method, particularly in the context of therapeutic cells. To achieve that, we need a better understanding of how cryoinjury affects therapeutic cells and alters their cellular components during the freeze/thaw process. More importantly, a detailed investigation of the physicochemical protection mechanism offered by the hydrogel matrix during the freeze/thaw process is necessary in order to develop a cryopreservation methodology for therapeutic cells using hydrogel encapsulation in the absence of DMSO.

1.2 Objectives

The main objective of this dissertation research is to develop a novel cryopreservation method for mammalian cells using hydrogel encapsulation, and further optimize this method using NK cells as a model for therapeutic cells. To accomplish this objective, the following specific aims were pursued:

Specific Aim 1: Analysis of molecular changes associated with warming Injury in cryopreserved cells

This specific aim focused on investigating the cooling rate, DMSO concentration, and thawing protocol on the post-thaw viability of frozen human white blood cells (WBCs). Additionally, Fourier Transform Infrared (FTIR) spectroscopy was utilized to analyze the change of molecular structure and conformation of the WBCs during warming, with the aim to establish a correlation between the cellular damages and low-temperature kinetic processes.

Specific Aim 2: Design and manufacture a hydrogel matrix for the cryopreservation of mammalian cells and determine the physicochemical mechanisms of protection offered by hydrogel encapsulation

This specific aim focused on the development of an encapsulation cryopreservation method that utilizes agarose hydrogel and trehalose to preserve mammalian cells, without the need for any membrane-permeable cryopreservation agents. Additionally, we conducted a thorough analysis of the kinetic and thermodynamic changes that occur within the agarose hydrogel matrix with trehalose during freeze/thaw events using FTIR and differential scanning calorimetry (DSC). Through these analyses, we were able to establish the physicochemical mechanisms of cryoprotection offered by hydrogel encapsulation.

Specific Aim 3: Validation and optimization of the hydrogel encapsulation method for cryopreservation of NK-92 cells

This specific aim focused on the optimization of the cell extraction protocol and validation of the cryopreservation of NK-92 cells using agarose hydrogel encapsulation with trehalose. Also, the feasibility of using alginate as an alternative hydrogel material for reversible encapsulation and cryopreservation of NK cells was explored. The post-thaw viability (before and after cell extraction), cytotoxicity, extraction rate, and recovery rate were assessed for the NK cells extracted from these two hydrogels.

The outline of these specific aims is shown in ***Figure 1.2***. These specific aims are addressed in Chapters 3, 4, and 5, respectively. The research summary and future work are presented in Chapter 6 and Chapter 7, respectively.

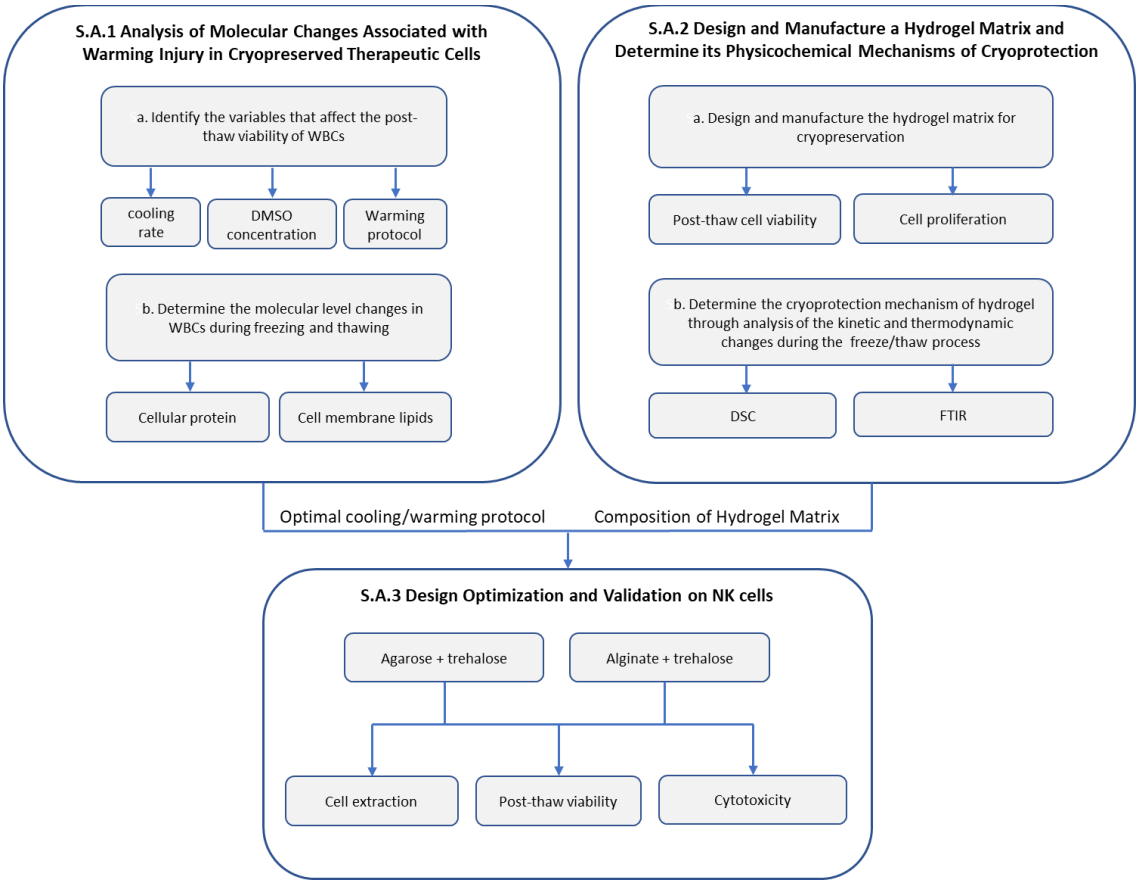

Figure 1.2 Outline of the specific aims for the dissertation.

Chapter: 2 Background

2.1 Methods of Cryopreservation

In cryopreservation, the post-thaw survival of cells is highly dependent on the concentration of CPAs, the cooling/warming rates, and the storage temperature. Based on the difference in these factors, cryopreservation methods can be categorized into two approaches: conventional freezing and vitrification.[3] (***Figure 2.1***)

2.1.1 Conventional Freezing Method

Typically, the conventional freezing method involves two cooling stages (***Figure 2.1***): (1) controlled cooling (slow cooling with ice nucleation), and (2) rapid cooling to the final temperature. The controlled cooling stage typically employs a slow cooling rate (~ 1°C /min) followed by ice nucleation in the extracellular solution. The slow cooling rate and the presence of CPAs can make sure the cells have enough time to dehydrate before ice nucleation. During this process, the intracellular water diffuses out through the plasma membrane, which gradually increases the osmolarity of the cytoplasm. As a result, intracellular ice formation (IIF) is minimized when the sample is deep freezing. For certain types of cells which are sensitive to freezing, the ice nucleation temperature needs to be precisely controlled and induced.[37] The second stage of freezing involves rapidly cooling the sample from a low temperature (between −60°C~ -80°C) to the final temperature (between − 140°C ~ -196°C, in the vapor or liquid phase of liquid nitrogen) for long-term storage.[2] Currently, this method has been widely used for

the preservation of cell suspensions; however, it is not suitable for the preservation of larger biological samples (such as organs) because of the progressive formation of extracellular ice.

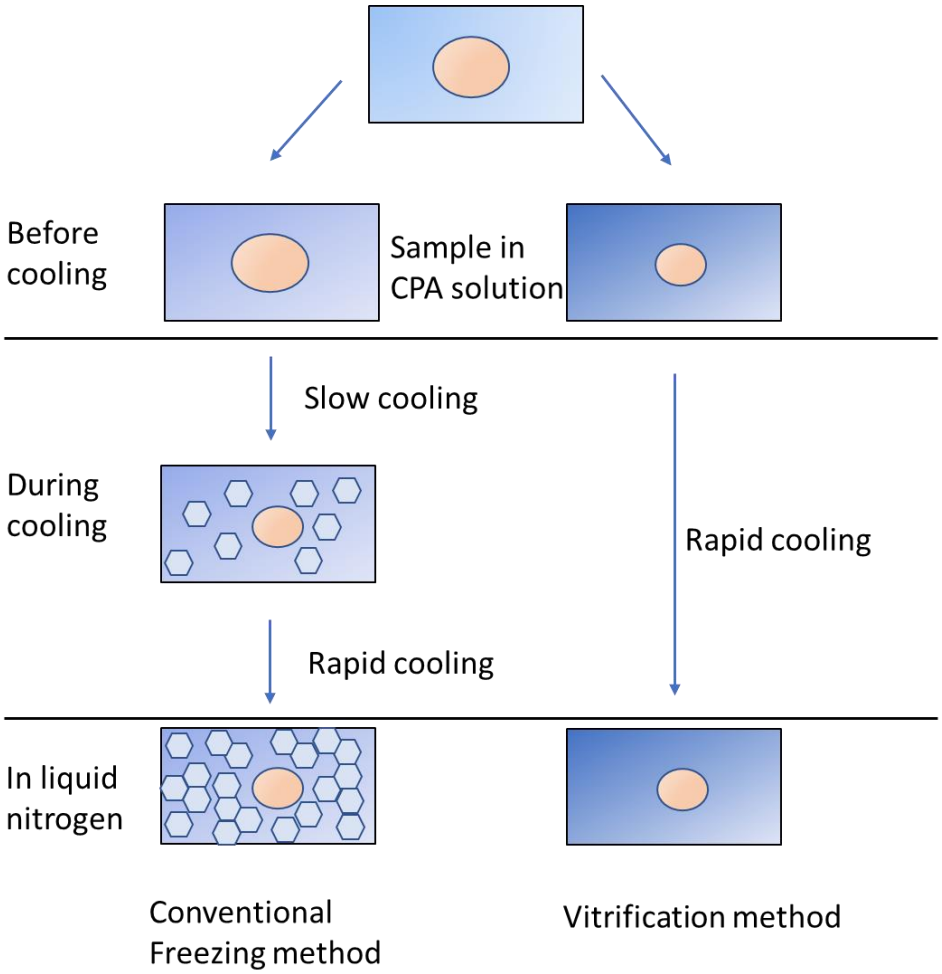

Figure 2.1. Schematic of a cell cooling protocol using conventional freezing and vitrification.

2.1.2 Vitrification

Ice formation can be avoided by vitrification method. Vitrification is achieved by cooling the biological sample into an amorphous glassy state, which has an extremely high viscosity. As a result, the vitrified sample behaves like a solid however without any crystallization even at ultra-low temperatures. The temperature at which this phenomenon takes place is known as glass transition temperature (T_g), and the vitrified sample is biologically inert when it's cooled below this temperature.[38] Unlike the conventional freezing method, vitrification requires rapid cooling rates above the critical cooling rates (usually >100°C /min) and/or higher concentrations of CPAs (40%~60%, w/v) to avoid ice nucleation.[39, 40] However, the increased CPA concentration can be cytotoxic to cells, inducing metabolic and osmotic injuries. [41] In order to mitigate toxicity, multiple steps are required to gradually load (before cooling) and unload (after warming) the CPAs,[40, 42] which is time-consuming and stressful. Vitrification method also requires high warming rates to ensure that the system avoids ice nucleation from glass during the warming process. Currently, vitrification method is mainly used for the preservation of gametes and larger biological samples such as tissues and organs.

2.2 Cryoprotectant Agents (CPAs)

2.2.1 Types of CPAs

A big hurdle to the success of cryopreservation is freezing. Freezing is fatal to most living organisms, since the formation of intra- and extracellular ice crystals may lead to a dramatic increase in osmotic stress and cellular mechanical damage on cells. Therefore, CPAs are necessary for cryopreservation because of their ability

to inhibit the formation and growth of ice crystals.[2] Based on the ability to diffuse across cell membranes, CPAs can be categorized into two types: (1) penetrating CPAs, such as dimethyl sulfoxide (DMSO), glycerol, ethylene glycol, and propanediol; (2) non-penetrating CPAs, including antifreeze proteins, polymers and various sugars (for mammalian cells).[43, 44] Penetrating CPA can pass through the cell membrane, so it plays a critical role in minimizing the osmotic stress on cells and thus preventing cells from over-dehydration during freezing. Also, the CPAs inside cells can effectively prevent the formation and growth of intracellular ice.[43, 45] On the other hand, non-penetrating CPA can effectively inhibit ice formation in the extracellular solution. Also, the presence of non-penetrating CPA will increase the osmolality of the extracellular solution. The elevated extracellular osmolarity forces intracellular water flow out through the cell membrane and leads to cell shrinkage before freezing. As a result, the concentration of electrolytes increases in the cytoplasm, which inhibits IIF during cryopreservation,[43, 46] even though it's not as effective as the penetrating CPA. Typically, at least one membrane-permeable CPA is needed for cryopreservation, and the nonmembrane-permeable CPAs are often used as additives to improve cell survival further. Although CPAs are effective in inhibiting ice formation at cryogenic temperatures, these chemical reagents can also be damaging to cells, mainly due to the "solution effects" when used at high concentrations.[9, 47]

2.2.2 DMSO

DMSO has been widely used for cell cryopreservation since the 1960s.[48] While it is known to effectively inhibit ice formation, numerous studies have shown that DMSO can also have detrimental effects on biological samples. Specifically, DMSO can bind to proteins irreversibly through hydrophobic interactions, resulting in protein unfolding at supra zero temperatures,[16] in contrast to its stabilizing effects at lower temperatures through preferential exclusion.[16, 17] Furthermore, at higher concentrations or temperatures, DMSO has been shown to damage the structure of the lipids cell membrane, leading to pore formation, reduced membrane thickness, and decreased stability.[49, 50] For therapeutic cells, the use of DMSO has been found to cause not only a reduction of cell viability, but also negative effects on various aspects of cell function, including proliferation,[19, 51] differentiation,[21, 52] phenotype,[22, 53] and cytotoxicity[20, 51] (in the case of immune cells). For example, Ford et al. reported a reduction in the cluster of differentiation CD3+ and CD4+ T cells from cryopreserved peripheral blood mononuclear cell (PBMC) samples of patients following vaccination.[52] Worsham et al. reported that cryopreservation with 10% DMSO resulted in reduced viability of CD4+ T cells and a decrease in their proliferative and cytotoxic response to immunological stimuli.[51] Additionally, Holthaus and colleagues have demonstrated that even small amounts of DMSO (0.25%) in the cell culture medium can impair CD4+ T-cell activation and signaling pathways, while higher concentrations (1%) can completely eliminate CD4+ T-cell proliferation.[53] Besides that, the expression of activation markers such as CD69, CD25, and CD154, as well as glucose uptake, have also been found to be inhibited in the presence of DMSO.[53] These findings highlight the need for

alternative cryoprotectants that can preserve therapeutic cells in a safe and more effective way.

2.2.3 Trehalose

Trehalose has emerged as a potential alternative to DMSO for the cryopreservation of cells. Unlike DMSO, trehalose is an inert, biocompatible, and non-toxic compound to cells,[54, 55] which makes it a good option for use in cell cryopreservation. Studies have demonstrated that trehalose is capable of stabilizing the cell membrane, decreasing the freezing temperature, and increasing the glass transition temperature. [4, 55, 56] However, trehalose alone is not a suitable cryoprotectant, since it's impermeable to mammalian cell membranes. As a result, trehalose has to be used at a high concentration to inhibit the extra- and intracellular ice formation (through dehydration), which can result in significant osmotic stress on the cell and lead to cell death.

Studies have shown the presence of a small amount of trehalose on both sides of the membrane can afford excellent protection against cryoinjury during cryopreservation.[57, 58] A lot of approaches have been developed to deliver trehalose into mammalian cell membranes, such as genetic modification[4, 59], microinjection[57], and thermal poration[56, 60]. Genetic modification involves the use of a genetically engineered pore-forming protein derived from Staphylococcus aureus a-hemolysin.[61] This polypeptide can spontaneously bind to the plasma membrane and forms a heptameric functional pore. After replacing five sequential

native residues with histidine (H5) using genetic engineering, the “open” or “closed” of the heptameric pore can be controlled by the addition or removal of Zn^{2+} ions. [4, 59, 61] Studies have shown that the delivery of intracellular trehalose (at a concentration as low as 200mM) using H5 α-hemolysin resulted in a significant improvement in the post-thaw survival of mammalian cells. [4, 59, 61] On the other hand, microinjection is done by directly injecting trehalose molecules directly into individual cells using micropipettes. [57] It has been reported that the injection of small amounts of intracellular trehalose (0.15M) can offer good protection to human oocytes during cryopreservation, in the absence of any other CPAs.[57] Thermal poration is applicable because of the characteristic of the plasma membrane: the liquid crystalline-to-gel phase transition at a specific temperature range (around 0^{o}C). [56, 60] It has been found that the permeability of the plasma membrane increases significantly during its phase transition,[60] which allows the diffusion of trehalose intracellularly due to the osmotic gradient.

Despite the promising results of these techniques, none of them have been widely accepted for practical use. This is likely due to the complicated and time-consuming nature of these operations, which can be costly and difficult to implement in large-scale cryopreservation procedures. Therefore, further research is needed to develop more efficient and practical methods for utilizing trehalose (which may effectively inhibit the intra- and extracellular ice formation without the increase of osmotic stress) in cryopreservation.

2.3 Cryoinjuries

2.3.1 Cryoinjuries associated with the cooling process

a. Two-factor hypotheses:

Ideally, cryopreservation should ensure the viability and functionality of the sample are maintained after thawing. However, the mechanical, thermal, and osmotic stresses applied to cells during cryopreservation may lead to cell damage and therefore compromise the viability and functionality of the biological samples. A significant factor determining if cells can be protected from freezing damage is the cooling rate.

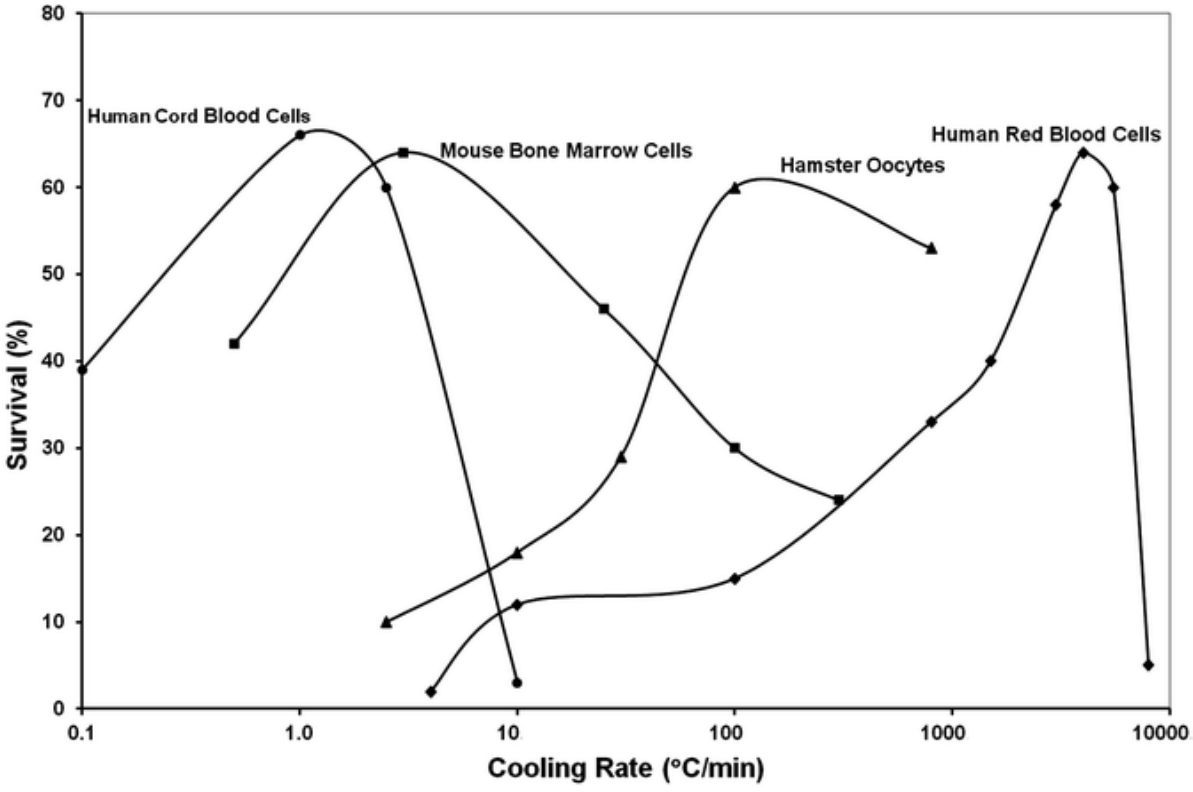

Figure 2.2. The effect of cooling rate on the survival following the freezing of four types of cells. [2]

As shown in ***Figure 2.2***, the plot of cell survival vs. cooling rate is an inverted U: a cooling rate that is either higher or lower can kill cells, and the maximum survival occurs at an intermediate rate. This phenomenon can be explained by the water transport model[62]:

$$dV/dt = L_p ART\,(\pi_i - \pi_e) \quad (1)$$

where V is the water volume in the cell, t is time, L_p is the permeability coefficient for water (hydraulic conductivity), A is cell surface area, R is gas constant, T is temperature, π_e and π_i are the osmolarities of extracellular media and cytoplasm, respectively.

During the cooling process, the intracellular water gradually leaves the cells (cell dehydration) and freezes extracellularly, which is driven by the vapor pressure or chemical potential difference between the intra- and extracellular environment. The rate and extent of cell dehydration depend primarily on two factors: The hydraulic conductivity (Lp) of the cell membrane and the cooling rate. For the cell of a given L_p, the slower it gets cooled, the more water it loses to remain in chemical potential equilibrium with the external solution and ice. On the other hand, the faster the cell is cooled, the less it can dehydrate, and the more cell water will become supercooled as the temperature falls. This mechanism was initially quantitatively expressed by Peter Mazur in 1963,[62] and further elaborated in his two-factor hypothesis of cell injury, [9] which identifies solution effects and intracellular ice formation as the main causes of damage.

Solution Effect

At slow cooling rates, cryoinjury occurs due to solution effects. Solution effects originate from the freezing of extracellular solution. As the extracellular ice crystals form, they progressively withdraw pure water in the solution and thus significantly increase the concentration of extracellular solutes.[9, 62] The elevated concentration of extracellular solutes applies enormous osmotic stress on cells, which leads to severe cell dehydration. In addition, the freeze-concentrated electrolytes in the isotonic solution (such as NaCl and PBS) are toxic to the cells.[63] Too slow cooling rate results in cell death.

Intracellular Ice Formation (IIF)

IIF usually occurs when the intracellular liquid is supercooled, and the cell is unable to maintain equilibrium with the external environment.[62, 64] During rapid cooling, the formation of ice and the concentration of extracellular solutes occurs too fast for the cell to lose water. As a result, the cytoplasm becomes increasingly supercooled, which significantly facilitates the freezing of intracellular water.[65] The greater the extent of supercooling, the higher probability of IIF and cell death.

b. Eutectic crystallization

Another mechanism to explain the cryoinjuries during the cooling process is eutectic crystallization. Electrolytes (such as NaCl), which are the main composition in the physiological solution, can form a eutectic mixture with water.[66] The eutectic mixture has a specific eutectic temperature, which is lower than the

melting point of any of the constituents. Therefore, when the sample is cooled, ice crystalizes first at the freezing temperature, and then the sample crystallizes again at the eutectic temperature. The degree of eutectic crystallization depends on the concentration of each constituent in the mixture.

Similar to ice crystallization, eutectic crystallization is a kinetic solidification process, which consists of nucleation and crystal growth. Therefore, it is also a process detrimental to cells. Kristiansen reported the damage of liposomes in saline solution significantly increased after the onset of the eutectic formation.[67] Han et al. found that the post-thaw viability of rat prostate tumor cells in the NaCl – Water solution with eutectic crystallization decreased by over 40% compared to the group without the induction of eutectic crystalization.[68] They also reported that the cell viability decreased with the increase in the temperature of eutectic formation. In other words, cell injury may be more severe when solutes with higher eutectic temperatures are added. The main mechanisms of cell injury associated with eutectic crystallization include mechanical damage to the cell membrane (such as membrane disruption) and intracellular eutectic formation.[68] However, it has been found that a variety of CPAs (such as glycerol and trehalose) could significantly inhibit or eliminate the eutectic formation of electrolytes during cryopreservation.[69] This highlights the importance of incorporating suitable CPAs into the cryopreservation process to mitigate the detrimental effects of eutectic crystallization on cells.

2.3.2 Cryoinjury associated with the warming process

a. Devitrification:

As to the warming process, one of the major cell injuries is devitrification. Devitrification is the transition process of formerly crystal-free, amorphous glass solution to the supercooled liquid. This process is often followed by ice crystalizaion.[12, 15] The formation of ice nuclei and/or the progressive growth of formed small crystals in the cytoplasm and the surrounding extracellular medium can lead to significant damage to cells. [2, 14] Devitrification may occur in the cryopreserved sample regardless of the methods of cryopreservation.

b. Ice Recrystallization:

Another primary source of cell injury during warming is ice recrystallization. In the process of ice recrystallization, larger ice crystals start to grow and gradually increase in size at the expense of smaller ice crystals for a given ice phase volume. [70] The formation of larger ice crystals intracellularly may cause detrimental damage to cellular structures.[3, 7, 71] It has been reported that the rate of ice recrystallization increases significantly with increasing temperature, until the frozen sample starts to melt(including eutectic melting).[72] This can explain why temperature fluctuations(such as transient warming that happened during the long-term storage) have a significant negative impact on the post-thaw survival of biological samples. This phenomenon also indicates that when the warming process is slow, it may provide more time for ice recrystallization at higher subzero temperatures.

Note that although fast warming is generally recommended to minimize devitrification and ice recrystallization, experimental and theoretical evidence indicates that there are some situations in which post-thaw viability could improve with slow warming.[10-12] One of the hypotheses supporting slow warming is that it enables osmotic re-equilibration, thus improving cell recovery after thawing.[73] Therefore, it's important to carefully evaluate the optimal warming rate based on the specific cell type and cryopreservation protocol.

2.4 Introduction of Cell Encapsulation

2.4.1 Hydrogel encapsulation

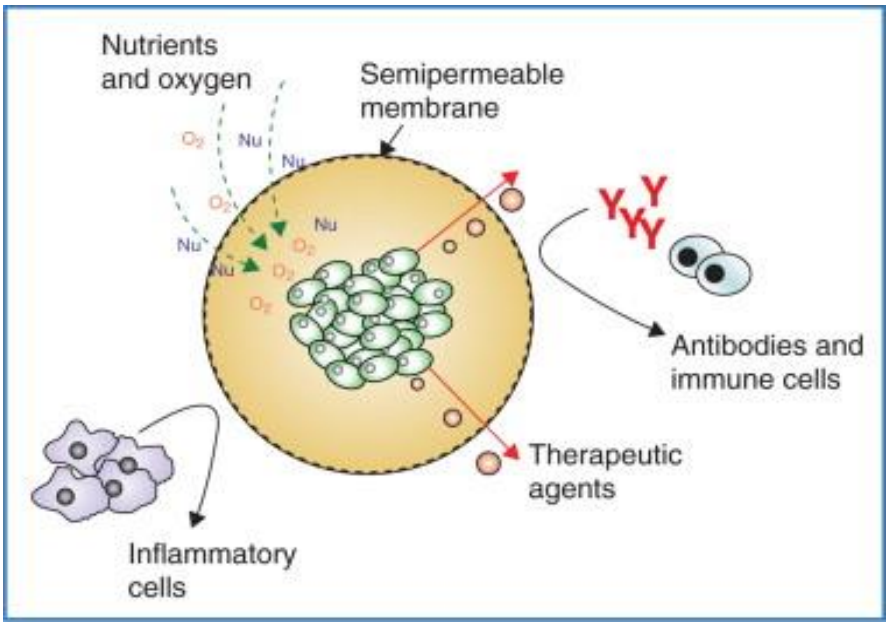

Figure 2.3. Schematic diagram of cell encapsulation.[46]

Cell encapsulation is a technique of entrapment of viable and functional cells within a semi-permeable matrix.[74-76] The presence of the semi-permeable matrix allows

the diffusion of nutrients and oxygen to the encapsulated cells, as well as the release of waste products and other functional agents to the environment through the small matrix pores(***Figure 2.3***).[46] Besides, the matrix could protect the encapsulated cells from being threatened by the antibodies or immune cells after transplantation, therefore maintaining the viability and functionality of encapsulated cells in the immune system of the host.[75, 77, 78] Because of these advantages, cell encapsulation has been used for a variety of biomedical applications including drug delivery, tissue engineering, and regenerative medicine over the past few decades.[78-80]

Considering the broad applications of this technology, an optimum material for cell encapsulation should be flexible, porous, and soft, but mechanically stable. Also, these materials can be processed under conditions compatible with cells and avoid inflammatory responses in humans.[76, 81] Some naturally-derived carbohydrate polymers, such as cellulose, chitosan, alginate, and agarose(***Figure 2.4***), have shown these promising properties and thus have been used extensively in cell encapsulation.[76, 82].

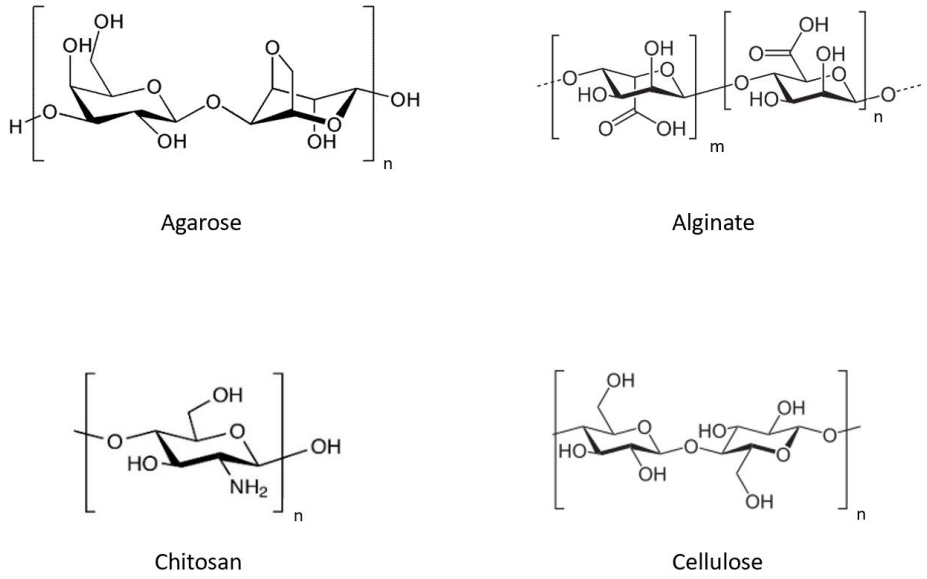

Figure 2.4. Chemical structure of naturally derived carbohydrate polymers commonly used for cell encapsulation.

Typically, carbohydrate-based polymers are composed of hydrophilic polymer chains, which can easily form a three-dimensional hydrogel structure by cross-linking. Based on the chemical or physical nature of the crosslink junctions, hydrogels can be divided into two categories: physically crosslinked hydrogel and chemically crosslinked hydrogel. Physically crosslinked hydrogel has transient or reversible junctions, which originate from physical interactions such as hydrogen bonds, ionic interactions, and hydrophobic interactions.[83, 84] These physical crosslinks in hydrogel may not be mechanically stable, but they are sufficient to make hydrogels insoluble in an aqueous media. On the other hand, the chemically crosslinked hydrogel is based on covalent bonding between the polymer chains. The formation of chemical crosslinks was carried out by the addition of small cross-linker molecules, polymer-polymer conjugation, and photosensitive agents.[83] Due

to the formation of covalent bonds, hydrogels generated in chemical crosslinking are much more stable and less reversible.[84] After gelation, the hydrogel matrix is soft, highly porous, and can be processed under mild conditions which are compatible with cell survival.

2.4.2 Hydrogel encapsulation for cell cryopreservation

In recent years, lots of studies have exploited the feasibility of cryopreserving encapsulated cells, given the growing application of cell encapsulation. Various hydrogels and preservation protocols (such as controlled rate freezing and vitrification) have been tested on different types of cells, with a summary of results presented in ***Table 2.1***. Through the tests on different hydrogel materials including agarose [85], alginate[27, 28, 31, 86-88], collagen[89-91], and synthetic polymers hydrogels,[92, 93] it is found that cells encapsulated in hydrogel suffered fewer injuries during the cooling and warming process. This is due to the ability of hydrogels to confine ice crystal growth within their three-dimensional networks, minimize osmotic shock when cryoprotectants permeate the cells, and preferentially vitrify the encapsulated cells at lower concentrations of CPA. This advantage makes hydrogel encapsulation a promising cryopreservation technique, with the potential to reduce the use of toxic CPAs such as DMSO.

Material	Cell Line	CPA	Preservation Protocol	Post-thaw viability / functionality	Year
Agarose	mouse oocytes/ embryos	EFS 20, EFS 40 (Sucrose, BSA, 20% or 40% Ethylene glycol)	Rapid cooling in LN2	Oocytes without a zona pellucida (ZP) had a survival rate of 5–18%, however, almost all agarose capsule embryos survived	2017 [85]
Collagen	human dermal fibroblasts	culture medium+ 5%~25% CPA (DMSO, glycerol, ethanediol)	Cooled at -1°C/min from ambient to -70°C, then -5°C/min to –170 °C	Significantly more viable cells were recovered from gels then frozen with 10% DMSO	1993 [89]
Collagen	rat cells, MEF cells mouse ES cells	culture medium+ 10% DMSO	Immediately transferred the sample into LN2 and stored from 1 week to 3 months	For rat hepatocyte cells, 52.1% recovered, nearly zero for control. For MEF cells, 58.6% recovered, nearly zero survival for the control group. For ES cells, 88.6% recovered after thawing, no viable cells were observed for the control group.	2009 [90]
Collagen	hASCs	Collagen + DMSO (3D printing scaffold)	Precooled in an isopropanol container (−20 °C), the container was then stored in a deep freezer (−80 °C) up to 14 days	After 1, 7, 14, and 20 days of cryostorage. the fabricated scaffold maintained high cell viability (>90%) at day 1 after thawing. All scaffolds showed similar increases in the cell proliferation indicators (cell viability and F-actin area per cell) and doubled in the bone differentiation indicator from 7 to 14 days of the cell-culture period.	2018 [91]
Alginate	mESCs, hMSCs	culture medium+10 %DMSO	Incubated at -80 °C one day	mESCs: 74% viability hMSC: 80% viability	2013 [28]
Alginate	hMSCs	5,10% DMSO +10% FCS	(1) −1 °C/min to −80 °C (2) −1 °C/min to −40 °C with ice nucleation at -7 °C, then −10 °C/min until −80 °C (3) one-stage rapid cooling	10% DMSO in CPA solution displayed better results than 5% DMSO. The second protocol, which included induced ice nucleation, showed the best viability and metabolic activity after thawing.	2013 [27]

Alginate	Primate MSCs	Culture medium + 10% DMSO +17.5% FBS	Incubated the sample at 4 °C for 12 min, then cooled at −1 °C/min r, then incubated at −80 °C overnight, and stored at −150 °C.	Encapsulated and cryopreserved MSCs showed better metabolic activities than unencapsulated cells	2014 [86]
Alginate	mESCs, hADSCs	2M PROH + 1.3M trehalose	The sample was cooled from room temperature to -60°C at a rate of 60°C/min.	Most of the microencapsulated cells could survive.	2015 [31]
Alginate	MG63 cells	DMSO Glycerol trehalose	The sample was cooled from 37 to -80°C at -1°C /min. The next day, vials were transferred to liquid nitrogen.	Cell survival after thawing: DMSO: (85% – 2%) Glycerol: (71% – 4%) DMSO/trehalose: (71% – 2%) Glycerol/trehalose: (72% – 6%).	2018 [87]
Alginate	C2C12 and D1MSC cell	CryoStor CS10 10% DMSO 5% Sodium Hyaluronate (Low MW-HA)	First incubated the sample on ice for 20 min and then in −80 °C freezer overnight. Finally stored the sample in LN2 for three weeks	The survival of encapsulated C2C12 and D1MSCs with 5% low MW-HA did not show statistical differences with 10% DMSO and CS10, however, the metabolic activity of the cells cryopreserved with low MW-HA was the lowest compared to 10% DMSO or CS10	2018 [88]
Alginate	β cells	0.4M Trehalose (in nano-capsules)	Cryovials were kept in the fridge (4 °C) for 20 min and then transferred to -40°C freezer overnight. Long-term storage in LN2.	great cell recovery rates (≈85%) were obtained and cell function was well preserved by evaluating the adherence, proliferation, and insulin expression of cells post-cryopreservation.	2019[94]
Alginate	RBCs	2.5, 5, 10% Glycerol or DMSO	Rapid cooling in LN2	Encapsulated RBCs with ultralow concentrations (2.5% and 5%) of CPAs can improve the RBC recovery by 15%–35%.	2020[30]

Alginate	RBCs	0.3M~1M Trehalose	Samples were placed in LN2 for rapid freezing,	The recovery of RBCs is the highest (86.76 ± 0.52%) with 0.7M Trehalose. No significant difference in morphology and ATP level.	2022[32]
Polymer (PVA/gelatin)	bovine thoracic arterial smooth muscle cells	Culture medium + 0-10% DMSO + 0-10%FBS	Incubated the sample at 4 °C for 1 h; and then stored at -70 °C overnight.	Post-thaw viability is ~50% (affected by the concentration of the serum and DMSO)	2009 [92]
Polymer (HEMA/agarose/gelatin)	HepG2, HUVECs cells	Freezing medium (DMEM:FBS: DMSO ratio 7:2:1)	The samples were stored in a -80 °C freezer for 1 day and 30 days.	Cryopreserved cells did not alter with the duration of cryopreservation and was able to grow and proliferate.	2017 [93]

Table 2.1. Articles reporting on natural polymer and synthetic polymer hydrogel for cell cryopreservation. (EFS: ethylene glycol + Ficoll + sucrose; BSA: bovine serum albumin; MEF: mouse embryonic fibroblasts; ES: embryonic stem; hADSCs: human adipose-derived stem cells; mESCs: murine embryonic stem cells; hMSCs: Human mesenchymal stem cells; hESCs: Human embryonic stem cells; FBS: fetal bovine serum; FCS: fetal calf serum; HUVECs: Human umbilical vein endothelial cells; HepG2 hepatocellular cells; HEMA: Hydroxyethyl methacrylate; PVA: poly(vinyl alcohol); DMEM: Dulbecco's modified Eagle's medium)

2.5 Introduction of Natural Killer (NK) Cells and Their Cryopreservation

2.5.1 Primary NK cells and NK-92 cells

In recent years, the impressive responses achieved with chimeric antigen receptors (CARs) T cells in cancer patients, especially those with relapsed/refractory B-cell malignancies[95, 96], demonstrate the ability of immune cells to become effective therapeutic agents. The encouraging results obtained with CAR T cells have attracted people to investigate the clinical utility of other immune cell types, such as natural killer (NK) cells, which may be able to address some of the limitations of CAR T cells. Different from T cells, human NK cells are

potent innate effectors with a set of stimulatory and inhibitory receptors, which are capable of targeting and killing virally infected and malignant cells without priming or prior activation.[97, 98] In addition, NK cells secrete not only cytotoxic granzyme and perforin that kill the target cells, but also cytokines and chemokines, such as IFNγ and TNFα, to modulate the subsequent immune responses,[99] thus minimizing the probability of serious adverse events including Cytokine Release Syndrome (CRS) or Graft versus Host Disease (GvHD) in patients.[100-102] These unique characteristics make NK cells an attractive cell type for adoptive immunotherapy.

Although clinical studies have shown that NK cell immunotherapy is effective and safe, challenges still exist, particularly in the process of manufacturing therapeutic NK cells. Since NK cells represent only 10% of peripheral blood mononuclear cells (PBMCs),[103] it is difficult to extract them in sufficient quantities to generate a high effector-to-target ratio in vivo. Hence, ex vivo expansion is necessary to generate clinically relevant levels of primary NK cells for multiple infusions. However, because of cell division, the cell expansion procedure may shorten the telomere, lowering the cytotoxicity of NK cells.[104] Besides, although the allogeneic transfer of NK cells is considered safe, it is crucial to deplete the contaminating allogeneic T cells to prevent GvHD.[105] Other factors including the logistics and costs associated with the preparation of primary NK cells also restrict patients' accessibility to NK cell immunotherapy.

As a potential alternative to primary NK cells, NK-92 has demonstrated promising anti-cancer activities, and it's so far the only FDA-approved cell line to be used in clinical trials.[106] It's found that NK-92 cells express virtually all major NK activating receptors, lacking only CD16 surface expression.[106, 107] Given their strong resemblance to primary NK cells, NK-92 cells have also proven highly effective against both solid and liquid tumors, as well as nontoxicity towards healthy cells.[104] Besides, the unlimited proliferation ability of NK-92 cells generates a consistent supply for both lab research and clinical treatment, greatly improving the logistics and reducing the cost of preparing NK cells.[104]

2.5.2 Cryopreservation of NK cells

Cryopreservation has been recognized as one of the major obstacles for NK cells to become the first "off-the-shelf" cell product for the treatment of cancer.[108] As highly active cells that are involved in numerous biological processes, NK cells are delicate and sensitive to the stresses associated with freeze/thaw (including temperature change, osmotic pressure, oxidation, and other environmental factors), especially when they are cytokine-activated.[73, 109] Currently, the commonly used freezing medium for NK cells contains 10% DMSO. While some studies indicated that using the freezing medium with DMSO does not result in a significant decrease in the immediate viability after thawing, these post-thawed cells showed different cell phenotypes, reduced motility, and lower cytotoxicity.[110, 111] For example, Mark and colleagues reported that NK cells have a 6-fold decrease in the fraction of motile and a 5.6-fold decrease in the numbers of killed

solid tumor cells after being cryopreserved with 10% ~ 20% DMSO.[110] In another study, Mata et al. found that the expanded NK cells cryopreserved with 5% DMSO showed a reduction of surface expression of NKG2D and TRAIL, as well as reduced cytotoxicity to K562 cells.[111] The decrease in cell motility and change in cell phenotypes are believed to be correlated to the decreased cytotoxic function of NK cells. Although some studies suggest that cytotoxic activity can be partially recovered after incubation with interleukin-2 (IL-2) following thawing, the viability of post-thaw cultured NK cells tends to decline significantly over time, particularly in the first few days.[112]

A few preliminary studies have explored the possibility of cryopreserving NK cells without DMSO. For example, Assal and colleagues developed a method for cryopreserving NK-92 cells using a cocktail of cryoprotects composed of dextran and carboxylated ε-poly-L-lysine.[113] Their results demonstrated that the cryopreserved NK cells maintained their viability immediately after thawing at a level comparable to that of cells cryopreserved with DMSO. Also, the recovered cells showed a higher cytotoxic potency against leukemia cells compared to controls. However, the viability of cells cryopreserved with the cocktail CPA dropped significantly in the first day of culture, and it took one week in culture for the cells to reach a comparable level to controls. Although these findings suggest that DMSO may not be necessary for the cryopreservation of NK cells, further research is needed to thoroughly confirm the efficacy of these techniques, and to elucidate their underlying mechanisms. Furthermore, cryopreserving primary NK

cells remains a challenging area of research, and thus far no successful cryopreservation of primary NK cells has been reported without the use of DMSO.

Chapter 3: FTIR Analysis of Molecular Changes Associated with Warming Injury in Cryopreserved Leukocytes

Much of the text and figures in this chapter have previously appeared in the publication below:
Wang, Mian, et al. (2018). FTIR analysis of molecular changes associated with warming injury in cryopreserved leukocytes. Langmuir, 35(23), 7552-7559.

3.1 Introduction

Human leukocytes, or white blood cells (WBCs), have been widely used in various medical treatment modalities. For example, in hematopoietic stem cell transplantation, WBCs from allogeneic donors are used clinically to speed up immune system recovery and to prevent disease relapse in transplant recipients.[114] In addition, autologous WBCs extracted from tumors have been successfully used in immunotherapy for the treatment of leukemia and lymphoma.[115] However, the practicality and safety of such cell therapies, whether using WBCs or any other cell type, typically necessitate cryogenic storage of the living cell product prior to transplantation.[116] Consequently, it is important to minimize the extent of irreversible cell damage caused by the cryopreservation of WBCs. Nonetheless, scant attention has been paid to the optimization of the preservation techniques currently used for WBCs, and the causes of WBC injury during cryopreservation are still not well understood.

Even though little is known about the exact pathways of the cryoinjury mechanisms that lead to loss of viability and function in cryopreserved cells, two variables known to significantly influence post-thaw cell viability are the rate of cooling and

the presence of cryoprotective agents (CPAs). According to Mazur's two-factor hypothesis,[9] slow cooling rates are associated with osmotic dehydration injury due to solute rejection during extracellular ice growth,[9, 117, 118] whereas fast cooling is associated with deleterious intracellular ice formation (IIF).[8, 119-121] Therefore, cell survival is maximized at some optimal intermediate rate of cooling; the magnitude of this optimum cooling rate is dependent on cell type.[119, 120]

To improve the outcome of cell cryopreservation procedures, CPAs are added to the samples before the start of the cooling process.[122] The addition of a cell membrane permeable CPA, such as the widely used dimethyl sulfoxide (DMSO),[21, 123] is known to increase post-thaw cell survival by mitigating cryoinjury mechanisms associated with both slow and fast cooling.[119] Because CPAs are less effective at insufficient concentrations but become cytotoxic at elevated concentrations,[124, 125] development of cryopreservation protocols requires optimization of the CPA concentration.[21, 126]

Mechanisms of cryoinjury dominant during the thawing of cryopreserved cells are poorly understood, despite the known sensitivity of post-thaw survival to the rate of warming from cryogenic storage temperatures.[10, 119, 127, 128] In fact, recent studies indicate that the rate of warming may be the process parameter that has the largest effect on cell survival, for both ice-free and conventional cryopreservation techniques.[129, 130] Although rapid warming rates are generally preferred,[128, 130] experimental and theoretical evidence indicate that there are some situations in which post-thaw viability should improve with slow warming.[10-12] Cryoinjury during

slow warming has conventionally been attributed to non-equilibrium ice crystal growth mechanisms that are known as devitrification[10, 12, 131] (active near the glass transition temperature, T_g) and recrystallization[15, 119] (active near the melting temperature), respectively. However, evidence to support the devitrification and recrystallization hypotheses of slow-warming injury is largely circumstantial in nature, and almost nothing is known about the possible role of biomolecules in cell damage mechanisms that manifest during the thawing process.

An ideal technique for near real-time probing of freeze/thaw-induced changes to the structure and conformation of cellular biomolecules in *in situ* is thermal Fourier Transform Infrared (FTIR) spectroscopy. Many techniques have been exploited to study biomolecule-lipid membrane interactions or membrane structure change at low temperatures,[132-134] however, only FTIR analysis can simultaneously supply information on the structural transitions of the lipid membranes and cellular proteins, as well as the thermodynamic state of extracellular environment.[135-137] Specifically, δ-OH (OH bending) and libration combination bands (~2200 cm^{-1}) of water have been used to detect crystallization and melting of ice in aqueous solutions.[135] On the other hand, ν-CH_2 bands (2950 -2830 cm^{-1}) have been used extensively to analyze the phase transitions of isolated lipid layers, liposomes, as well as the lipid membranes of cells.[135, 137, 138] Amide I (~1650 cm^{-1}), and Amide II (~1550 cm^{-1}) bands arising from vibrations of the protein backbone have widely been used to determine the secondary structures of isolated proteins,[139-141] and cellular proteins.[135, 142] However, the potential for freezing and thawing processes

to irreversibly alter molecular components of the cell, including cell proteins and membrane lipids, and the influence of such changes on the post-thaw viability of cryopreserved cells, are important avenues of research that remain underexplored. In this chapter, we investigate the major modes of cryoinjury during the freezing and thawing of human WBCs using DMSO as a cryoprotectant. In addition to optimizing the DMSO concentration and cooling rate for WBC cryopreservation, we report on the observation of slow-warming injury in WBCs at low temperatures. We used thermal FTIR spectroscopy to characterize cell molecular changes during the freeze-thaw cycle, providing insights into possible mechanisms for the cell damage process associated with the slow warming of WBCs.

3.2 Materials and Methods

3.2.1 WBC isolation from whole blood

Human blood samples were collected from volunteers by University of Minnesota Biological Materials Procurement Network (BioNet) staff following a University of Minnesota Institutional Review Board (IRB) approved protocol (Study Number: 1011E92892). Informed consent was obtained by BioNet from all volunteer subjects and all samples were de-identified. The experimental methods and procedures followed were approved by University of Minnesota IRB, and experiments were carried out in accordance with the approved guidelines.

To isolate WBCs, the whole blood sample (~10 ml) collected in an EDTA tube was centrifuged at 300g for 5 mins and the plasma layer was discarded. 1 ml of the cell

aggregate was diluted with 9 ml red blood cell lysis buffer (BioLegend, San Diego, CA, USA). After dilution, the solution was gently shaken for 10 mins at room temperature, and centrifuged at 500g for 5 mins. The supernatant was then discarded and the white blood cell pellet was resuspended in phosphate buffered saline (PBS) and centrifuged at 300g for 5 mins to remove the lysis buffer. Finally, the cell pellet was resuspended in 10 µL of 5% or 10% DMSO (Sigma-Aldrich, St Louis, MO, USA) solution (v/v prepared in PBS) to be used in FTIR analysis or for viability testing.

3.2.2 WBC viability measurements

After the WBCs were resuspended in DMSO solutions, 1 µL of the solution containing the cells was sandwiched between two CaF_2 windows and loaded into a cryostage (FDCS 196, Linkam, Tadworth, UK). All of the samples were first cooled down from 20°C down to 0°C at a rate of 10°C/min to minimize the intrinsic toxicity of DMSO [143] to cells at room temperature. To determine the optimal cooling rate and DMSO concentration for the highest post-thaw viability for WBCs, different cooling rates (1, 2, 5, 10, 20, and 50°C/min) and DMSO concentrations (5, and 10% v/v) were tested when samples were cooled from 0°C to -120°C. Extracellular ice nucleation was not controlled during the cooling process, and was observed to generally occur in the range of -15 to -25°C. Once the temperature reached -120°C, the sample was rewarmed to 20°C at a warming rate of either 100, 5 or 2°C/min. On the other hand, in order to study the effect of low-temperature kinetic factors, a 100°C/min warming ramp from -120°C was interrupted at an intermediate

temperature (-40°C, -50°C, -60°C, -70°C, -80°C, -90°C, -100°C, -110°C) and held constant for 6 or 30 minutes before resuming rapid warming (100°C /min) to 20°C.

After rewarming back to 20°C, 1 µL of 20 µg/ml acridine orange (AO) / propidium iodide (PI) fluorescent dye (Nexcelom, Lawrence, USA) diluted from a 1 mg/ml stock solution was added to the sample, and the number of live and dead cells were counted (in five representative areas for each sample) using a Nikon Eclipse TE200 inverted fluorescence microscope (Melville, NY, USA). The final percentage viability of the sample was calculated with respect to the control (unfrozen WBCs) using the following equation:

$$\text{Viability} = \frac{\text{percentage of live cells}}{\text{percentage of live cells in the control}} \times 100\%$$

3.2.3 FTIR spectroscopy

Fourier Transform InfraRed (FTIR) spectroscopy was used to analyze the WBC solutions during the cooling and warming processes. Experimental solutions of 1µL were sandwiched between two CaF_2 windows and sealed with vacuum grease to avoid evaporation of the solution. The assembly was then transferred to the cryostage attached to an infrared microscope, which was connected to an FTIR spectrometer (Thermo-Nicolet Continuum equipped with a mercury cadmium telluride detector, Thermo Electron, Waltham, MA). IR spectra were collected form a sample area of 200 µm x 200 µm as the temperature of the sample was varied from 20°C to 0°C at a rate of 10°C/min and from 0°C down to temperatures as low as −120°C at a rate of 2°C/min. Three different warming rates (2, 5 or 100°C/min)

were utilized to warm the samples. During cooling and thawing, IR spectra were collected every 5°C (or every 10°C during the experiments at 100°C/min warming rate) at a resolution of 4 cm^{-1} and a total of 32 IR scans were averaged to obtain each spectrum analyzed. The IR spectra were analyzed using the OMNIC software (Thermo-Nicolet, Madison, WI, USA). Changes in the water combination band (2200 cm^{-1}) arising from OH bending and libration, CH_2 symmetric stretching band (2850 cm^{-1}), the Amide II band (1550 cm^{-1}), and the asymmetric CH_3 deformation band (1440cm^{-1}) were examined as the sample was cooled and heated.

3.2.4 Statistical Analysis

Viability data are reported as the mean ± standard deviation of n = 2–5 replicates for each experimental condition. Effects of DMSO concentration and cooling rate were analyzed by two-way ANOVA, whereas effects of warming rate or hold temperature were analyzed by one-way ANOVA. Post hoc testing was performed using the Holm-Sidak method. All effects were considered statistically significant at $p < 0.05$.

3.3 Results and Discussion

3.3.1 Cell viability

(a) Effect of cooling rate and DMSO on WBC viability

The cooling rate dependence of viability followed an inverted-U shape (***Figure 3.1***), as expected from Mazur's two-factor hypothesis.[9] ANOVA revealed statistically significant effects of cooling rate ($p < 0.001$) and DMSO concentration ($p < 0.005$),

with a significant interaction term ($p < 0.05$). All of the WBC samples frozen in 5% DMSO solutions had higher post-thaw viability than those in 10% DMSO when cooled at the same rate, although the difference between the two CPA concentrations was only statistically significant ($p < 0.001$) at the cooling rate optimum (2°C/min). This result is consistent with findings of published studies, which have reported that reduction of DMSO concentration from 10% to 5% yields improved outcomes in cryopreservation of WBCs[18] and peripheral blood progenitor cells.[18, 144]

The maximum post-thaw viability was 65.7 ± 9.8% for WBCs cooled at 2°C/min in 5% DMSO. For WBCs in 5% DMSO, the difference in viability between the optimum cooling rate and all other cooling conditions was statistically significant ($p <0.005$). WBC post-thaw viability was lower at supra-optimal cooling rates than at sub-optimal cooling rates ($p < 0.005$), and dropped down to zero when the cooling rate reached 50°C/min. In interpreting the results in ***Figure 3.1***, it is important to keep in mind that extracellular ice formation was not controlled in our experiments, which is likely to have resulted in reduction in the amount of cell dehydration possible at rapid cooling rates (due to depressed extracellular ice nucleation temperatures); thus, considering the interplay between cell dehydration and cryoinjury[9, 145], it is possible that the cooling rate optimum would shift if the extracellular ice formation were induced at the start of the cooling ramp. In our present study, all further experiments were performed using a DMSO

concentration of 5% and a cooling rate of 2°C/min (without induction of extracellular ice nucleation).

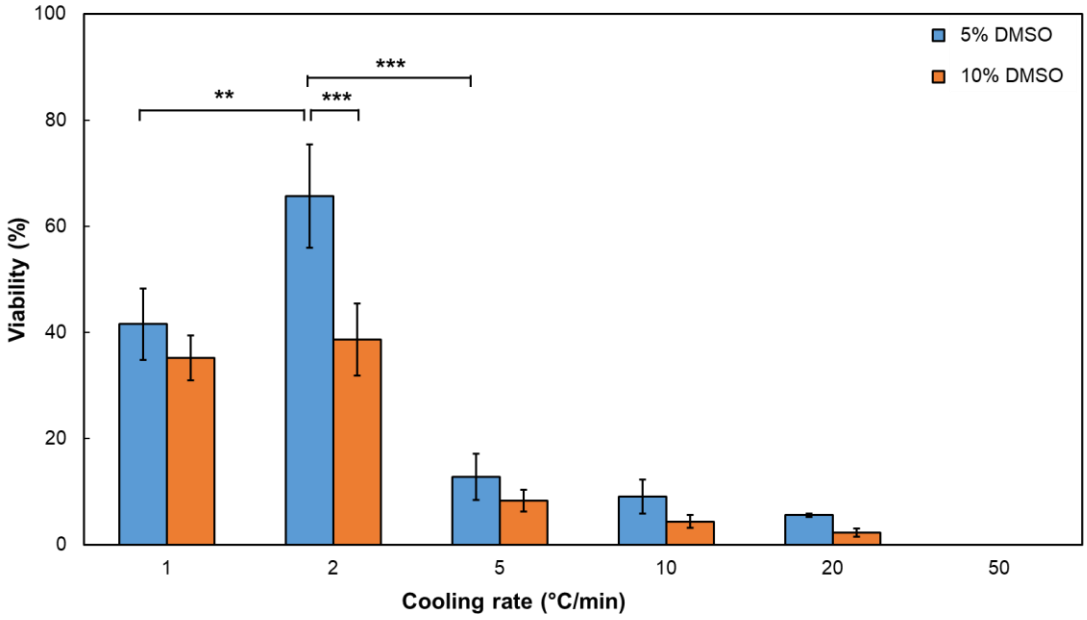

Figure 3.1. Post-thaw viability of WBCs suspended in DMSO solutions at different cooling rates when exposed to the same warming rate of 100°C /min. Note that the viability of the sample cooled at 50°C /min is zero. (** indicates p<0.01, and *** indicates p<0.001)

(b) Effect of warming protocol on WBC viability

The effect of warming rate on the post-thaw viability of frozen WBCs was tested at constant warming rates of 2, 5, and 100°C/min. ***Figure 3.2A*** shows that for WBCs frozen at 2°C/min in 5% DMSO, the fastest warming rate tested (100°C/min) yielded the highest viability (65.7 ± 9.8%). The effect of warming rate on viability was statistically significant ($p < 0.001$), and the viability after thawing at 100°C/min was significantly higher than the post-thaw viability for warming at either 5°C/min ($p < 0.001$) or 2°C/min ($p < 0.001$). Transmitted light images of WBCs captured at 20°C before freezing and after thawing (***Figure 3.2B***) revealed that WBCs warmed

rapidly (100°C/min) retained their structure and round shape after thawing, but slow warming (2°C/min) resulted in an abnormal morphology of the thawed WBCs, which correlated with the observed decrease in cell viability.

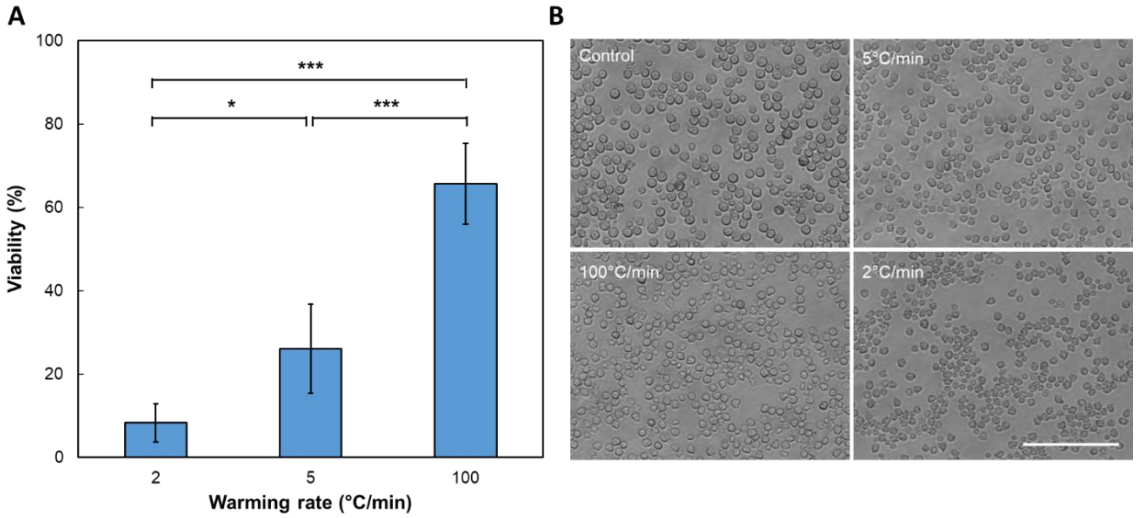

Figure 3.2. (A) Post- thaw viability of WBCs cooled at 2°C/min, and warmed at different rates (2, 5 or 100°C/min). (B) Transmitted light images of WBCs suspended in 5% DMSO at 20°C before freezing, and after thawing at different warming rates (scale bar =100μm). (*indicates $p<0.05$, and *** indicates $p<0.001$)

To determine the temperature range in which warming injury occurs, the rapid warming (100°C/min) of frozen WBCs was interrupted at an intermediate temperature, where the temperature of the samples was kept constant for 6 minutes and 30 minutes, respectively, before resuming with the rapid warming protocol. As shown in ***Figure 3.3***, the post-thaw viability was sensitive to the interruption of rapid warming, and the mean viability was highest when rapid warming was uninterrupted for both 6-min and 30-min hold groups. Specifically, when WBCs underwent isothermal holds for 6 minutes at -70°C and -80°C, their viability was substantially reduced compared to WBCs warmed without any interruptions. Furthermore, for WBCs subjected to isothermal holds lasting 30

minutes during warming, post-thaw viability exhibited a significantly lower value than the control group across a more extensive temperature range (between -60°C and -100°C). Additionally, WBCs held for 30 minutes at -60°C, -70°C, and -80°C exhibited significantly lower viability than those held for 6 minutes at the same temperatures ($p<0.05$). These observations suggest that cells experience increased damage over time at consistent holding temperatures, particularly within the -60°C to -80°C range.

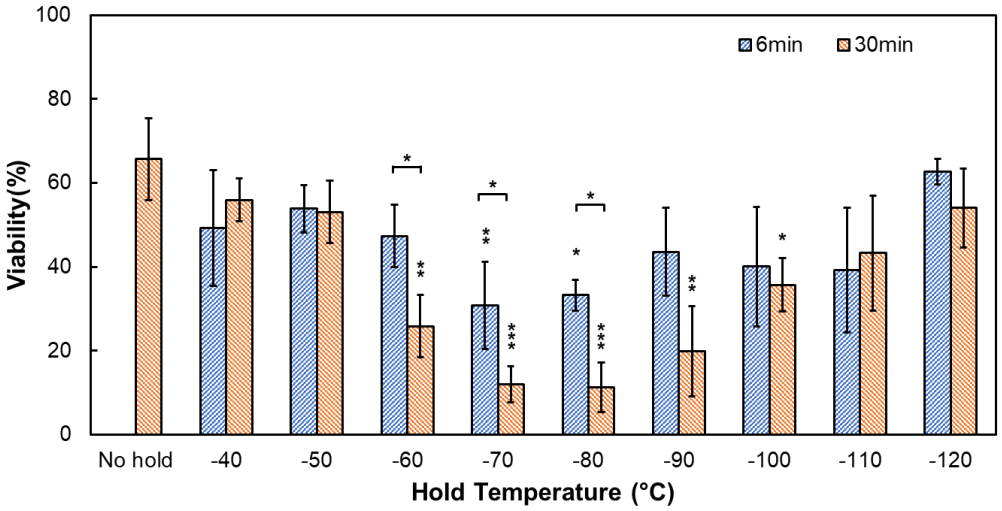

Figure 3.3. Post-thaw viability of WBCs suspended in 5% DMSO solutions cooled at 2°C/min, and warmed at 100°C /min, interrupted by a 6-minute or 30-minute constant temperature hold. (* indicates $p<0.05$, ** indicates $p<0.01$, *** indicates $p<0.001$, * above the bars indicates the significant difference with the No hold control group)

3.3.2 Molecular level changes in cells during freezing and thawing

Figure 3.4 depicts the mid-infrared IR spectra collected from WBCs suspended in 5% DMSO solution during the freezing and thawing processes. Water exhibits strong bands at 1650, and 2200 cm^{-1} arising from the O-H bending, and the

combination of bending/libration vibrational modes, respectively. Characteristic bands arising from cellular components can also be identified in the spectra. Cellular proteins exhibit three bands: The Amide I band (around 1650 cm^{-1}) mainly arises from C=O stretching vibrations but overlaps significantly with the δ-OH band of water. The Amide II band arises from δ-NH vibrations and is located around 1550 cm^{-1}. The Amide III protein band is composed of a couple of weak bands in the region 1200 – 1350 cm^{-1}.[146] The bands at 2850 cm^{-1}, and 2920 cm^{-1} are associated with the methylene symmetric, and asymmetric stretching vibrations of the acyl chains, respectively.[138]

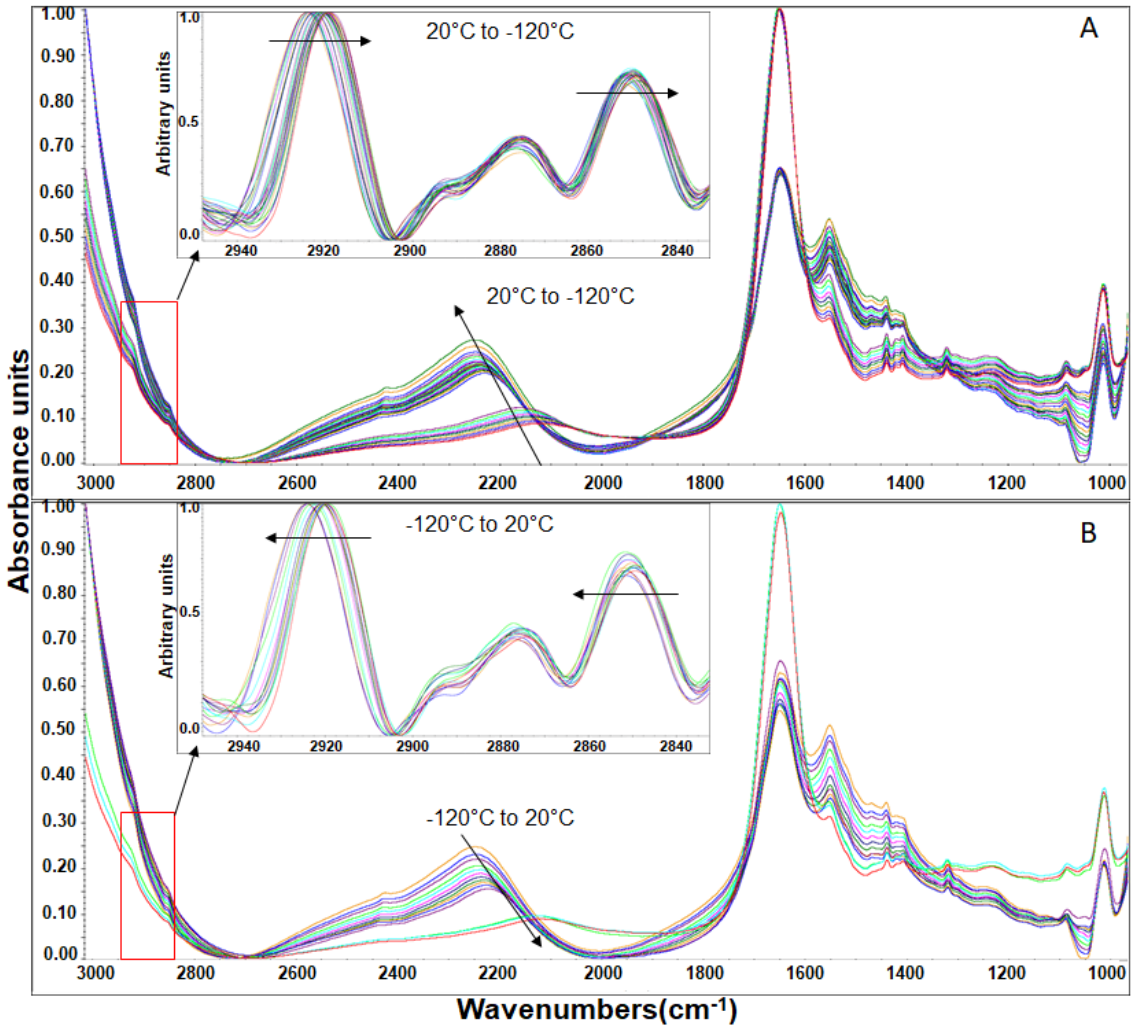

Figure 3.4 FTIR spectra of WBCs suspended in 5% DMSO **(A)** during cooling, and **(B)** warming processes **(B)**. Insets show the second derivative spectra in the CH_2 stretching region (2950 -2830 cm^{-1}). The sample shown here was cooled from 20°C down to -120°C at 2°C/min, and warmed back up to 20°C at 100°C/min. Spectra were collected every 5°C, and 10°C during cooling, and warming, respectively.

(a) Lipid membrane phase change

Phase change behavior of lipid bilayers,[147, 148] liposomes,[149] and cellular membranes[136, 137, 150, 151] can be explored by FTIR spectroscopy by analyzing the lipid CH_2 stretching vibration band in the 2800~3000 cm^{-1} region. The second derivative of the original spectra was taken to analyze the two small lipid bands in this region in detail (insets, ***Figure 3.4***). The change in the position of ν-(CH_2) with temperature was evaluated by calculating the peak position at 90% of band height in the second derivative spectra.

During cooling from room temperature, the symmetric CH_2 stretching mode arising from the membrane lipids exhibited a shift to lower wavenumbers, which indicated dehydration,[137] and an increase in the order and compactness of the lipid membrane (***Figure 3.5B, E, H***).[135, 138] Extracellular ice nucleation (marked by a sudden shift in the water combination band as shown in ***Figure 3.5A, D, G***) had a strong effect on the lipid bilayer, and induced membrane phase transition. This was reported earlier by others as well.[135-136] For the samples warmed at 100, and 5°C /min the plots of ν-(CH_2) versus temperature obtained during cooling and warming have highly overlapped, suggesting that the dehydration lipid groups experienced during cooling was reversible, and there was no permanent change

in the cell membrane structure after warming back to room temperature (***Figure 3.5B, E***). However, in the sample warmed at 2°C /min, a clear hysteresis appeared above 0°C during warming (***Figure 3.5H***).

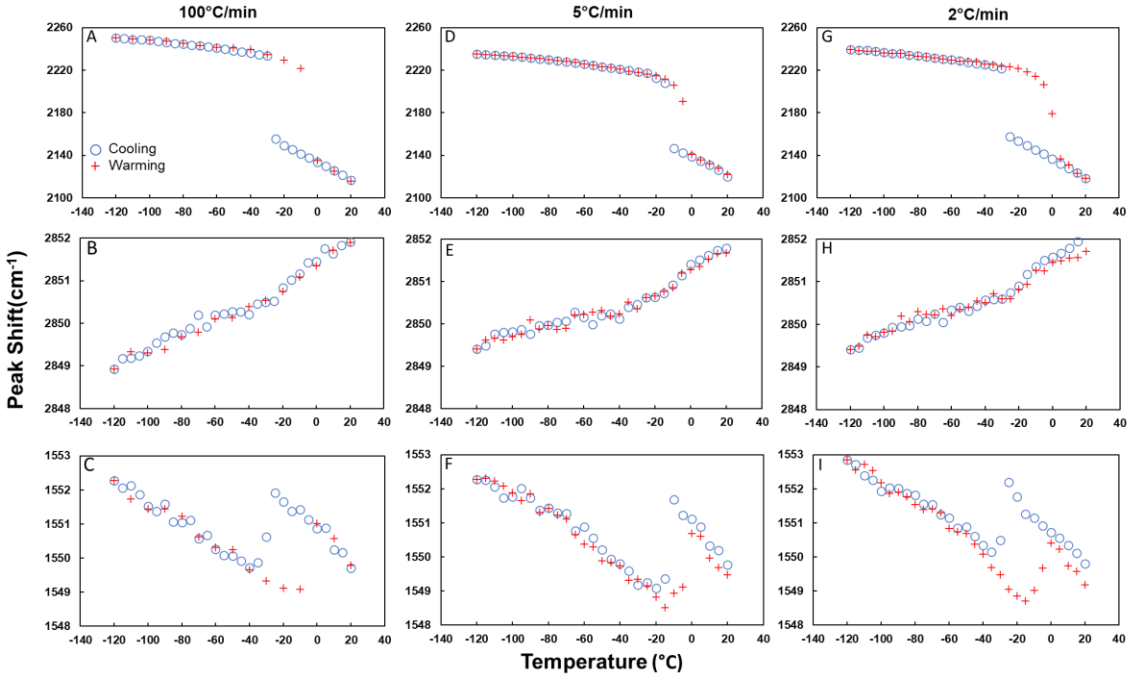

Figure 3.5 Variation of bending + libration OH peak (**A, D, G**), symmetric ν–CH_2 (**B, E, H**), and Amide II peaks (**C, F, I**) during freeze/thaw cycling of WBCs suspended in 5%DMSO. Samples were cooled at 2°C /min from 20°C down to -120°C and warmed back up to 20°C at 100°C/min (**A-C**), 5°C/min (**D-F**), and 2°C/min (**G-H**).

(b) Changes to cellular proteins

IR spectra reveal the changes in protein secondary structure as the peak position and shape of the Amide bands are highly sensitive to the extent of hydrogen bonding of the protein with its surroundings.[152, 153] The Amide I band has been used widely for analysis of the secondary structures of proteins [139-141] however, it overlaps with δ-OH of water. As opposed to the Amide I band, the Amide II band

has no spectral contributions from water, and therefore is more suitable for protein structural analysis.

As shown in ***Figure 3.5C,F,I***, the Amide II peak position shifted to higher wavenumbers with decreasing temperature, which indicated an increasing level of cellular protein hydration.[141, 152] An abrupt change in peak location was observed at the temperature of ice nucleation, due to rapid dehydration of cellular proteins with loss of hydrogen bonding with liquid water. For the samples thawed at a rate of 100°C /min, the plots of Amide II peak position versus temperature recorded during cooling and warming processes have fully overlapped (except for the range between ice nucleation and melting temperatures, as expected), suggesting that the change in the hydration levels of cellular proteins were highly reversible. This followed the same trends observed above in cell membrane lipids. However, for the samples warmed at slower rates, the wavenumbers showed a red shift after the samples were thawed (above 0°C), which indicated that the hydration level of cellular proteins decreased (with respect to their pre-freeze states) after the freeze/thaw cycle. The difference in Amide II location at 20°C increased with decreasing warming rate, showing that lowering the warming rate had changed the hydration levels of cellular proteins, pointing out to irreversible damage accumulation.

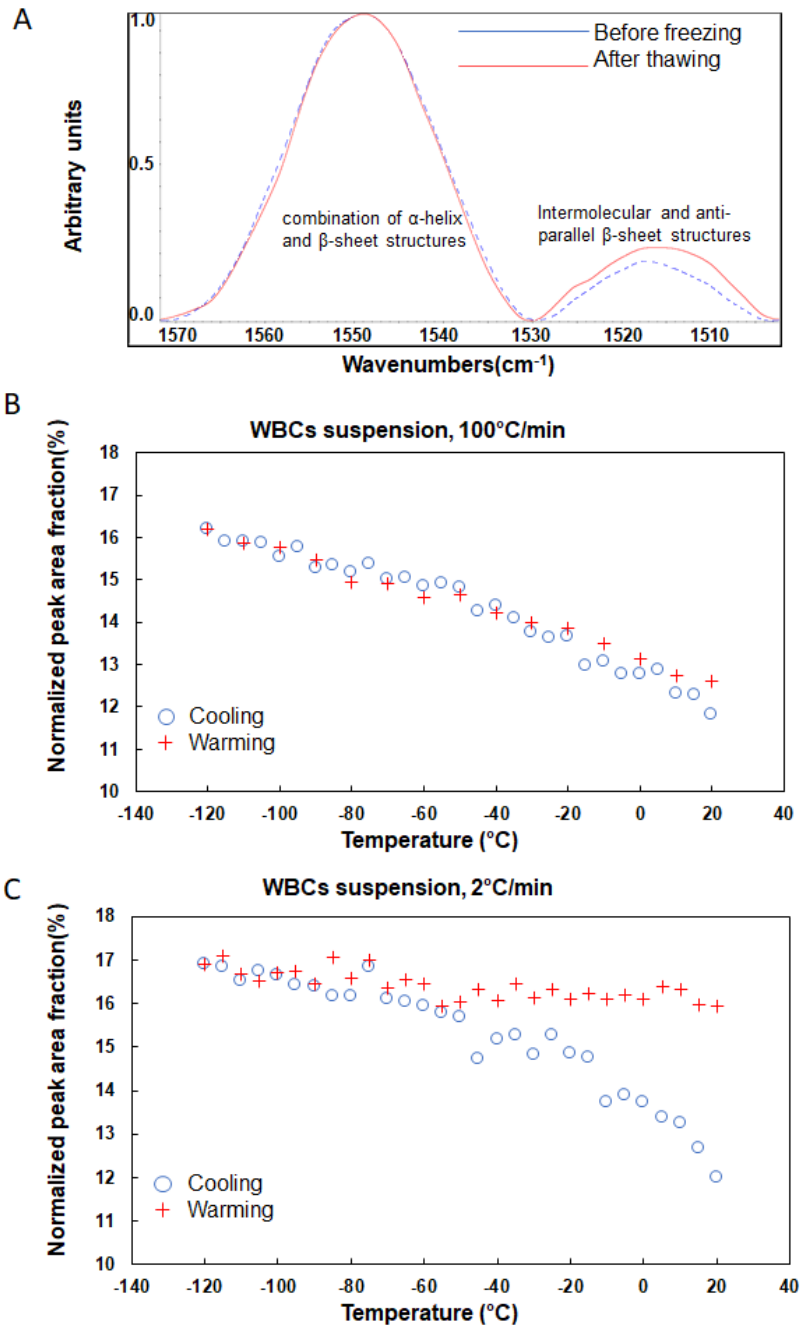

Figure 3.6 (A) Second derivative spectra in Amide II region collected from WBCs suspended in 5% DMSO at 20°C before freezing (dashed blue line), and after thawing (solid red line). The sample was cooled from 20°C down to -120°C, and warmed back up to 20°C at a rate of 2°C/min. (B) Variation in the area fraction of intermolecular and (C) antiparallel β-sheet structures of cellular proteins in WBCs suspended in 5%DMSO and subjected to freeze/thaw. Both of the samples were cooled down at 2°C /min, but warmed at different rates: (**B**) 100°C /min, (**C**) 2°C /min.

To further investigate the structural changes in cellular proteins, the two bands in the Amide II region (1590~1500 cm^{-1}) appearing in the second derivative spectra were studied using their baseline corrected band areas (***Figure 3.6A***). The band at 1590−1530 cm^{-1} was assigned to a combination of α-helix and β-sheet structures,[142, 154] and the band at 1530−1500 cm^{-1} was assigned to intermolecular and antiparallel β-sheet structures.[142, 154-156] Earlier studies report that the change in the area fraction of these bands is a direct outcome of protein secondary structure change,[157, 158] which is supported by the findings presented in ***Figure 3.6B*** and ***Figure 3.6C***, where the area fraction of intermolecular and antiparallel β-sheet structures increased with decreasing temperature.

In the sample warmed at 100°C/min, the traces obtained during cooling and warming were highly similar, and there was no significant difference in the spectra collected at 20°C before freezing and after thawing (***Figure 3.6B***). This suggested that even though cooling and freezing might change the secondary structure of the cellular proteins, the change was fully reversible if the sample was thawed at a very high rate. However, for the sample thawed at a slow warming rate of 2°C/min, the peaks of the intermolecular and antiparallel β-sheet structures, which increase with aggregation of proteins,[155, 159] became stronger after thawing when compared to the IR spectra collected at 20°C before freezing (***Figure 3.6C***). This suggested irreversible protein damage in the cells thawed at a slow warming rate.

In addition, for the sample warmed at 2°C/min, the slope change in the plot (***Figure 3.6C***) occurred around -60°C, suggesting the occurrence of cellular protein denaturation at this temperature. This is consistent with the significant decrease in viability observed for WBCs rapidly warmed with an isothermal hold between -60°C and -80°C.

3.4 Conclusion

Post-thaw viability and IR spectroscopy analysis of white blood cells established causality between cellular protein/lipid membrane damage sustained at low cryogenic temperatures (T < -60^{o}C) and loss of viability observed post-thaw. The evidence suggests that these deleterious events were mediated by kinetic processes active at cryogenic temperatures lower than -60°C, which may include: a) eutectic crystallization and melting;[160, 161] b) ice recrystallization. [13, 45]

During warming of vitrified water-DMSO solutions, eutectic crystallization starts at approximately -70^{o}C, and is followed by eutectic melting at -64^{o}C.[162] Rapid phase change, involving crystallization and melting, would be highly likely to create significant mechanical and chemical stresses, damaging cells. The plot slope change around -60 ^{o}C during warming (***Figure 3.6B***), as well as the U-shaped post-thaw viability curve (***Figure 3.3***) with its nadir between -60 ^{o}C and -70 ^{o}C, suggests that cells experience heightened damage due to eutectic crystallization and melting.

Moreover, devitrification (new ice crysat formed) and ice recrystallization (growth of ice crytals) may occur if the temperature is higher than the glass transition temperature of freeze-concentrated water-DMSO solutions (-124°C), and the rate of ice recrystallization increases with rising temperature,[13] which is lethal to cells. Consequently, the post-thaw viability of cells may decrease with increasing hold temperature. However, the viability data indicate that this hypothesis is only applicable to the low-temperature region (below -70°C). When the viability reaches its nadir in the region between -70°C and -80°C, it begins to increase with a rising holding temperature(***Figure 3.3***). This phenomenon might be attributed to the melting of the eutectic mixture of DMSO-water around -64°C,[162] which would substantially inhibit ice recrystallization. Above the eutectic point, the solutes from the eutectic mixture begin to dissolve by melting the nearest ice, and then diffuse to fresh ice surfaces and initiate melting.[163] Consequently, holding the temperature higher than the eutectic melting temperature may be less detrimental than holding it lower, resulting in a U-shaped curve for the post-thaw viability (***Figure 3.3***), particularly when the time of isothermal hold is extended.

It is important to note that the mode of warming injury observed here may only be applicable to the specific freezing procedure and cryoprotectant solution that were investigated. Nonetheless, further research is warranted to elucidate these and other damage mechanisms active during the warming of cryopreserved cells, so that strategies to prevent warming injury can be developed.

Chapter 4: Physicochemical Mechanisms of Protection Offered by Agarose Encapsulation during Cryopreservation of Mammalian Cells in the Absence of Membrane-Penetrating Cryoprotectant

Much of the text and figures in this chapter have previously appeared in the publication below: Wang, Mian, et al. (2023) "Physicochemical Mechanisms of Protection Offered by Agarose Encapsulation during Cryopreservation of Mammalian Cells in the Absence of Membrane-Penetrating Cryoprotectants." ACS Applied Bio Materials.

4.1 Introduction

During freeze/thaw, cells are exposed to mechanical, thermal, chemical, and osmotic stresses, which cause loss of viability and function.[2, 9] Specifically during cooling, nucleation and growth of ice intra/extra-cellularly physically damages the cellular structures such as the cytoskeleton, the organelles, and the plasma membrane.[64, 164] Extracellular ice formation also dehydrates cells, inducing osmotic and chemical stresses.[9, 63] At lower cryogenic temperatures, pH changes due to selective precipitation of the buffer electrolytes,[165] and eutectic formation[66] induce further chemical, and mechanical stresses on the cell.[68] During warming, primary sources of cryoinjury are eutectic crystallization/melting, devitrification (ice crystallization in the amorphous phase following glass melting), and ice recrystallization (formation of larger ice crystals through the fusion of smaller ones),[3, 7, 70, 71] as discussed in Chapter 3. To minimize cryopreservation-induced cellular injuries, cryoprotective agents (CPAs) such as polyols, disaccharides, sugar alcohols, and polar solvents are routinely added to the cells to be cryopreserved, and dimethyl sulfoxide (DMSO) is the most widely used one since it can easily penetrate the cell membrane and effectively inhibit both intra- and

extracellular ice formation. However, the toxicity of DMSO may have a variety of adverse effects on cell metabolism, enzymatic activity, cell differentiation and viability.[23, 166] Therefore, many studies have focused on reducing the amount of DMSO needed in the cryoprotectant formulations[110, 113, 167-171] using additives such as albumin,[110, 170, 172] FCS/FBS,[168, 169] and growth media.[113] However, there is an ongoing debate on the safety and ethicality[173, 174] of using FCS/FBS as they are not clinical reagents that can be safely used in injectable/infusible cell therapy products.

Encapsulation of cells in hydrogels for cryopreservation has been shown to be beneficial in decreasing the need for using high concentrations of membrane-permeable cryopreservation agents, relaxing fast cooling requirements.[87, 175-177] For a very detailed analysis of the studies conducted with DMSO and other membrane permeable cryoprotectants used to cryopreserve encapsulated cells, please see the reviews by Gurruchaga et al.[176] and Zhang et al.[35] As detailed in the Gurruchaga review, none of the studies to date have been successful in eliminating the need for membrane permeable cryopreservation agents such as DMSO, ethylene glycol or 1,2-propanediol and still depended heavily on the use of FCS/FBS. Furthermore, some of these methods require direct liquid nitrogen immersion of the encapsulated cells loaded in microcapillaries are therefore not scalable and pose a very high risk of contamination. Therefore, cryopreservation of cellular therapy products is an ongoing challenge.[178-180]

In this chapter, we present an encapsulation-based cryopreservation method capable of preserving mammalian cells without using membrane-permeable cryopreservation agents (e.g., DMSO) or FCS/FBS at slow cooling rates (2^{o}C/min) and without controlling ice nucleation. We have chosen agarose because of its cytocompatibility, ease of use, and reversibility (by agarase digestion) and extracellular trehalose to cryopreserve a model cell line (MDA-MB-231). Trehalose is a widely used kosmotrope cryoprotectant,[181] which disrupts water-water hydrogen bonding, and therefore inhibits ice formation while increasing the glass transition temperature of the freeze-concentrated liquid.[55, 182] Furthermore, trehalose is biocompatible and nontoxic to cells, and thus approved as an injectable inactive ingredient by the FDA.[54, 55] All of these characteristics, make this method suitable for cryopreservation of cellular therapy products.

Furthermore, using Differential Scanning Calorimetry (DSC) and Fourier Transform Infrared (FTIR) microspectroscopy analyses, we show that the mechanisms of cryoprotection offered by agarose encapsulation in the presence of trehalose are: 1) Decreasing the amount of free water within the sample, 2) increasing the volume of the freeze-vitrified solution, 3) creating smaller ice crystals of uniform size distribution, and 4) inhibition of devitrification, ice recrystallization, and eutectic phase transition damages. Therefore, the model cells encapsulated in the agarose hydrogel with trehalose are well protected from mechanical damage during the freeze/thaw process,[183] as reflected by high cellular viability and proliferation post-thaw.

4.2 Materials and Methods

4.2.1 Cell culture

MDA-MB-231 cells were obtained from ATCC (ATCC, Manassas, VA) at passage number 38. Cells were grown in Dulbecco's Modified Eagle Medium (Gibco, Waltham, MA) supplemented with 10% FBS (Gibco, Waltham, MA), and 1% penicillin/streptomycin (Fischer Scientific, Hampton, NH). Cells were passaged at 80 - 90% confluence. To resuspend the MDA-MB-231 cells, the cells attached to the culture dish were washed with isotonic phosphate-buffered saline solution (1xPBS) and then treated with 0.05% trypsin-EDTA (Gibco, Waltham, MA) at 37°C and 5% CO_2. After 5 minutes of incubation, the cell culture medium was added to stop trypsinization, and the cell suspension was pelleted by centrifugation at 250 x g for 2 minutes.

4.2.2 Hydrogel encapsulation

To prepare agarose hydrogels, 0.25, 0.5, 0.75, 1.5, 2.5, or 4% (w/w) of agarose powder (low-gelling temperature agarose, Sigma-Aldrich, Saint Louis, MO) was added to 1xPBS. To prepare agarose-trehalose hydrogels, 10 or 20% trehalose (w/w) (Sigma-Aldrich, Saint Louis, MO) was also added to the solution. The solution was incubated in a water bath (>65°C) to accelerate dissolution and mixing. After the solution was completely transparent, the agarose solution was transferred to and kept in a 37°C water bath until use. To encapsulate the cells in an agarose-trehalose hydrogel, the cell pellet was first suspended and incubated in a cell culture medium containing 10% trehalose and then in 20% trehalose for

15 minutes. This was done to minimize the hyperosmotic stress experienced by the cells during encapsulation. To encapsulate the cells in an agarose hydrogel, the cell pellet was resuspended in 1xPBS agarose solution containing trehalose at 37°C to achieve a cell concentration of 10^7 cells/ml. The solution was gently and thoroughly mixed in a microtube and then stored at 4°C to induce gelation. After a few minutes, the gels hardened and uniformly encapsulated the cells.

3. Freeze/thaw protocol and post-thaw viability measurements

In control experiments, the cell pellets were suspended in 10% DMSO in 1xPBS (v/v), 10%, and 20% trehalose (w/w) prepared in 1xPBS or directly in 1xPBS solution. Agarose and agarose-trehalose solutions were prepared, and cell encapsulation was conducted following the protocols described above. Note that the sample of 0.25% agarose + 20% trehalose remained liquid but, did not form a gel.

In freeze/thaw experiments conducted in the cryostage, a small amount of the sample (2-4 μL solution or hydrogel containing the encapsulated cells) was sandwiched between two CaF_2 windows and loaded into the cryostage (FDCS 196, Linkam, Tadworth, UK). The sample was then cooled down from 10°C to −150°C at a rate of 2°C/min. Note that since DMSO is toxic to cells at room temperature, the experiment was started at 10°C. Extracellular ice nucleation was not controlled during the cooling process. Ice nucleation generally occurred in the range of −15 to −25°C. Once the temperature reached −150°C, the sample was rapidly

rewarmed to room temperature at a warming rate of 100°C/min. Note that the rapid warming protocol was only applied in the freeze/thaw experiments used for viability measurements as a high warming rate is necessary to maximize viability. For the experiments used to identify kinetic and thermodynamic transitions, both the cooling and the warming rates were fixed at 2°C/min. Post-thaw viability of the encapsulated cells was measured using 20 μg/mL acridine orange (AO)/propidium iodide (PI) fluorescent dye (Nexcelom, Lawrence, USA). The live (green) and dead (red) cells in the sample were counted in five representative areas for each sample using a Nikon Eclipse TE200 inverted fluorescence microscope (Melville, NY, USA). The final percent viability of the cells was calculated with respect to the freshly harvested MDA-MB-231 cells.

4.2.3 Cell extraction/recovery from hydrogel

To extract encapsulated cells from agarose hydrogel, a solution of cell culture media containing 100 U/ml β-Agarase I (New England Biolabs, Ipswich, MA) was added and mixed with an equal volume of the hydrogel. Agarase is a glycoside hydrolase enzyme that can cleave agarose into oligosaccharides.[184] The mixture was homogenized for a few seconds to break down the hydrogel matrix into smaller pieces. After gently and thoroughly mixing the hydrogel with agarase solution, the sample was incubated on a temperature-controlled shaker (~39°C) at 300 rpm for 1 hour. Viability of the cells after extraction was also measured using the AO/PI dye using the method outlined above.

4.2.4 Cell proliferation assay

Frozen/thawed and extracted cells were centrifuged and suspended in cell culture media at a cell concentration of 10^4 cells/ml. Cell suspensions from each experimental group were added to a 96-well plate at a concentration of 3000 cells per well. In parallel, freshly harvested MDA-MB-231 cells were seeded as the positive control group. For background subtraction and instrument gain modification, some wells were left empty or only contained cell culture media. The 96-well plate was incubated at 37°C for up to 3 days. On day 0, 1, 3, or 10 μL WST-8 solution (Abcam) was added to each well that contained the control or experimental groups. After 4 hours of incubation at 37°C at an atmosphere of 5% CO_2 and 95% humidity, absorbance at 460 nm were measured using a microplate reader (INFINITE 200 PRO, Tecan, Zurich, Switzerland). Cells were normalized with control sample, wells containing growth medium. Absorbances recorded for each experimental conditions were also normalized to their respective day 0 absorbances to calculate the proliferation rate.

4.2.5 Differential Scanning Calorimetry (DSC) analysis

A differential scanning calorimeter (Q2000, TA Instruments, New Castle, DE) equipped with a refrigerated cooling accessory was used to analyze the experimental and control samples during freeze/thaw. To prepare DSC samples, 2-10 mg solution or hydrogel was weighed in a Tzero hermetic pan (TA Instruments, New Castle, DE) and sealed with a lid. Each sample was initially cooled from room temperature to −150°C at 2°C/min, then heated back to 10°C at 2°C/min. Dry

nitrogen was used to purge the sample chamber continuously at a flowrate of 50 ml/min. The DSC scans were analyzed using the TA Universal Analysis software (V4.5A, TA Instruments, New Castle, DE)

4.2.6 Fourier Transform Infrared Spectroscopy (FTIR) analysis

Fourier transform infrared spectroscopy was also used to monitor the thermodynamic and kinetic changes of the sample during freeze/thaw. 0.1-1 µL of experimental and control samples spiked with 5% D_2O (99.8% purity, Sigma-Aldrich, St. Louis, MO) were sandwiched between two CaF_2 windows and sealed with vacuum grease to avoid evaporation. The assembly was then transferred to the cryostage attached to an infrared microscope, which was connected to an FTIR spectrometer (Thermo-Nicolet Continuum, Thermo Electron, Waltham, MA) equipped with a mercury cadmium telluride detector (Thermo Electron, Waltham, MA). The sample was first cooled from 10°C to -150°C at a rate of 2°C/min, then warmed back to 10°C at 2°C/min, following the identical freeze/thaw protocol used in the DSC analysis. Infrared (IR) spectra were collected from a sample area of 100 µm × 100 µm every 2°C, and 64 IR scans at a resolution of 4 cm^{-1} were averaged in 9000 to 900 cm^{-1} wavenumber range to obtain each spectrum. The IR spectra were analyzed using the OMNIC software (Thermo-Nicolet, Madison, WI,). Changes in the *v*-(OD) band (2500 cm^{-1}),[185] δ-(OH) band (1650 cm^{-1}),[186] and the glycosidic band (995 cm^{-1})[187, 188] were examined as the sample was cooled and heated. Note that since the v-(OH) band is saturated due to the high-water content

in the samples, 5% D_2O was added to all samples. Therefore, the v-(OD) band could be analyzed to study transitions of water.

4.2.7 Statistical analysis

All of the experiments (and control measurements) were repeated 3 times. Results are presented as mean ± standard deviation. Two-tailed Student's t-test was used to determine the statistical significance. The difference in results was considered to be statistically significant if $p < 0.05$. In plots, * indicates $p < 0.05$, ** indicates $p < 0.01$, and *** indicates $p < 0.001$.

4.3 Results and Discussion

4.3.1 Thermodynamic and kinetic transitions of agarose hydrogel with trehalose during freeze/thaw

We first utilized Differential Scanning Calorimetry (DSC) analyses to detect the effects of agarose encapsulation on the kinetic and thermodynamic transitions of the trehalose solution and determined that while not contributing to the vitrification kinetics of the solution, encapsulation had significant effects on ice kinetics during cooling and warming.

As a control, frozen ultrapure water was warmed at a heating rate of 2°C/min from -150°C to 10°C, and a single endothermic peak was observed in the DSC scan at 0°C (T_m) caused by the release of heat of fusion (data not shown). Note that the area under this endotherm is proportional to the amount of ice formed during cooling, and is therefore used to calculate the enthalpy of heat of fusion, ΔH of

water.[189] When a similar warming experiment was conducted with frozen 1xPBS, a much smaller lower temperature peak corresponding to eutectic melting (T_e ~ -22°C) also became apparent (***Figure 4.1A***). Analysis of the eutectic melting peak (***Figure 4.1A*** inset) revealed a small shoulder starting around -25°C, a very sharp peak around -22°C, and a broad shoulder persisting up to higher temperatures (up to around -17°C). This relatively complex behavior is due to melting of the NaCl•2H_2O-ice phase.[190, 191] The smaller amounts of KCl, Na_2HPO_4, and KH_2PO_4 also contribute to the complexity of this peak, but their contributions are considered negligible when compared to NaCl.

When encapsulated by an agarose gel, a significant change in the transitions of 1xPBS solution became apparent as the eutectic melting peak gradually disappeared with increasing agarose concentration (see ***Figure 4.1B*** and its insert for eutectic melting of 1xPBS encapsulated in a 2.5% agarose gel). Furthermore, ΔH decreased as the concentration of agarose in the sample increased (***Figure 4.1C***), indicating that the amount of ice crystallized during cooling (the "free water" in the sample) decreased with increasing agarose concentration. Addition of 20% w/w (584 mM) trehalose further depressed eutectic melting (***Figure 4.1C***) - consistent with previous findings[191, 192] - and enabled vitrification of the freeze-concentrated solution during freezing. Glass-amorphous liquid transition could be detected by the lower temperature baseline shift in specific heat capacity (C_p) measured during warming (***Figure 4.1C*** inset). The midpoint temperature of this shift is assigned as the glass transition temperature (T_g) of the solution.[193-195] As

the concentration of agarose increased, T_g moved very slightly to lower temperatures (within experimental error) without significant change in ΔC_p (***Table 4.1***). This observation, coupled to the persistence of the ice exotherms in the presence of trehalose showed that agarose encapsulation did not result in uniform vitrification of the trehalose solution, but vitrification was confined to the initially freeze-concentrated solution.

In the DSC scans, the small shoulder observed at higher temperatures (denoted as T_m') is due to the onset of melting of the impure ice crystals that contain solutes trapped within during nonequilibrium freezing,[194, 196] and potentially due to some devitrification (i.e., ice formation in the amorphous liquid above the glass transition temperature). This shoulder disappeared at high agarose concentrations (***Figure 4.1C*** inset), suggesting that less trehalose was trapped within the ice during freezing, resulting in the formation of more homogenous (and pure) ice and freeze-concentrated liquid phases and/or the ice crystal sizes have decreased in size in high agarose content gels. The latter explanation is more logical as the agarose pore size decreases with increasing agarose concentration.

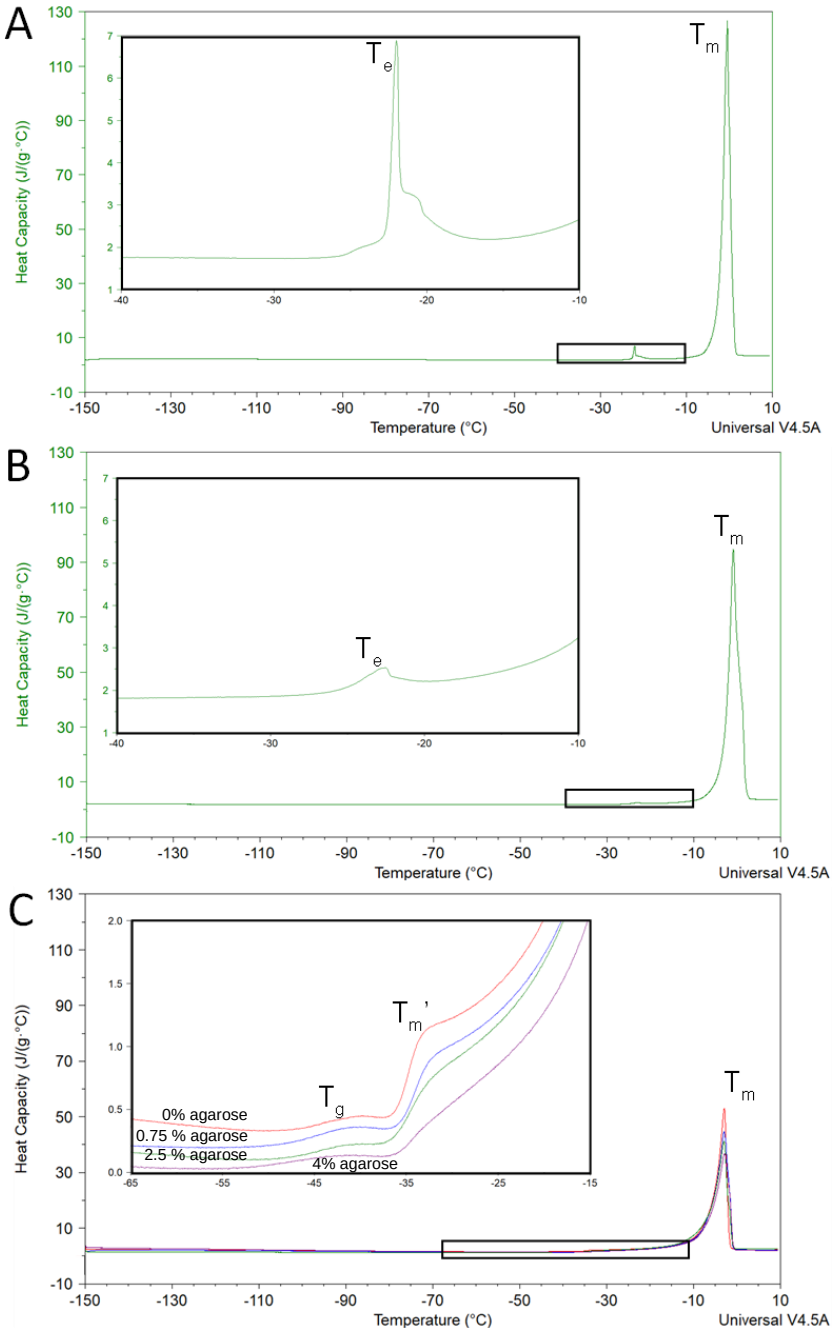

Figure 4.1 DSC warming scans of (A) 1xPBS solution, (B) 2.5% agarose in 1xPBS, and (C) 0, 0.75%, 2.5%, and 4% agarose + 20% trehalose in 1xPBS. (T_e: eutectic melting temperature, T_g: glass transition temperature, T_m': onset of ice melting endotherm, T_m: ice melting temperature.

The ΔH values of samples containing trehalose and agarose were much lower than that of the 1xPBS solution, which could be attributed to either the inhibition of

ice formation by these compounds or a decrease in water content within the sample. To eliminate the influence of lower water content on ΔH with the increase in concentrations of agarose and trehalose, we calculated the water weight percentage in each sample and normalized ΔH by this value, calculating ΔH_N (as presented in ***Table 4.1***). The normalized parameter, ΔH_N, is a more direct indication of the efficacy of agarose and/or trehalose suppressing ice formation. No significant difference in ΔH_N was found between 1xPBS and 4% agarose solutions, suggesting that similar amounts of ice have formed during freezing (i.e., that agarose binding of water was insignificant).

Sample	**T_g (°C)**	**ΔC_p (J/g °C)**	**$T_{m'}$ (°C)**	**T_m (°C)**	**ΔH (J/g)**	**ΔH_N (J/g)**
1x PBS	N/A	N/A	N/A	-0.45 ± 0.13 [a]	291.5 ± 12.8 [a]	291.5 ± 12.8 [a]
2.5% agarose	N/A	N/A	N/A	-0.81 ± 0.17 [b]	284.2 ± 10.7 [a]	291.3 ± 11.0 [a]
4% agarose	N/A	N/A	N/A	-0.62 ± 0.07 [b]	286.7 ± 7.4 [a]	298.1 ± 7.7 [a]
20% trehalose	-44.77 ± 0.53 [a]	0.0983 ± 0.008 [a]	-34.01 ± 0.60 [a]	-2.87 ± 0.07 [c]	178.9 ± 2.9 [b]	223.6 ± 3.6 [b]
0.75% agarose + 20% trehalose	-45.09 ± 0.41 [a]	0.1088 ± 0.013 [a]	-33.74 ± 0.71[a]	-2.80 ± 0.02 [c]	170.3 ± 5.2 [b, c]	212.9 ± 6.6 [b]
2.5% agarose + 20% trehalose	-45.48 ± 0.76 [a, b]	0.1097 ± 0.014 [a]	-33.93 ± 0.65 [a]	-2.89 ± 0.14 [c]	163.4 ± 7.1 [c]	208.4 ± 9.1 [b]
4% agarose + 20% trehalose	-46.89 ± 1.03 [b]	0.0931 ± 0.025 [a]	-34.89 ± 0.98 [a]	-2.64 ± 0.22 [c]	157.7 ± 12.3 [c]	203.5 ± 15.9 [b]

Table 4.1 Glass transition temperature (T_g), change in specific heat capacity during glass transition (ΔC_p), the onset temperature of ice melting (T_m'), ice melting temperature (T_m), the heat of fusion (ΔH), and normalized heat of fusion (ΔH_N) for

1xPBS, trehalose and different agarose hydrogels containing 20% trehalose. Values are shown as mean ± standard deviation from the mean. Values marked with different superscripts (a, b, c) within a column are statistically significantly different ($p < 0.05$).

On the other hand, ΔH_N of 20% trehalose was significantly lower than that of 1xPBS, indicating that trehalose greatly inhibited ice formation during freezing (i.e., the vitrified water content of the sample was higher). In addition, ΔH_N slightly decreased with increasing agarose concentration from 0 to 4% in trehalose solution but this was not quite statistically significant ($p < 0.1$). Although ΔH decreased with increasing agarose concentration, the insensitivity of ΔH_N to increasing agarose concentration (tested up to 4%) shows that the agarose gel did not facilitate trehalose vitrification. This observation is in opposition to the previous reports advocating that encapsulation enables vitrification.[177, 197] However, those studies were based on indirect observations made by transmitted light cryomicroscopy experiments, and therefore are subjective. Note that agarose gels in the 1-4% w/v range form pores in the range of 40 to 300 nm [198, 199], which is not sufficient to promote confinement-induced vitrification.

To complement our observations made by the DSC analyses, further experiments were conducted using Fourier Transform Infrared Spectroscopy (FTIR). These experiments provided in-depth molecular level detail on the behaviors of the individual components of the solutions tested in response to temperature changes and further verified our conclusions.

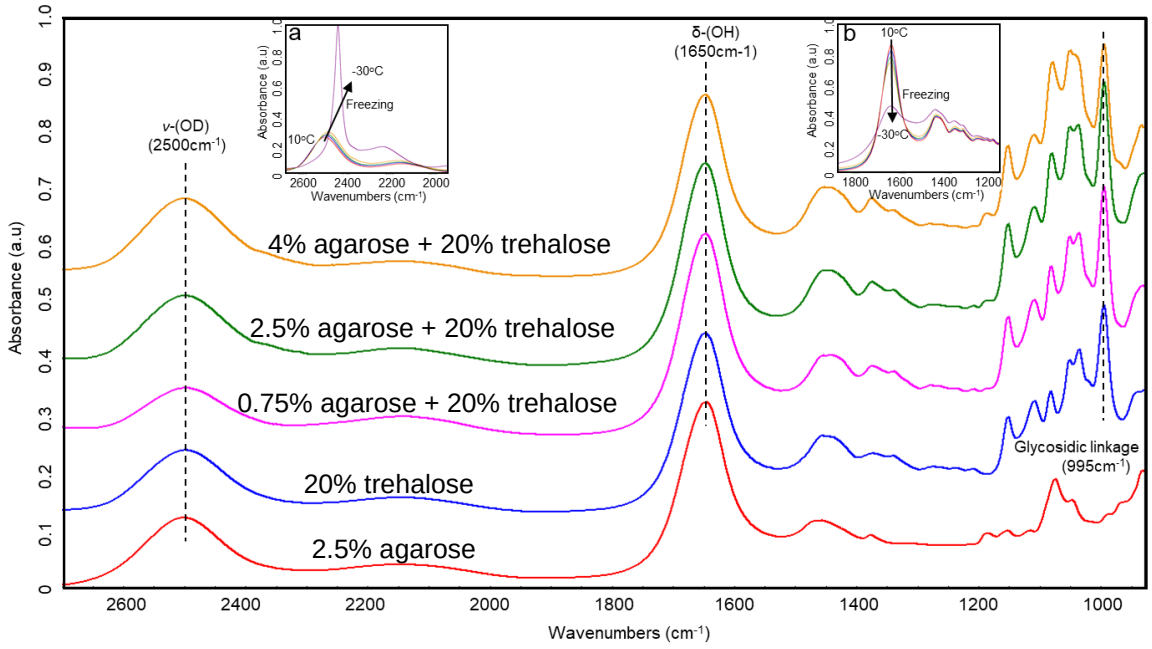

Figure 4.2 Representative IR spectra of 2.5% agarose, 20% trehalose, 0.75% agarose with 20% trehalose, 2.5% agarose with 20% trehalose, and 4% agarose with 20% trehalose at 10°C. All samples included 5% D_2O.

Representative IR spectra collected from 2.5% agarose, 0, 0.75, 2.5, 4% agarose + 20% trehalose solutions and gels at 10°C are shown in ***Figure 4.2***. Since the *ν*-(OH) band (3500 cm^{-1}) [200, 201] was saturated because of the high water content of the samples, 5% D_2O was added to each solution, and the *ν*-(OD) (2500 cm^{-1}) band [185] was used to study the phase change behavior of water during the freeze/thaw event. During cooling, *ν*-(OD) gradually shifts to lower wavenumbers (***Figure 4.2***), indicating that more hydrogen bonds (HBs) form between water molecules.[201, 202] Upon freezing, an abrupt drop in wavenumber and a significant increase in peak intensity (inset "a" in ***Figure 4.2***) were observed due to the formation of fully tetrahedrally hydrogen-bonded water molecules (ice). On the

other hand, the *v*-(OD) band shifted to higher wavenumbers during the warming process, and a sudden spike was seen when the sample melted.

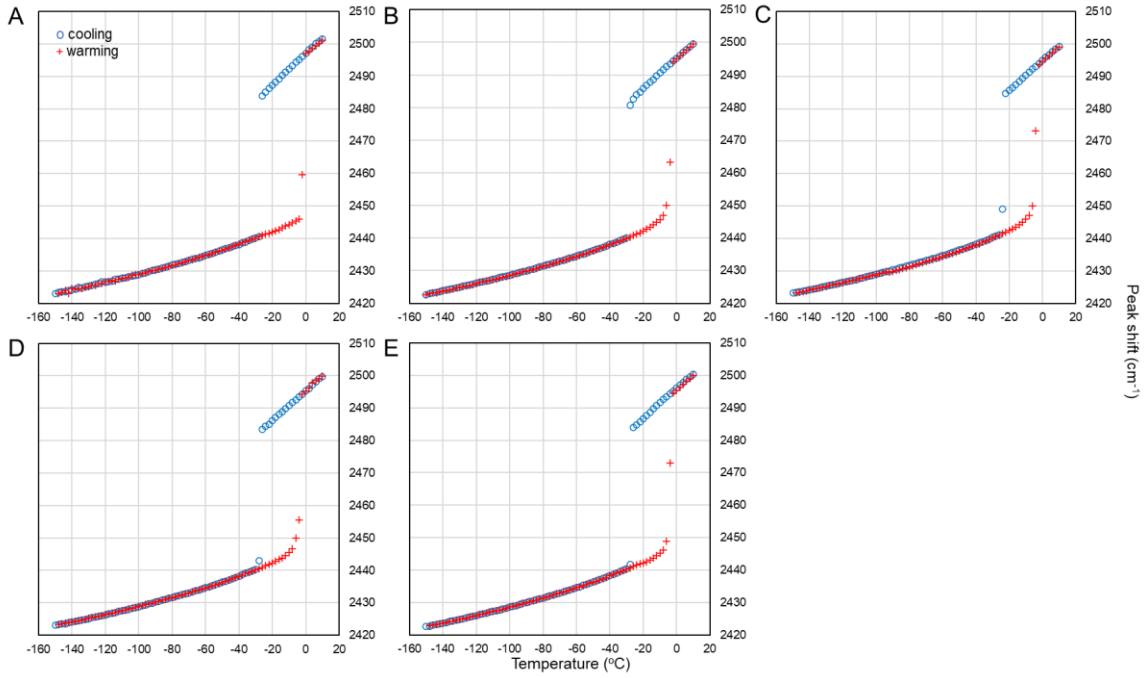

Figure 4.3 Peak shift of the *v*-(OD) band (~2500 cm^{-1}) during cooling and warming processes of; (A) 2.5% agarose (B) 20% trehalose, (C) 0.75% agarose + 20% trehalose (D) 2.5% agarose + 20% trehalose, and (E) 4% agarose + 20% trehalose solutions. Samples were cooled from 10°C to -150°C and then warmed back to 10°C at 2°C /min.

To further investigate the water structure change with temperature in the agarose hydrogel containing trehalose, δ-(OH) band (1650 cm^{-1}) was also analyzed. Different from the water stretching band (which is strongly affected by the hydrogen bonding between water and carbohydrates),[186, 203, 204] δ-(OH) band mainly originates from the water population that is not fully hydrogen bonded.[186, 205] Therefore, this peak is hardly affected by HB between water and trehalose.[186] Due to more tetrahedral HBs forming during the cooling process, peak intensity of δ-

(OH) reduced with decreasing temperature, and a sudden drop was observed upon freezing (inset "b" in ***Figure 4.2***). When the samples reached -150°C (***Figure 4.4A***), 2.5% agarose hydrogel showed a very weak δ-(OH) band, suggesting that the amount of unfrozen (i.e., vitrified) water in the sample was small, and almost all the water molecules were tetrahedrally hydrogen-bonded. On the other hand, the 20% trehalose solution showed a stronger δ-(OH) band, indicating that the amount of vitrified water in the sample was higher than that in the 2.5% agarose hydrogel. This is expected as trehalose is a strong glass-former.[55, 141, 186] In addition, the peak intensity of the δ-(OH) band was further increased when the concentration of agarose in the 20% trehalose solution was increased, indicating that the vitrified volume in the combination system was even higher than trehalose or agarose alone. This supported the DSC measurements and trends shown in ***Table 4.1***. A similar trend was observed in δ-(OH) peak location during the cooling process (***Figure 4.4B***). Upon cooling of the 2.5% agarose hydrogel, an abrupt decrease in δ-(OH) peak location was observed upon freezing. The peak location continued to shift to lower wavenumbers with decreasing temperature. The redshift of the δ-(OH) band with decreasing temperature after freezing indicated that the structure of ice got more ordered (transitioning from noncrystalline to polycrystalline),[206] due to an increase in HB networking among the water molecules. On the other hand, in the presence of trehalose δ-(OH) peak location showed a smaller drop upon freezing, and the temperature-induced redshift of δ-(OH) was greatly inhibited after freezing. This indicated that water molecules in the combination system (agarose + trehalose) undergo very little structural change,

especially in the 4% agarose + 20% trehalose gel, during ice nucleation and subsequent cooling. These results are consistent with our findings in DSC analysis that the amount of ice formed in the combination system is less than that in trehalose or agarose alone, indicating that more water was vitrified in the combination system during cooling.

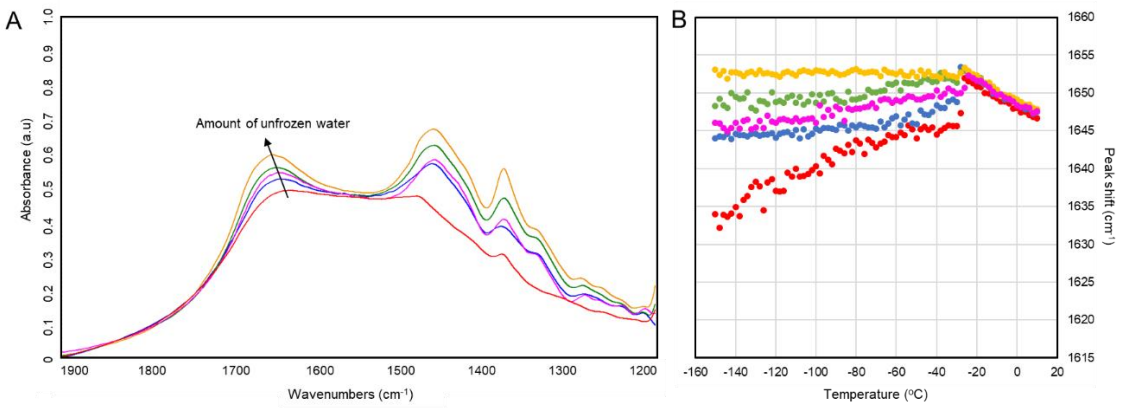

Figure 4.4 (A) IR spectra (from bottom to top) of 2.5% agarose, 20% trehalose, 0.75% agarose + 20% trehalose, 2.5% agarose + 20% trehalose, and 4% agarose + 20% trehalose at -150°C. (B) Peak shift of *δ*-(OH) band of these four samples during the cooling process. Samples were cooled at 2°C /min from 10 °C to -150 °C. All samples included 5% D_2O.

To investigate the water-trehalose and trehalose-trehalose HB interactions during the freeze/thaw event, the temperature-induced shift of the trehalose glycosidic linkage (connecting the two glucose pyranose rings in trehalose)[188] peak located at 995 cm^{-1} was analyzed (***Figure 4.5***). Both peaks at 1150 cm^{-1} and 995 cm^{-1} originate from the *v*-(CO) vibration of the glycosidic linkage[187, 188] however, only the 995 cm^{-1} peak was studied since the interference from agarose at this frequency is negligible. Peak shift magnitude of the glycosidic linkage is a measure of the flexibility of the carbohydrate:[186, 207, 208] At higher concentrations, more

inter/intramolecular carbohydrate-carbohydrate HBs form, which causes the folding of the carbohydrate around its glycosidic linkage.[186] As a result, flexibility of the carbohydrate molecule decreases and the glycosidic band shifts to lower wavenumbers.

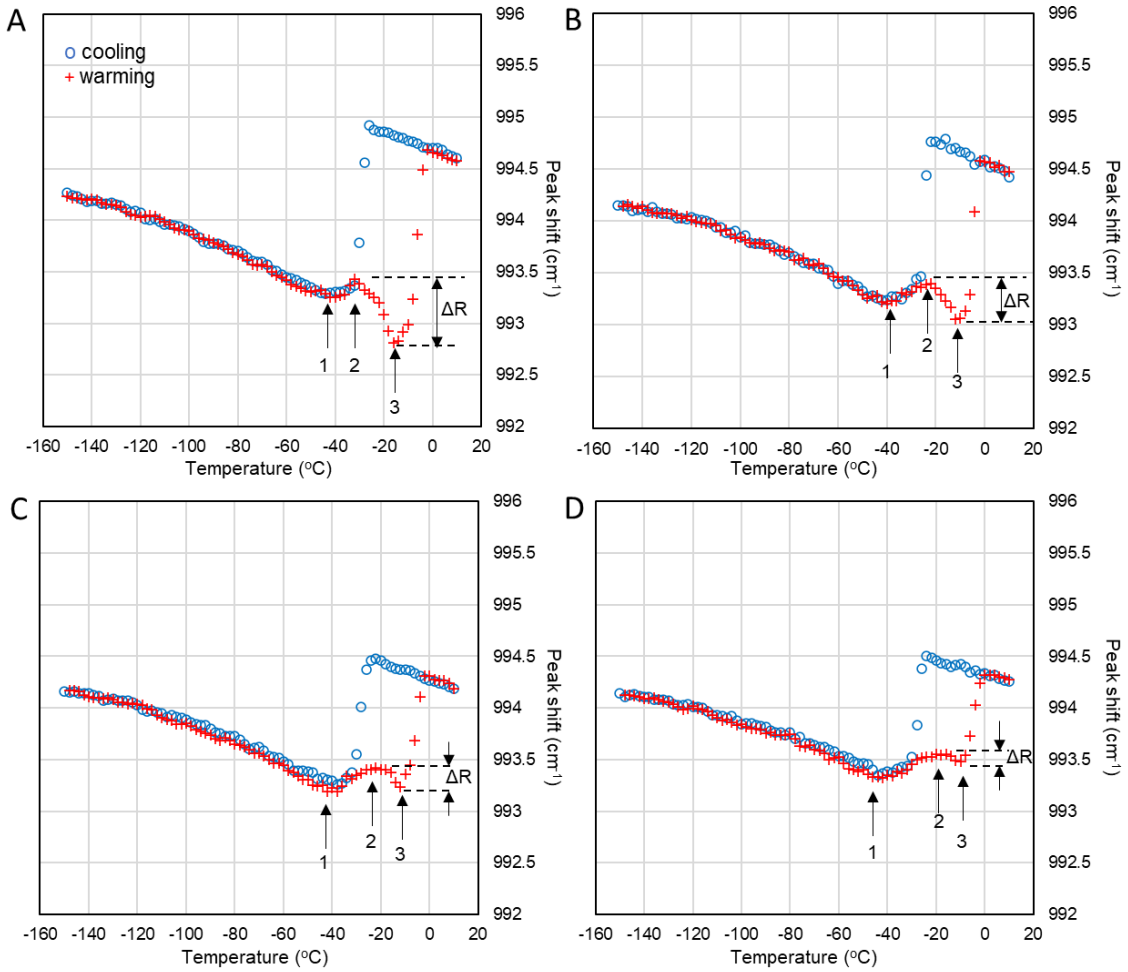

Figure 4.5 Peak shift of the glycosidic band (~995 cm^{-1}) during cooling and warming processes of; (A) 20% trehalose, (B) 0.75% agarose + 20% trehalose (C) 2.5% agarose + 20% trehalose, (D) 4% agarose + 20% trehalose solutions. Samples were cooled from 10 °C to -150 °C and then warmed back to 10 °C at 2 °C /min.

During cooling, the glycosidic band (995 cm^{-1}) gradually shifted to higher wavenumbers, experiencing an abrupt drop around -30°C, which corresponded to

the freezing of the sample. The blueshift of glycosidic linkage peak location with decreasing temperature is due to the increase in hydration level for trehalose.[186, 207] More water-trehalose HBs form at lower temperatures, decreasing the amount of trehalose-trehalose intermolecular HBs (note that trehalose does not form intramolecular HBs),[187, 209] also increasing the flexibility of trehalose around the glycosidic linkage.[186] On the other hand, the abrupt redshift during freezing was because of the formation of the freeze-concentrated liquid (FCL). Compared to the supercooled liquid, FCL has a much higher trehalose concentration (therefore, more trehalose-trehalose HBs are formed) than the supercooled liquid. Therefore, the flexibility of trehalose decreases significantly when ice forms.

During the warming process, three transitions were observed in the IR spectra. The first transition (at the lowest temperature) is located around -45°C (which very gradually decreases with increasing concentration of agarose), corresponding to the glass melting temperature of the FCL in the sample. This is in perfect agreement with the DSC data listed in ***Table 4.1***. During glass melting, previously vitrified FCL transitions into a supercooled liquid, which increases the mobility of the trehalose molecules. As a result, the glycosidic band shifts to higher wavenumbers. Similarly, a significant increase in peak position was observed after the third transition, corresponding to the melting of the bulk ice. Upon melting, HBs are formed extensively between liquid water and trehalose, which increases the hydration level and flexibility of trehalose.

On the other hand, the mechanism of the second transition is more difficult to interpret than either transition 1 or 3 (***Figure 4.5)***. During the second transition, the glycosidic band shifts to lower wavenumbers with increasing temperature. Since the peak shifts very fast (especially for 20% trehalose) during this transition, the redshift cannot simply be explained by a reduction in the hydration level of trehalose with increasing temperature. To further investigate the mechanism of transition 2, two additional experiments were performed:

(1) 20% trehalose solution was frozen and thawed following the protocol described in the Materials and Methods section. When the sample reached -20°C (a temperature between transition 2 and transition 3), it was held isothermal for 1 hour and then warmed back to 10°C.

(2) 20% trehalose solution was frozen and thawed following the same protocol as above. When the sample was warmed to -20°C, it was re-cooled down to -50°C (below the temperature of transition 1, i.e., T_g). This cooling/warming cycle (between -20°C and -50°C) was repeated twice before the sample was warmed back to 10°C.

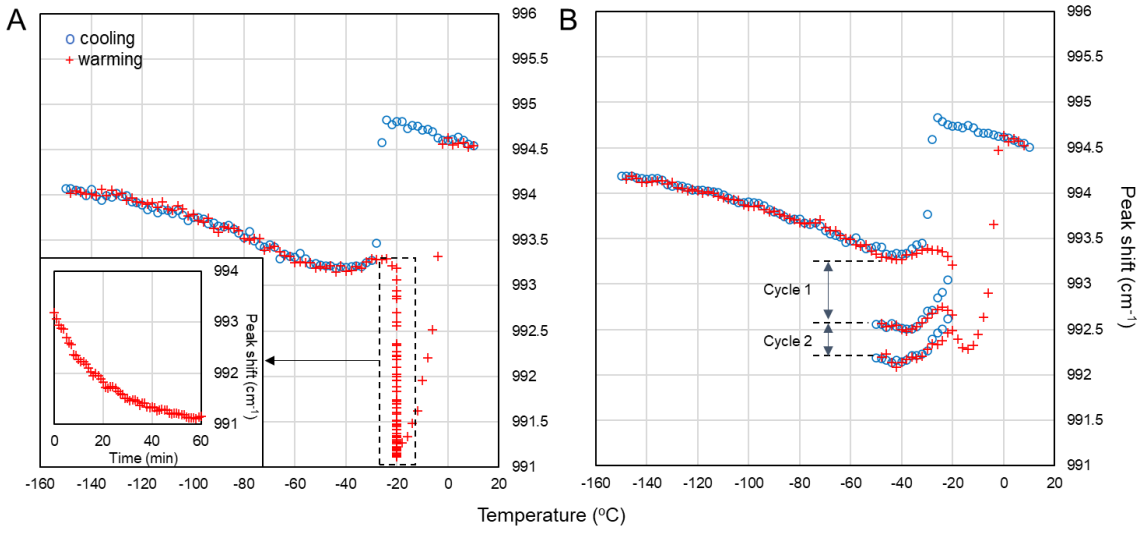

Figure 4.6 Peak shift of the glycosidic band (995cm^{-1}) of 20% trehalose solution during the cooling and warming processes. (A) A one-hour isothermal wait step was applied at -20°C during the warming process (inset). (B) Two cooling/warming cycles (between -50°C and -20°C) were applied during the warming process.

The 20% trehalose solution was chosen for these experiments since the peak shift of the glycosidic linkage during transition 2 was much more significant than the samples containing agarose. The plots of wavenumbers versus temperature/time are shown in ***Figure 4.6***. In the first experiment, the shift in the glycosidic band continued to evolve towards lower wavenumbers when the sample was kept isothermal at -20°C (***Figure 4.6A***). The shift rate gradually decreased with time. In the second experiment, the wavenumbers of the glycosidic band decreased with increasing temperature when the sample was warmed from transition 2 to -20°C. Interestingly, when the cooling step (from -20°C to -50°C) was applied, this peak didn't shift back to higher wavenumbers. Instead, its wavenumbers further dropped until the temperature of the sample reached transition 1 (T_g). As a result, a significant drop in wavenumbers was observed between successive cycles in the range of -50°C to -20°C (***Figure 4.6B***). These findings suggest that transition 2 is a nonequilibrium process that takes place in the temperature range between T_g and T_m. According to previous studies, both ice recrystallization,[70, 208] and trehalose crystallization[208, 210, 211] may occur in this temperature range (both processes decrease the flexibility of trehalose significantly). However, trehalose crystallization in a frozen solution is a rather slow process, which may take tens of hours (with seeding) to a couple of days (without seeding) during annealing.[210, 211] Since the hold time we applied (1 hour) was much shorter, we attributed transition

2 to ice recrystallization, where the rapid growth of ice crystals in the FCL decreased the hydration level and the flexibility of trehalose. To determine the magnitude of ice recrystallization (ΔR), the peak shift between the second transition (onset of ice recrystallization) and the third transition (melting of bulk ice) for each sample was measured. By increasing the concentration of agarose in the sample, ΔR decreased from 0.7 cm^{-1} (20% trehalose) to 0.1 cm^{-1} (4% agarose + 20% trehalose). The significant decrease of ΔR indicates that the ice recrystallization was greatly inhibited by agarose in the combination system.

4.3.2 Post-thaw viability and proliferation of MDA-MB-231 cells frozen/thawed in the agarose hydrogel with extracellular trehalose

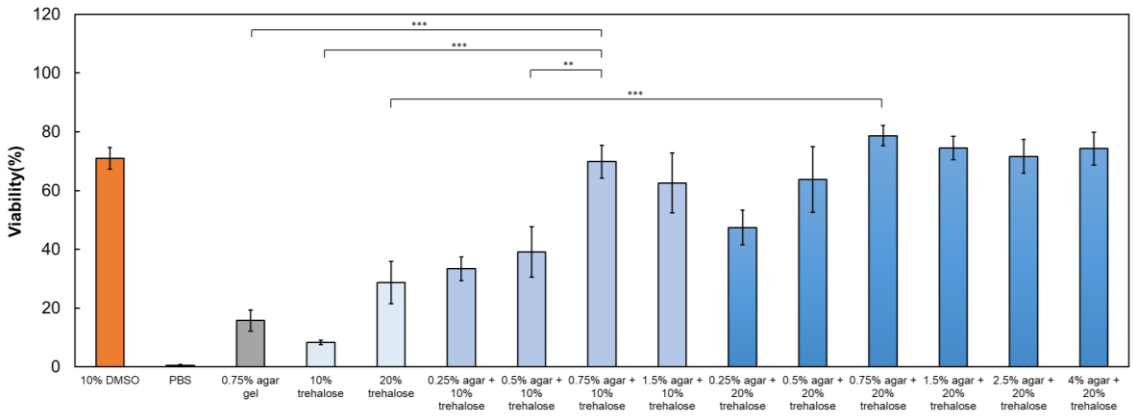

Figure 4.7 Post-thaw viability of MDA-MB-231 cells cooled at 2°C/min to -150°C, and warmed at 100°C/min to 10°C (* indicates p<0.05, ** indicates p<0.01, and *** indicates p < 0.001)

Post-thaw viability of MDA-MB-231 cells measured by AO/PI staining is shown in ***Figure 4.7***. Poor survival was observed when the encapsulated cells (in 0.75% agarose) were frozen and thawed in the absence of any trehalose. Also, when the

unencapsulated cells were frozen in 1xPBS solution containing extracellular trehalose, post-thaw viability was lower than 40%. It is known that trehalose needs to be present intracellularly to offer any cryoprotection. Therefore, it was not surprising that extracellular trehalose or agarose alone does not protect cells effectively at cryogenic temperatures. The viability of the cells increased significantly (to 69.8 ± 5.6%) when they were encapsulated and frozen/thawed after encapsulation in 0.75% agarose hydrogel in the presence of 10% trehalose. The viability could be further improved (to 78.7 ± 3.4%) when the concentration of trehalose was increased from 10% to 20% but further increase in agarose concentration (up to 4%) did not increase viability further. The post-thaw survival of cells encapsulated in 0.75% agarose hydrogel with trehalose was comparable to the positive control group, where cells were frozen in 10% DMSO (70.9 ± 3.6%).

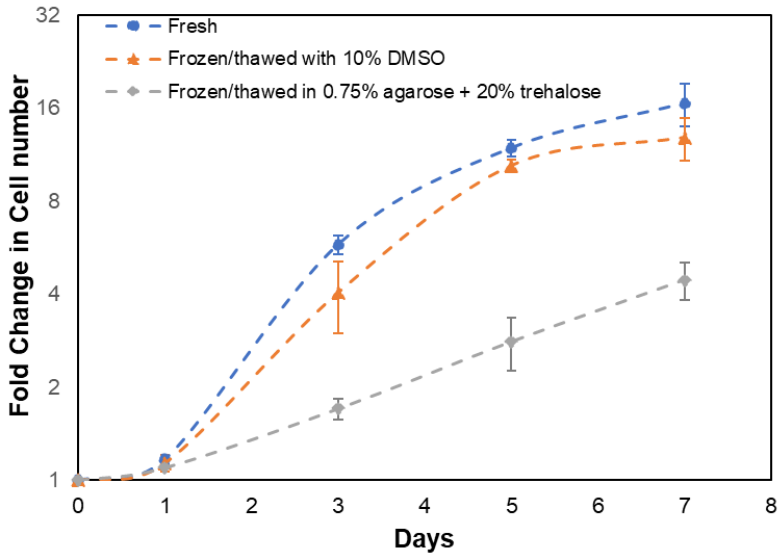

Figure 4.8 MDA-MB-231 proliferation post-thaw. Cell proliferation was measured using WST-8 assay at days 0, 1, 3, 5, and 7. The experimental condition includes fresh (not frozen) cells, cells frozen/thawed in 10% DMSO, and encapsulated cells extracted post-freeze/thaw.

Lastly, cell proliferation post-thaw was measured for fresh and cryopreserved cells using WST-8/CCK-8 assay (***Figure 4.8***). Absorbance values recorded with the growth medium were subtracted from the experimental conditions containing cells. A standard curve was used to calculate the number of cells in each sample for each day of experiment. The proliferation rate was calculated by taking the ratio of the number of cells each day to the respective day 0 cell number. Fresh and cells frozen using 10% DMSO proliferated at similar rates. Proliferation rates for encapsulated and extracted cells were lower (almost by half as measured on day 7). One possible explanation for this is the incomplete extraction of cells from agarose gels. Also, we have observed that there are still small residues of agarose left in the samples post-extraction (***Figure 4.9***). While these residues may not affect the immediate viability of the cells, they could prevent the cells from attaching to the plate surface. This shows that the extraction process we apply needs to be further optimized.

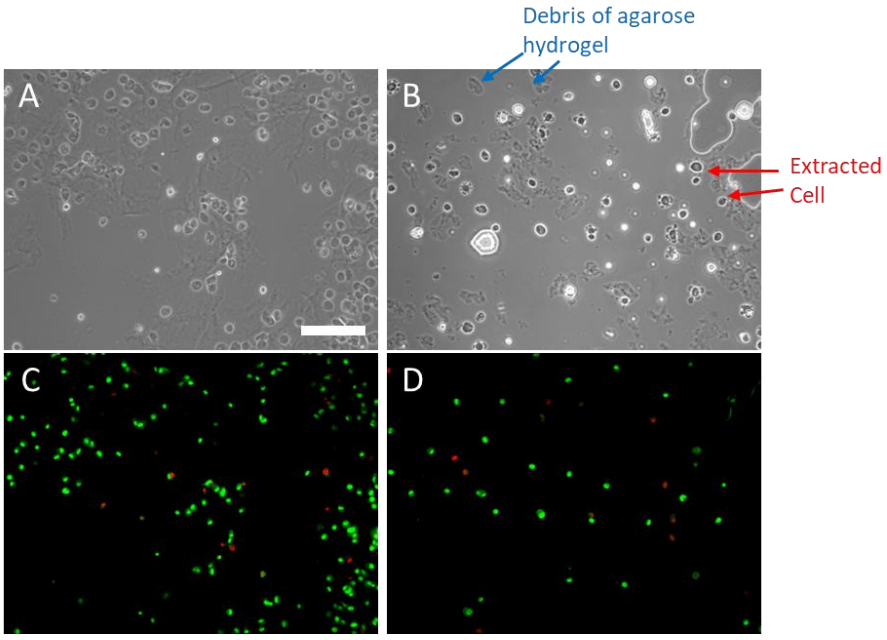

Figure 4.9 Bright-field images of encapsulated MDA-MB-231 cells before (A) and after isolation(B) from 0.75% agarose gel. Live/dead fluorescence images of MDA-MB-231 before (C) and after extraction (D). (scale bar: 200μm)

4.4 Conclusion

In this chapter, we present an encapsulation-based cryopreservation method that eliminates the need for DMSO. This is achieved by encapsulating the cells in a cytocompatible agarose hydrogel in the presence of extracellular trehalose, a membrane-impermeable cryoprotective agent. The study demonstrates that the method offers effective cryoprotection through the following mechanisms: First, as proven by the DSC and FTIR analyses, hydrogel encapsulation decreased the amount of free water in the solution, resulting in a smaller ice phase volume (***Figure 4.1, Table 4.1,*** and ***Figure 4.4A***) with a less ordered water structure (***Figure 4.4B)***, resulting in a higher vitrified volume. Second, devitrification and ice recrystallization during warming were inhibited (***Figure 4.5***), potentially due to the hydrogel network mechanically inhibiting the formation, progression, and fusion of ice crystals. And finally, damaging eutectic crystallization/melting transitions were inhibited (***Figure 4.1***). Therefore, cells encapsulated in the agarose hydrogel in the presence of trehalose are well protected against detrimental mechanical damage observed during freeze/thaw [183] as reflected by a very high viability post-thaw (***Figure 4.7***). The lower proliferation rate observed in the first few days post-thaw/extraction (***Figure 4.8, Figure 4.9***) on the other hand suggests the need for further optimization of the extraction process post-thaw.

Chapter 5: Optimization and Validation of Hydrogel Encapsulation for Cryopreservation of NK Cells

5.1 Introduction

Manufactured NK and T cells are mainly used in cancer immunotherapy.[212] In the past decade, industrial and academic labs have focused on the engineering and expansion of these native immune cells to develop enhanced effector cells, including chimeric antigen receptor T cells (CAR-T cells), which exhibit heightened targeting capabilities and specificity against cancer cells.[1, 213, 214] These innovative approaches have yielded remarkable clinical responses to previously untreatable malignancies. Significant progress has been made in the treatment of lymphomas and leukemias with multiple FDA-approved products using patient-derived CAR-T cells in the market, but success with allogeneic “off-the-shelf" products from healthy donors has been elusive so far.

To enable the utilization of allogeneic cell therapy products, one of the key factors is to effectively and safely cryopreserve large quantities of manufactured cells. Moreover, it is important to establish a reliable and repeatable cryopreservation methodology that allows for the availability of these cells to clinicians for transfusion with minimal pre-infusion preparation and processing requirements. Currently, therapeutic cell cryopreservation is conducted using commercially available freezing media, the majority of which are DMSO-based.[73] Examples of such commercially available freezing media include BloodStor by Stem Cell Technologies and CryoStor by BioLife Solutions. Alternatively, cryopreservation

solutions can also be prepared in-house using formulations that include DMSO as a key component.

DMSO is a cell membrane-permeable molecule with a strong affinity for water. Due to its great ability to inhibit both intracellular and extracellular ice formation, DMSO has been widely used for the preservation of a variety of cell lines used in research laboratories.[17, 48] Currently, the commonly used freezing medium for NK cells contains 10% DMSO. While some studies indicated that using the freezing medium with DMSO does not result in a significant decrease in the immediate viability after thawing, it has been observed that these cells exhibit a relatively lower level of cytotoxicity.[110, 111] Furthermore, in vivo persistence of frozen-thawed NK cells is also reported to be orders of magnitude lower than fresh cells.[215] The main reason for cytotoxicity loss is ascribed to the loss of motility,[110] and significant changes in NK cell phenotype, specifically a decrease in the cytotoxic CD16+ populations.[110, 216, 217] Transcriptomic, phenotypical changes, and heterogeneity loss due to DMSO-based cryopreservation are not unique to NK cells but have been reported widely for most cells in major single-cell transcriptomic studies.[218-221]

To resolve the issues associated with cell number and cytotoxicity loss, therapeutic cells need to be expanded for 3-7 days post-thaw to increase cell numbers and activated through interleukin stimulation for a minimum of 12-16 hours to recover cytotoxic capability.[222, 223] However, the extra processing required in the clinic, including additional quality control and lot testing requirements, will increase costs,

delay the treatment, and also increase the risk of contamination during the expansion of the cells. Furthermore, most of the cell therapy clinics or hospitals would not even have facilities for post-thaw cell re-culture. Therefore, these extra processing steps after thawing are impractical for cell therapy products. Another problem with the use of DMSO in cryopreservation formulations is the side effect on patients. Incomplete removal of DMSO from cryopreserved therapeutic cells before infusion can lead to adverse side effects in patients, including nausea, chills, hypotension, heart arrhythmias, and stroke [24-26] (Detailed information on the toxicity of DMSO can be found in Section 2.5.1). Therefore, the elimination of DMSO from therapeutic cell products holds significant importance, driving the advancement of alternative approaches, including the combination of different types of biocompatible cell membrane-impermeable CPAs[224, 225] and hydrogel encapsulation [27, 35].

Hydrogel encapsulation has shown promise in the cryopreservation of therapeutic cells, including human mesenchymal stem cells[27] and embryonic stem cells[35], to minimize the use of toxic cryoprotectants such as DMSO. A detailed summary can be found in ***Table 2.1***. Different hypotheses have been proposed to explain the efficacy of hydrogels in cryopreservation, including their ability to inhibit ice crystal growth within their three-dimensional network,[29, 35] minimize osmotic shock,[35] and facilitate vitrification[29, 177, 226] of cryoprotectant solutions at lower cooling rates or cryoprotectant concentrations. However, our findings from Chapter 4 indicate that encapsulation in agarose gels (up to 4% concentration) does not significantly

promote vitrification or increase the glass transition temperature (***Table 4.1***) of trehalose solutions up to 20% concentration. Despite agarose encapsulation not facilitating vitrification, the structure and dynamics of confined water or cryoprotectant molecules in the micropores of the hydrogel matrix may still undergo significant changes due to their strong association with the hydrophilic surface of the hydrogel pores[227, 228] This phenomenon has been previously observed in silica gels[142] and polysaccharide hydrogels (such as alginate)[31, 197]. Based on the findings in Chapter 4, it was found that hydrogel encapsulation affects the kinetics of ice crystallization during the cooling process, resulting in the formation of smaller and more uniformly distributed ice crystals confined within the hydrogel matrix. In addition, it also reduces salt-water eutectic crystallization during cooling, and therefore, melting during warming. Moreover, potentially due to the association and hydrogel network acting as a mechanical impediment, ice recrystallization has been greatly inhibited during the warming process. Collectively, these findings comprehensively elucidate the physicochemical properties offered by hydrogel materials to protect cells during cryopreservation in the absence of DMSO.

In Chapter 4, MDA-MB-231 cells were selected as the model system to optimize the cryopreservation formulation and methodology using agarose hydrogel encapsulation. The results demonstrated the successful cryopreservation of cells with minimal viability loss, even in the absence of DMSO (***Figure 4.7***). Furthermore, the cells recovered from the agarose hydrogel after freeze/thaw exhibited

reasonable proliferation in 2D culture (***Figure 4.8***). However, the presence of residual agarose hydrogel debris and the observed relatively low post-thaw proliferation rate highlighted the need for a comprehensive evaluation and optimization of the cell extraction process. This is particularly important when considering the fragility and high sensitivity of NK cells, which possess unique functional characteristics and are susceptible to environmental stresses.[73] Therefore, the primary focus of the research conducted in Chapter 5 is to validate the effectiveness of agarose-trehalose hydrogel cryopreservation methods for NK-92 cells, while optimizing the cell extraction process from agarose hydrogel. This optimization involves adjusting the concentration of agarase enzyme and digestion time.

Moreover, we explored the feasibility of using alginate as an alternative hydrogel material for reversible encapsulation and cryopreservation of NK cells. As a biocompatible material, alginate has been extensively employed in cell encapsulation studies and has also demonstrated promise in cryopreservation applications.[31, 36, 176, 177] In addition to providing cryoprotective benefits, another advantage of alginate is that it's easily dissolvable in EDTA or sodium citrate solutions, which facilitates the digestion of hydrogel and the release of encapsulated cells after freeze/thaw. Through this comparative analysis between agarose and alginate, we aim to evaluate the cryopreservation outcomes (post-thaw viability before and after cell extraction), cell extraction efficiency, and recovery rate associated with both hydrogel materials, providing a comprehensive

understanding of their respective advantages and limitations used for the cryopreservation of NK cells.

5.2 Materials and Methods

5.2.1 Cell culture

NK-92 cells at passage number 1 were acquired from the American Type Culture Collection (ATCC, Manassas, VA). The cells were cultured in Minimum Essential Medium (MEM-α, Gibco, Waltham, MA) supplemented with 0.2 mM inositol, 0.1 mM 2-mercaptoethanol, 0.02 mM folic acid, 100 U/ml IL-2, 12.5% horse serum (Gibco, Waltham, MA), and 12.5% fetal bovine serum (Gibco, Waltham, MA). The cells were maintained in the incubator at 37°C with 5% CO_2, and the cell culture medium was refreshed every two or three days. NK-92 cell pellet was obtained by centrifuging the cell suspension at 160 x g for 5 minutes.

MDA-MB-231 cells were obtained from ATCC (ATCC, Manassas, VA) at passage number 38. Cells were grown in Dulbecco's Modified Eagle Medium (Gibco, Waltham, MA) supplemented with 10% FBS (Gibco, Waltham, MA), and 1% penicillin/streptomycin (Fischer Scientific, Hampton, NH). Cells were passaged at 80 - 90% confluence. To resuspend the MDA-MB-231 cells, the cells attached to the culture dish were washed with isotonic phosphate-buffered saline solution (1xPBS) and then treated with 0.05% trypsin-EDTA (Gibco, Waltham, MA) at 37°C and 5% CO_2. After 5 minutes of incubation, the cell culture medium was added to

stop trypsinization, and the cell suspension was pelleted by centrifugation at 250 x g for 2 minutes.

5.2.2 Agarose hydrogel encapsulation and extraction

To prepare agarose hydrogels, 0.75% (w/w) of agarose powder (low-gelling temperature agarose, Sigma-Aldrich, Saint Louis, MO) and 20% trehalose (Sigma-Aldrich, Saint Louis, MO) were added to 1xPBS. The solution was incubated in a water bath (>65°C) to accelerate dissolution and mixing. After the solution turned completely transparent, the agarose solution was transferred to and kept in a 37°C water bath until use. To encapsulate the cells in an agarose-trehalose hydrogel, the cell pellet was first suspended and incubated in a cell culture medium containing 10% trehalose and then in 20% trehalose for 15 minutes. This was done to minimize the hyperosmotic stress experienced by the cells during encapsulation. To encapsulate the cells in an agarose hydrogel, the cell pellet was resuspended in 1xPBS agarose solution containing trehalose at 37°C to achieve a cell concentration of 10^7 cells/ml. The solution was gently and thoroughly mixed in a microtube and then stored at 4°C to induce gelation. After a few minutes, the gels hardened and uniformly encapsulated the cells.

To extract encapsulated cells from agarose hydrogel, a solution of cell culture media containing 100 U/ml β-Agarase I (New England Biolabs, Ipswich, MA) was added and mixed with an equal volume of the hydrogel. Agarase is a glycoside hydrolase enzyme that can cleave agarose into oligosaccharides.[184] The mixture

was homogenized for a few seconds to break down the hydrogel matrix into smaller pieces. After gently and thoroughly mixing the hydrogel with agarase solution, the sample was incubated on a temperature-controlled shaker (~39°C) at 300 rpm for 1 hour.

To determine the cell viability and cell extraction rate, a droplet of the solution (~2µL) was mixed with the same volume of AO/PI dye, and sandwiched between two microscope slides. In five representative areas, the number of live cells (green in fluorescence image), the number of dead cells (red in fluorescence image), and the number of extracted cells (bright-field image) were counted under the fluorescence microscope. Cell viability was calculated by dividing the total number of live cells by the total number of cells (including both live and dead cells) in these five representative areas. The cell extraction rate was determined by dividing the total number of extracted cells by the total number of cells (including both live and dead cells) in these five representative areas.

To determine the cell recovery rate, the total number of cells before encapsulation and the total number of cells following cell extraction were counted under the microscope using a hemocytometer. The cell recovery rate is calculated by dividing the total number of cells collected following cell extraction by the total number of cells before encapsulation.

5.2.3 Alginate hydrogel encapsulation and extraction

To prepare alginate hydrogel beads, different concentrations (0.5%, 1%, 1.5%, and 2% w/w) of sodium alginate powder (Sigma-Aldrich, Saint Louis, MO) and 20% trehalose (Sigma-Aldrich, Saint Louis, MO) were added to deionized water (dH_2O). The resulting solution was incubated and stirred at 37°C overnight for complete dissolution. Once the solution achieved complete transparency, the alginate solution was stored at 4°C until further use.

To encapsulate cells within the alginate-trehalose hydrogel, the NK-92 cell pellet was initially suspended and incubated in a cell culture medium containing 10% trehalose, followed by incubation in a 20% trehalose solution for 15 minutes. This step aimed to pre-dehydrate the cells and minimize the hyperosmotic stress encountered during the encapsulation process. Subsequently, the cell pellet was resuspended in an alginate solution containing 20% trehalose to achieve a cell concentration of 10^7 cells/ml. To form the alginate hydrogel beads incorporating NK cells, 10 µL aliquot of this cell suspension was dropped into the 100 mM $CaCl_2$ solution with 20% trehalose, and incubated at least for 3 minutes. to facilitate the crosslinking of the alginate and the formation of the hydrogel beads.

To release the NK-92 cells from the alginate beads, the beads were incubated in a 100 mM EDTA solution at a volume ratio of 1:2 (alginate beads: EDTA solution) and maintained at 37°C for 20 minutes. Once the alginate hydrogel was completely dissolved, the solution was centrifuged and the cell pellet was resuspended in the cell culture medium for further analysis and experimentation.

5.2.4 Freeze/thaw protocol and post-thaw viability measurements

In control experiments, the cell pellets were suspended in the freezing medium containing 10% DMSO, 40% FBS, and 50% cell culture medium. In parallel, cell encapsulation was conducted following the protocols described above. In freeze/thaw experiments conducted in the cryostage, a small amount of the sample (2-4 µL solution or hydrogel containing the encapsulated cells) was sandwiched between two CaF_2 windows and loaded into the cryostage (FDCS 196, Linkam, Tadworth, UK). The sample was then cooled down from 10°C to −150°C at a rate of 2°C/min. Note that since DMSO is toxic to cells at room temperature, the experiment was started at 10°C. Extracellular ice nucleation was not controlled during the cooling process. Ice nucleation generally occurred in the range of −15 to −25°C. Once the temperature reached −150°C, the sample was rapidly rewarmed to room temperature at a warming rate of 100°C/min. Post-thaw viability of the encapsulated and extracted cells was measured using 20 µg/mL acridine orange (AO)/propidium iodide (PI) fluorescent dye (Nexcelom, Lawrence, USA). The live (green) and dead (red) cells in the sample were counted in five representative areas for each sample using a Nikon Eclipse TE200 inverted fluorescence microscope (Melville, NY, USA). The final percent viability of the cells was calculated with respect to the freshly harvested NK-92 cells.

5.2.5 NK Cytotoxicity Assay

The cytotoxic activity of both fresh and frozen/thawed NK-92 cells was assessed through the measurement of lactic dehydrogenase (LDH) released from apoptotic

tumor cells in the supernatant. The LDH assay was performed using the CyQUANT™ LDH Cytotoxicity Assay Kit following the manufacturer's instructions (Invitrogen, Waltham, MA). Briefly, 100 µL suspensions of target cells (MDA-MB-231) at a density of 10,000 cells/well were seeded in multiple wells of a 96-well plate and incubated overnight for cell attachment. On the following day, viable fresh or frozen/thawed NK-92 cells (effector) in 100 µL of medium were co-cultured with the target cells at different effector-to-target (E/T) ratios of 2:1, 1:1, and 0.5:1 in triplicate wells for 24 hours. Additionally, triplicate wells containing MDA-MB-231 cells for spontaneous LDH activity controls were treated with fresh medium only, while another set of triplicate wells for maximum LDH activity controls were treated with lysis buffer. After the co-culture period, the supernatants were collected to measure the LDH released from the dead MDA-MB-231 cells. The absorbance was measured at wavelengths of 490 nm and 680 nm. The 680 nm absorbance value, representing the background, was subtracted from the 490 nm absorbance, and the cytotoxicity percentage was calculated using the following formula:

$$\text{Cytotoxicity (\%)} = \frac{\text{experimental LDH activity} - \text{spontaneous LDH activity}}{\text{maximum LDH activity} - \text{spontaneous LDH activity}} \times 100\%$$

5.2.6 FTIR studies with alginate hydrogel

0.1 ~ 1µL of the samples (20% trehalose solution, and 1% alginate + 20% trehalose hydrogel) were sandwiched between two CaF_2 windows and sealed with vacuum grease to avoid evaporation. The assembly was then transferred to the cryostage attached to an infrared microscope, which was connected to an FTIR spectrometer (Thermo-Nicolet Continuum, Thermo Electron, Waltham, MA) equipped with a

mercury cadmium telluride detector (Thermo Electron, Waltham, MA). The sample was first cooled from 10°C to -150°C at a rate of 2°C/min, then warmed back to 10°C at 2°C/min. Infrared (IR) spectra were collected from a sample area of 100 µm × 100 µm every 2°C, and 64 IR scans at a resolution of 4 cm^{-1} were averaged in 9000 to 900 cm^{-1} wavenumber range to obtain each spectrum. The IR spectra were analyzed using the OMNIC software (Thermo-Nicolet, Madison, WI,). Changes in the glycosidic band (995 cm^{-1})[187, 188] were examined as the sample was cooled and heated.

5.3 Results and Discussion

5.3.1 Agarose hydrogel encapsulation

5.3.1.1 Encapsulation and extraction of NK-92 cells from agarose hydrogel

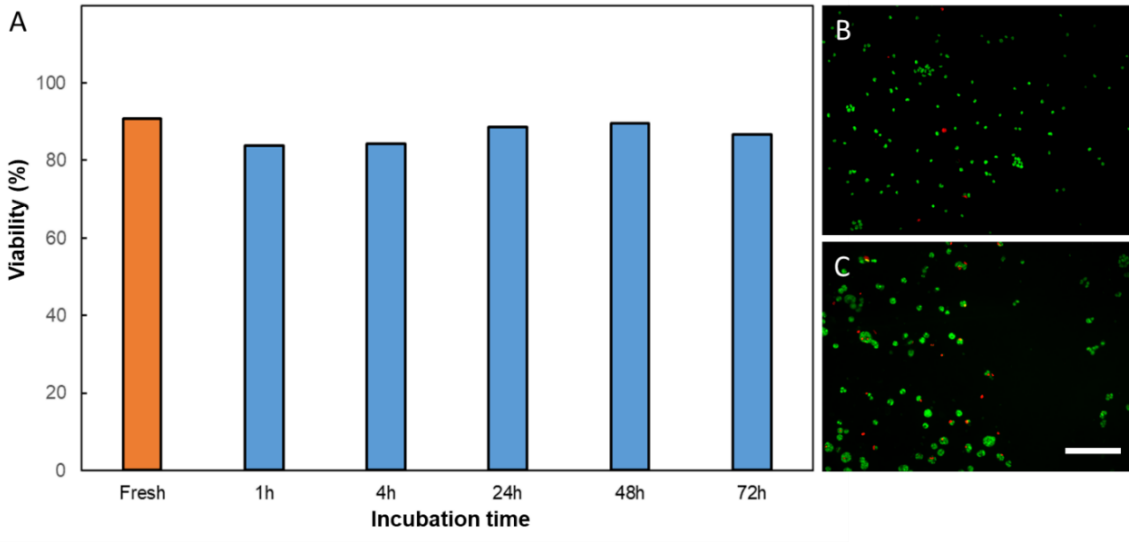

Figure 5.1. (A) Viability of encapsulated NK-92 cells (in 0.75% agarose hydrogel) incubated at 37°C, 5% CO_2 for up to 3 days (n=1). Live/dead fluorescence images of (B) fresh NK-92 cells, and (C) encapsulated NK-92 cells in 0.75% agarose hydrogel cultured for 72 hours. (scale bar: 200µm)

As shown in ***Figure 5.1A***, after the NK-92 cells were encapsulated in the 0.75% agarose hydrogel, no significant viability decrease was observed compared to the fresh control. Also, the encapsulated NK-92 cells exhibited sustained high viability and continued growth by forming cell clusters during the 3-day cell culture (***Figure 5.1C***). These results demonstrated the biocompatibility of agarose hydrogel with NK-92 cells.

To optimize the extraction process of NK-92 cells from the agarose hydrogel, three concentrations of agarase exposure (25, 100, and 250 U/ml) were tested, and the viability, as well as extraction rate data, were analyzed (***Figure 5.2A)***. It was found that the viability of NK-92 cells decreased gradually with increasing agarase concentration. Meanwhile, the cell extraction rate increased with increasing agarase concentration, with a statistically significant ($p<0.05$) difference observed between the 25 U/ml and 100 U/ml groups. Furthermore, the impact of different incubation times (0.5, 1, 2, and 4 hours) on the extraction rate of NK-92 cells was evaluated. As shown in ***Figure 5.2B***, the increase in the incubation time led to a higher cell extraction rate, and a significant difference was observed between 0.5-hour and 1-hour incubation ($p<0.05$). However, it is worthy of note that the increase in extraction rate was accompanied by a reduction in cell viability. Specifically, a significant decrease in cell viability ($p<0.05$) was observed during 0.5-hour incubation, and a more statistically significant ($p<0.01$) difference was observed during 2-hour incubation. Considering these results, we have determined that a

concentration of 100 U/ml for agarase and an incubation time of 1 hour are the optimal conditions for improving the cell extraction rate (***Figure 5.2C***) while preserving a satisfactory level of cell viability (***Figure 5.2D***).

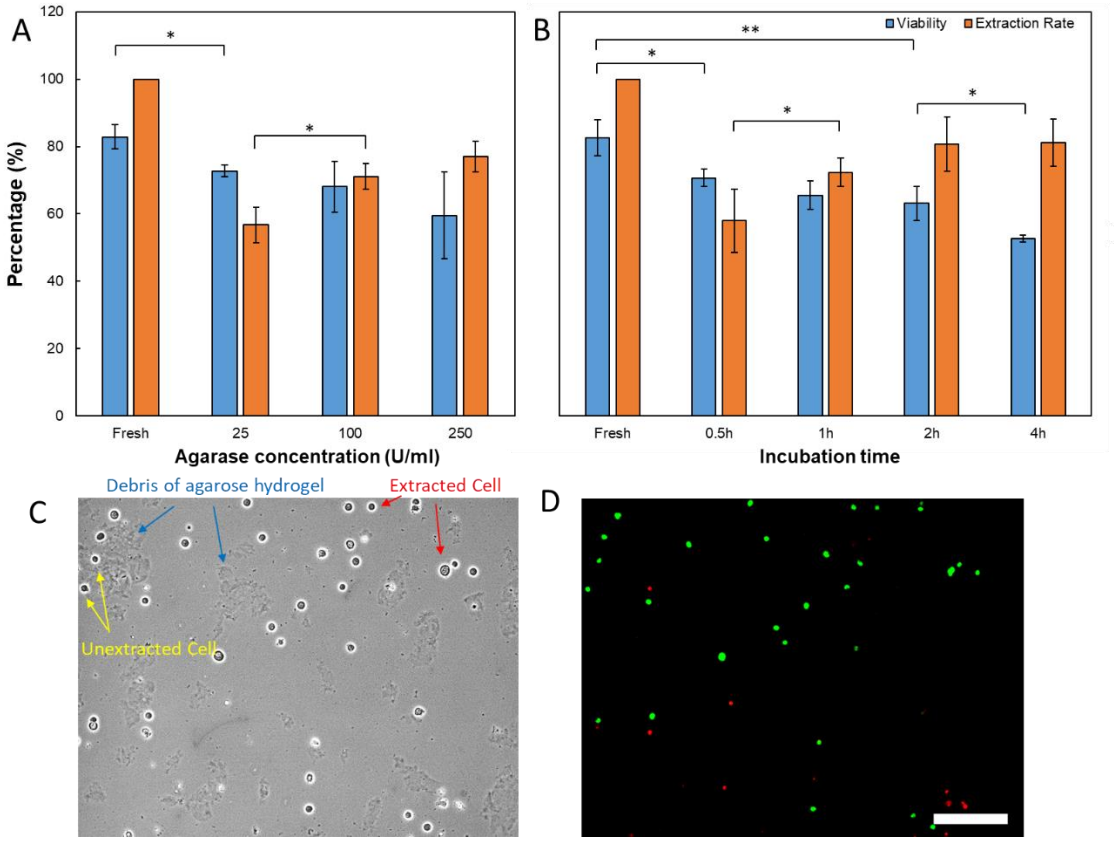

Figure 5.2 (A) Post-extraction viability and extraction rate of encapsulated NK-92 cells after incubation with different concentrations of agarase (25, 100, and 250U/ml) at 39°C for 1 hour. (B) Viability and extraction rate of encapsulated NK-92 cells after varying incubation times (0.5, 1, 2, and 4 hours) with 100U/ml agarase at 39°C. (C) Bright-field image and (D) live/dead fluorescence image showing extracted NK-92 cells from 0.75% agarose hydrogel after 1-hour incubation with 100 U/ml agarase at 39°C. (* indicates $p<0.05$, and ** indicates $p<0.01$, n=3, scale bar: 200µm)

However, it is important to note that even with the use of minimum agarase concentration and incubation time, the cell viability dropped significantly ($p<0.05$) compared to the fresh control (***Figure 5.2A*** and ***Figure 5.2B***). This result indicates

that the cell extraction process may still have some unfavorable effects on NK cells (e.g. the mechanical stresses during homogenization), which can lead to cell death. Additionally, the presence of hydrogel debris in the extracted cells (***Figure 5.2C***) may introduce additional negative effects, such as impeding NK cell migration and compromising their cytotoxicity. Therefore, ongoing efforts focused on further optimizing the extraction protocol of NK-92 cells from the agarose hydrogel.

5.3.1.2 Post-thaw analysis of NK-92 cells freeze/thawed in agarose hydrogel with trehalose

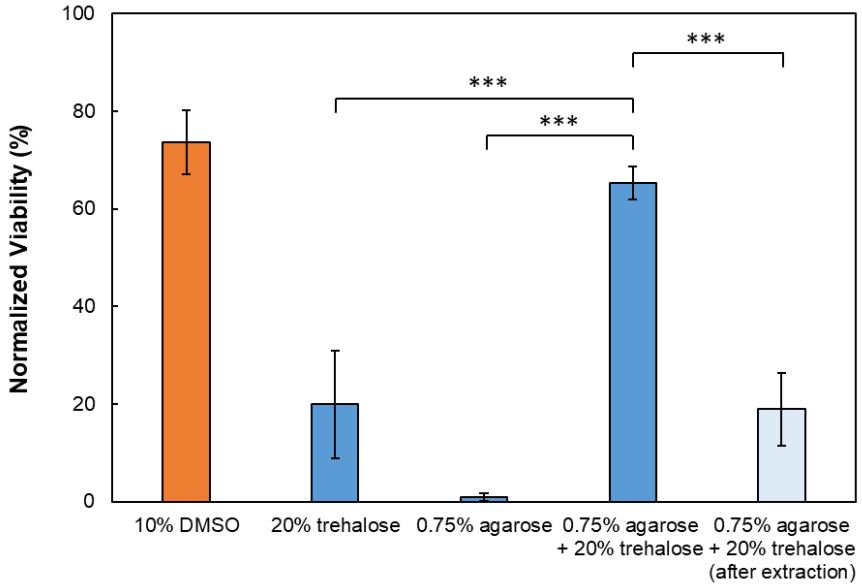

Figure 5.3 Post-thaw viability (normalized to fresh control) of NK-92 cells frozen in 10% DMSO solution (with 40% FBS and 50% cell culture medium), 20% trehalose in 1x PBS solution, 0.75% agarose hydrogel (before extraction), 0.75% agarose + 20% trehalose hydrogel (before extraction), and 0.75% agarose + 20% trehalose hydrogel (after extraction). (*** indicates $p<0.001$)

The post-thaw viability of NK cells frozen in different groups is shown in ***Figure 5.3***. The composition of 0.75% agarose + 20% trehalose was chosen since its

demonstrated high post-thaw viability for MDA-MB-231 cells. Similar to the observations made with MDA cells, poor survival was observed for NK-92 cells when they were frozen/thawed in the trehalose solution or encapsulated in agarose hydrogel (without trehalose). Encapsulation of NK-92 cells in 0.75% agarose hydrogel with 20% trehalose before freezing significantly increased their post-thaw viability to 65.2 ± 3.4%, which is comparable to the DMSO control (73.6 ± 6.4%). However, it is important to note that the post-thaw viability significantly decreased ($p<0.001$) to 18.9 ± 7.4% after cell extraction.

A cytotoxicity assay was performed to further analyze the post-thaw function of the extracted NK-92 cells (***Figure 5.4A***). In both the fresh and DMSO control, cytotoxicity increased with the effector-to-target (ET) ratio. Since the damage to the plasma membrane results in the release of LDH into the surrounding cell culture medium, the higher LDH activity means that more of the targeted MDA-MB-231 cells were damaged by NK-92 cells (higher cytotoxicity). The cytotoxicity of NK-92 cells frozen/thawed in 10% DMSO is slightly lower than that of the fresh control (particularly evident at ET ratio 2), although the difference was not statistically significant. Some studies have reported lower cytotoxicity for NK cells cryopreserved with DMSO, factors such as the use of different cytotoxicity assays and target cells may account for the variance, [217,222] a more detailed discussion is in the next section. In addition, the cytotoxicity data corresponds to our observations in ***Figure 5.4C, D***, where both the fresh and DMSO cryopreserved groups formed a number of NK-92 cell clusters after 1-day co-culture with MDA-

MB-cells, and the growth of MDA-MB-231 was also greatly inhibited compared to the MDA control without the seeding of NK-92 cells (***Figure 5.4B***). On the other hand, for NK-92 cells that were frozen/thawed and extracted from the 0.75% agarose + 20% trehalose hydrogel, no significant increase in cytotoxicity was observed with the increase in the ET ratio. Moreover, at an ET ratio of 2, the LDH activity was significantly lower than that of the fresh control. This finding indicates a severe impairment of the functionality of NK cells. This collaborates with the observation from ***Figure 5.4E***, where very few and small clusters of NK cells were formed and lots of MDA cells remained stretched and attached to the bottom surface.

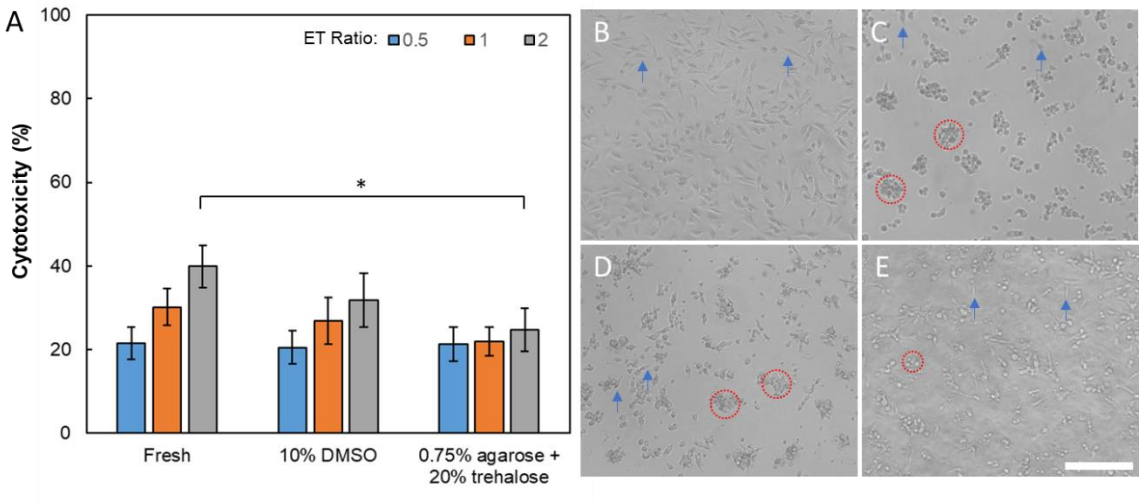

Figure 5.4 (A) Cytotoxicity assessment of NK-92 cells (fresh control, freeze/thawed in 10%DMSO, and freeze/thawed and extracted from 0.75% agarose + 20% trehalose) against MDA-MB-231 cells at different effector-to-target (ET) ratios (0.5, 1, and 2, for viable cells). Bright-field images of MDA-MB-231 cells after 24-hour co-culture with (B) no NK-92 cells, (C) fresh NK-92 cells, (D) NK-92 cells frozen/thawed in 10% DMSO, and (E) NK-92 cells frozen/thawed and extracted from 0.75% agarose + 20% trehalose, at the ET ratio of 2. (The blue arrow represents an example of attached and stretched MDA-MB-231 cells, the red dashed circle represents an example of NK-92 cell clusters. * indicates $p<0.05$. Scale bar: 200μm)25

Compared to the high post-thaw viability before cell extraction, the significant drop in post-thaw viability (***Figure 5.3***) and compromised cytotoxicity (***Figure 5.4***) of encapsulated NK-92 cells following cell extraction highlight the cell extraction process is detrimental to the NK cells, particularly for the cells after cryopreservation. Another explanation for the viability drop is the enhanced sensitivity and fragility of NK cells resulting from the freeze/thaw process. Cryopreservation-induced stresses have negative effects on cells (such as activating molecular responses)[229] and may trigger cell apoptosis and delayed-onset cell death (DOCD).[230, 231] Consequently, compared to the fresh NK-92 cells, the freeze/thawed cells become more vulnerable to the stresses encountered during the cell extraction process, such as the mechanical forces exerted during homogenization, as well as the hypoosmotic stress and elevated temperature during the incubation for agarose digestion. Another potential explanation for the compromised cytotoxicity could be the debris of agarose hydrogel. In comparison to the images of the other three groups, the background in ***Figure 5.4E*** appears to be blurred and indistinct, which is due to the accumulation of hydrogel debris at the bottom of the well. The presence of residual hydrogel debris could potentially impede the binding of NK-92 cells to MDA-MB-231 cells, resulting in the inhibition of NK cell activation and compromising their killing capabilities against tumor cells.

5.3.2. Alginate Hydrogel Encapsulation

5.3.2.1 Extraction of NK-92 cells from alginate hydrogel

The feasibility of using alginate as an alternative hydrogel material for reversible encapsulation and cryopreservation of NK cells was also explored. As shown in ***Figure 5.5C***, the majority of NK-92 cells remained viable after extraction from the 1% alginate hydrogel, with only a slight decrease in viability (~7%) compared to the fresh control (***Figure 5.5A***). This slight decrease in viability may be attributed to the incubation of NK cells in a relatively high concentration (100mM) of EDTA solution and prolonged exposure time (20 min) at 37°C. In contrast to the extraction of cells from agarose hydrogel, the extraction from the alginate hydrogel achieved a 100% extraction rate with no observed hydrogel debris (***Figure 5.5B***). Compared to agarose hydrogel, these findings indicate that the method of extracting NK cells from alginate hydrogel is more efficient and safer.

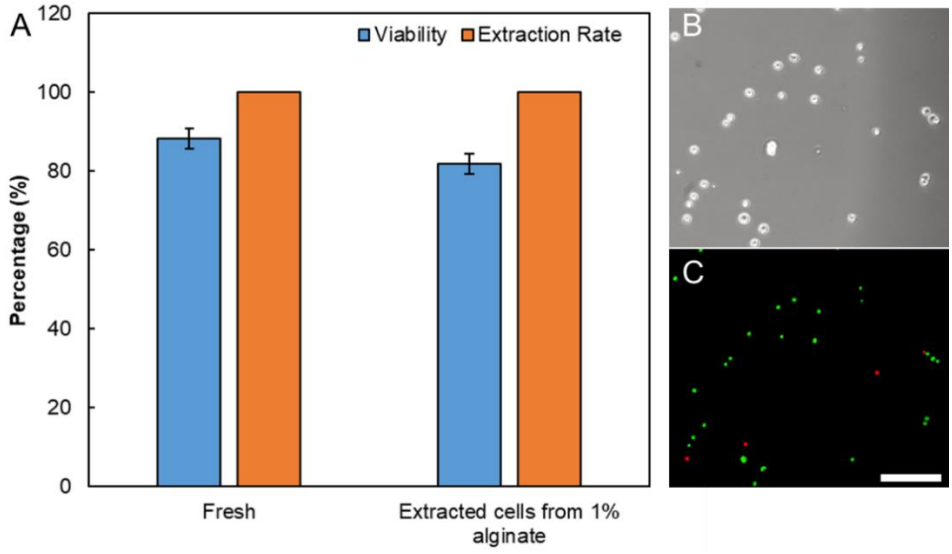

Figure 5.5 (A) Viability and extraction rate of fresh NK-92 cells and encapsulated NK-92 cells after being extracted from 1% alginate hydrogel. (B) Bright-field image and (C) live/dead fluorescence image showing NK-92 cells extracted from 1% alginate hydrogel. (scale bar: 200µm)

5.3.2.2 Post-thaw analysis of NK-92 cells frozen/thawed in alginate hydrogel with trehalose

The post-thaw viability of encapsulated NK cells frozen/thawed in different concentrations (from 0.5% to 2%) of alginate hydrogel is shown in ***Figure 5.6***. It's found that although encapsulation of NK-92 cells in alginate hydrogel with trehalose is beneficial for cryopreservation, it is less effective than the combination of agarose hydrogel with trehalose (***Figure 5.3***). Before cell extraction, the combination of 1% alginate + 20% trehalose yielded the highest post-thaw viability for NK-92 cells (48.1% ± 5.6%), which is significantly lower ($P<0.01$) than the 10% DMSO control (73.6 ± 6.5%). After extraction, the viability of NK-92 cells frozen/thawed in 1% alginate + 20% hydrogel further decreased to 28.3 ± 10.2 %. Comparing this approximately 20% viability decrease (***Figure 5.6***) to the approximately 7% viability decrease observed for the encapsulated fresh NK-92 cells after extraction(***Figure 5.5A***), it supports the finding that freeze/thawed cells become more vulnerable to stresses encountered during the cell extraction.

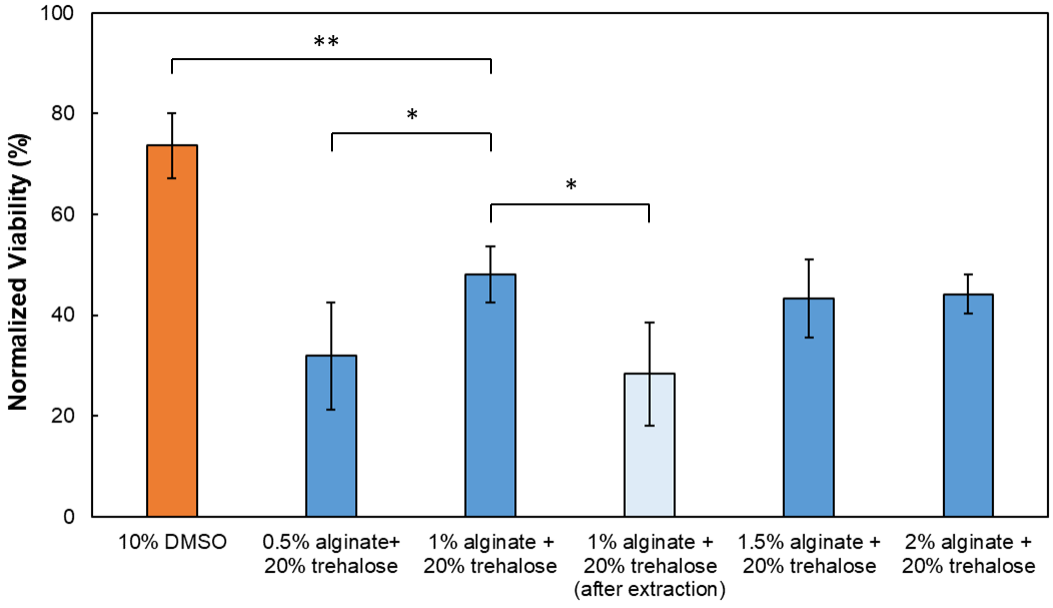

Figure 5.6 Post-thaw viability (normalized to fresh control) of NK-92 cells frozen/thawed in 10% DMSO solution (with 40% FBS and 50% cell culture medium), different concentrations of alginate hydrogel (0.5%, 1%,1.5%, 2%) with 20% trehalose (before extraction), and 1% alginate + 20% trehalose (after extraction). (* indicates $p<0.05$, ** indicates $p<0.01$)

Compared to the fresh control and DMSO group, the cytotoxicity of NK-92 cells frozen/thawed and extracted from 1% alginate + 20% trehalose hydrogel did not exhibit significant differences across all ET ratios (***Figure 5.7A***). Furthermore, bright-field images for all three groups (***Figure 5.7C, D, E***) showed the noticeable suppression of MDA-MB-231 cell growth and the aggregation of NK-92 cell clusters and after one day of co-culture, although the size of cell clusters in DMSO control and the 1% alginate + 20% trehalose group was slightly smaller compared to the fresh control. These results suggest that the cytotoxicity of viable NK-92 cells in alginate + 20% trehalose was slightly compromised after the freeze/thaw and cell extraction processes.

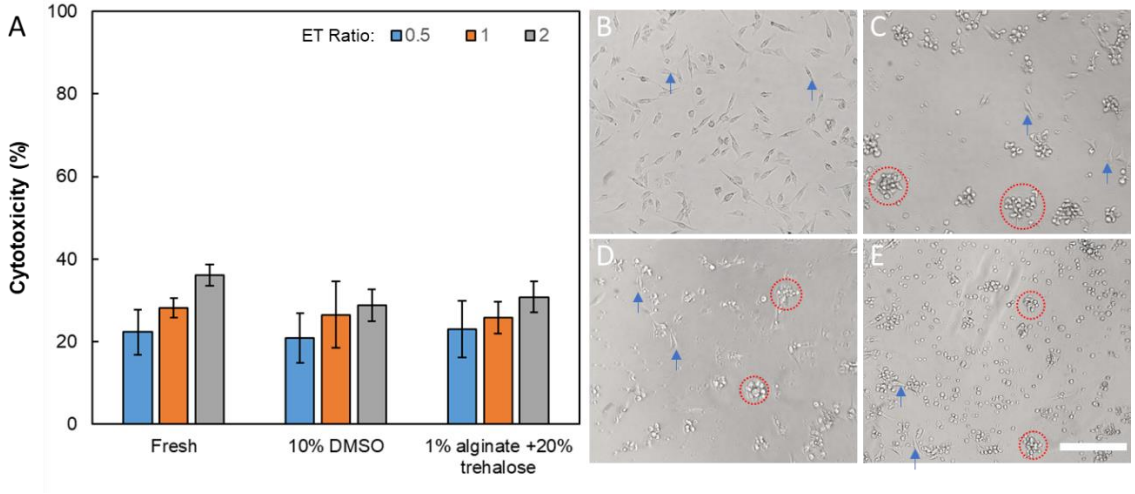

Figure 5.7 (A) Cytotoxicity assessment of NK-92 cells (fresh control, frozen/thawed in 10%DMSO, and frozen/thawed and extracted from 1% alginate + 20% trehalose) against MDA-MB-231 cells at different effector-to-target(ET)

ratios (0.5, 1, and 2, for viable cells). Bright-field images of MDA-MB-231 cells after 24-hour co-culture with (B) no NK-92 cells, (C) fresh NK-92 cells, (D) NK-92 cells frozen/thawed in 10% DMSO. and (E) NK- 92 cells frozen/thawed and extracted from 0.75% agarose + 20% trehalose, at the ET ratio of 2. (The blue arrow represents an example of attached and stretched MDA-MB-231 cells, and the red dashed circle represents an example of NK-92 cell clusters. Scale bar: 200μm)28

Since the maximum LDH activity of fresh NK-92 cells is relatively low (approximately 40% at an ET ratio of 2, as shown in ***Figure 5.4*** and ***Figure 5.7***), and the observed differences in cytotoxicity between different experimental groups or ET ratios are not very significant, we may need to increase the maximum ET ratio to obtain more conclusive results. Additionally, K562 cells, as employed in many previous studies, [217,232, 233] could be considered as an alternative to MDA-MB-231 cells. In contrast to the attached MDA-MB-231 cells, K562 cells are suspension cells (the same as NK cells), which facilitate NK cell migration and targeting. Furthermore, K562 cells lack expression of major histocompatibility complex (MHC) class I molecules, rendering them more susceptible to NK cell-mediated killing.[234] These may explain why some studies have observed a more significant drop in cytotoxicity after NK cells cryopreserved with DMSO.[110, 217, 222]

5.3.2.3 Preliminary study on the physicochemical mechanisms of protection offered by alginate encapsulation during freeze/thaw

FTIR studies were performed to investigate the thermodynamic and kinetic transitions that occurred during the freeze/thaw process in the alginate hydrogel with trehalose. Using the method described in Chapter 4, the temperature-induced

shift of the trehalose glycosidic linkage (located at 995 cm^{-1}) was analyzed. As shown in ***Figure 5.8***, during cooling, the glycosidic linkage peak shifted to higher wavenumbers with decreasing temperature, which is due to the increase in hydration level for trehalose,[186, 207] and the increase of the flexibility of trehalose around the glycosidic linkage.[186] The abrupt redshift upon freezing around -25°C (Blue arrow in ***Figure 5.8***) was because of the formation of the freeze-concentrated liquid (FCL), which significantly increased the trehalose concentration and thus decreased the flexibility of trehalose.

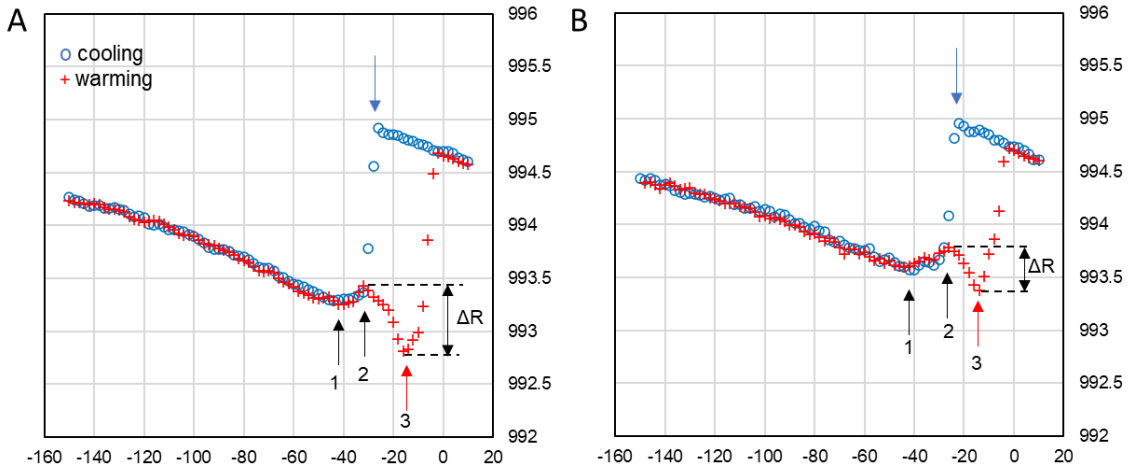

Figure 5.8 Peak shift of the glycosidic band (~995 cm^{-1}) during cooling and warming processes of: (A) 20% trehalose, (B) 1% alginate + 20% trehalose. Samples were cooled from 10 °C to -150 °C and then warmed back to 10 °C at 2 °C /min.

During the warming process, three transitions were observed in the IR spectra. As discussed in Chapter 4, these three transitions correspond to the glass melting of the FCL (transition 1), the onset of ice recrystallization (transition 2), and the melting of bulk ice (transition 3), respectively. ΔR between the onset of ice recrystallization (transition 2) and melting of bulk ice (transition 3) represents the

extent of ice recrystallization in the sample during warming. In comparison to the 20% trehalose, the ΔR value decreased from 0.7 cm^{-1} to 0.4 cm^{-1} in the 1% alginate + 20% trehalose group. This decrease suggests that alginate acts as an inhibitor of ice recrystallization during the warming process, similar to the effect observed with agarose hydrogel. Note that the ΔR value of 0.4 cm-1 for the 1% alginate + 20% trehalose group (***Figure 5.8B***) is similar to the ΔR value of 0.75% agarose + 20% trehalose group (***Figure 4.5B***), indicating their comparable abilities to inhibit ice recrystallization during warming. However, considering the relatively lower post-thaw viability of encapsulated NK-92 cells in the alginate hydrogel (48.1 ± 5.6%, ***Figure 5.6***) compared to the agarose hydrogel (65.2 ± 3.4%, ***Figure 5.3***), further investigations are underway to better understand the other factors such as the ability to inhibit ice formation and eutectic crystallization/melting in the system of alginate hydrogel with trehalose during freeze/thaw.

5.3.3 Comparative analysis and discussion of cryopreservation results of NK-92 cells: agarose hydrogel vs. alginate hydrogel

A comprehensive comparative analysis was summarized in ***Table 5.1***, which evaluates the cryopreservation outcomes of NK-92 cells in terms of post-thaw viability (before and after cell extraction), cytotoxicity for NK-92 cells, the efficiency of cell extraction, and recovery rates from both agarose and alginate hydrogel materials.

	Viability (%, before cell extraction)	Viability (%, after cell extraction)	Extraction Rate (%)	Recovery Rate (%)	Cytotoxicity (%, ET ratio = 2)
0.75% agarose +20% trehalose	65.2 ± 3.4 [a]	18.9 ± 7.4 [a]	72.4 ± 4.2 [a]	50.5 ± 7.4 [a]	65.1 ± 10.3 [b]
1% alginate + 20% trehalose	48.1 ± 5.6 [b]	28.3 ± 10.2 [a]	100 ± 0 [b]	73.1 ± 9.7 [b]	85.1 ± 4.1 [a]

Table 5.1 Comparison of the post-thaw assessment for cells frozen/thawed in agarose and alginate hydrogel. (All the data were normalized with fresh control. Values marked with different superscripts (a, b) within a column are statistically significantly different, $p < 0.05$)

The viability of NK-92 cells after freeze/thaw in 0.75% agarose + 20% trehalose hydrogel is significantly higher compared to 1% alginate + 20% trehalose, indicating the stronger protection offered by agarose hydrogel with trehalose during the freeze/thaw process. However, following cell extraction after freeze/thaw, cells extracted from both hydrogels showed a significant decrease in viability (~46% for agarose and ~20% for alginate, ***Table 5.1***). This decline can be attributed to the detrimental effect of the cell extraction process, as well as the stresses induced by cryopreservation, which may elevate the sensitivity and fragility of NK-92 cells, and potentially trigger cell apoptosis and DOCD. On the other hand, the lower viability drop during cell extraction, higher cell extraction, and recovery rates, as well as higher cytotoxicity (***Table 5.1***), suggest that the protocol used for extracting NK-92 cells from alginate hydrogel is less harmful and more efficient than the protocol for extracting cells from agarose hydrogel. These findings emphasize the need for further optimization of the extraction process (particularly for agarose hydrogel) to minimize cellular damage and maintain cell viability and functionality. Future studies should focus on mitigating the cryopreservation-induced stresses on NK cells and exploring alternative extraction

methods or modifications to the current procedure to mitigate the adverse effects associated with the cell extraction process and enhance overall cell recovery and viability.

5.4 Conclusion

This chapter evaluated the cryopreservation methods using agarose-trehalose hydrogel for NK-92 cells and optimized the cell extraction protocol from agarose hydrogel. Additionally, the potential of alginate as an alternative hydrogel material for reversible encapsulation and cryopreservation of NK-92 cells was investigated. Encapsulation of NK-92 cells in 0.75% agarose + 20% trehalose hydrogel demonstrated effective cell protection during the freeze/thaw process (***Figure 5.3***). However, poor post-thaw survival (***Figure 5.3***) and cytotoxicity (***Figure 5.4***) were observed after cell extraction, possibly attributed to (1) the detrimental effects of the extraction process and (2) the increased vulnerability of cells due to cryopreservation-induced stresses. On the other hand, 1% alginate + 20% trehalose hydrogel showed less effectiveness in the protection of NK cells during freeze/thaw (***Table 5.1***). Similar observations were made regarding the lower post-thaw viability (***Figure 5.6***) and compromised cytotoxicity (***Figure 5.7***) after cell extraction from alginate hydrogel. However, the process of NK cell extraction from alginate hydrogel appeared less detrimental and more efficient than from agarose hydrogel (***Table 5.1***). Further studies are needed to minimize cryopreservation-induced stress on NK cells and optimize the cell extraction process to alleviate the damage to cells.

Chapter 6: Research Summary

The main objective of this dissertation research is to develop a novel cryopreservation method for mammalian cells using hydrogel encapsulation to eliminate the use of toxic cell membrane-permeable CPA such as DMSO, and then validate and optimize this cryopreservation method for therapeutic NK cells. To achieve this goal, we have proposed the following specific aims:

Specific Aim 1: Analysis of molecular changes associated with warming Injury in cryopreserved therapeutic cells

In Chapter 3, we investigated the molecular changes and post-thaw viability of human therapeutic cells (leukocytes) associated with warming injury during cryopreservation. Our findings revealed that slow warming resulted in irreversible dehydration of cell membrane lipids and denaturation of cellular proteins (***Figure 3.5***), leading to cell death (***Figure 3.2***). Additionally, the post-thaw viability data for cells subjected to rapid warming with isothermal hold (***Figure 3.3***) indicated that human leukocytes are highly sensitive and vulnerable to the kinetic processes active at cryogenic temperatures, particularly in the range of -60°C and -80°C. These processes may involve (1) eutectic crystallization and melting (2) devitrification and extensive ice recrystallization.

Specific Aim 2: Design and manufacture a hydrogel matrix for the cryopreservation of mammalian cells and determine the physicochemical mechanisms of protection offered by hydrogel encapsulation

In Chapter 4, we developed an encapsulation-based cryopreservation method that eliminates the need for DMSO. This is achieved by encapsulating the cells in a cytocompatible agarose hydrogel in the presence of extracellular trehalose, a membrane-impermeable cryoprotective agent. The study demonstrates that the method offers effective cryoprotection through the following mechanisms: First, as proven by the DSC and FTIR analyses, hydrogel encapsulation decreased the amount of free water in the solution, resulting in a smaller ice phase volume (***Figure 4.1***, ***Table 4,1***, and ***Figure 4.4A***) with a less ordered water structure (***Figure 4.4B***). Second, ice recrystallization during warming was inhibited (***Figure 4.5***), potentially due to the hydrogel network mechanically inhibiting the formation, progression, and fusion of ice crystals. And finally, detrimental eutectic crystallization/melting transitions were inhibited (***Figure 4.1***). Therefore, the cells (MDA-MB-231) encapsulated in the agarose hydrogel with trehalose are well protected against detrimental mechanical damage observed during freeze/thaw, as reflected by a very high viability post-thaw (***Figure 4.7***). On the other hand, a lower proliferation rate was observed after the post-thaw cells were extracted from the hydrogel (***Figure 4.8, Figure 4.9***), which suggests the need for further optimization of the cell extraction process.

Specific Aim 3: Validation and optimization of the hydrogel encapsulation method for cryopreservation of NK cells

In Chapter 5, we validated the cryopreservation methods utilizing hydrogel encapsulation for NK-92 cells and optimized the protocol for extracting

encapsulated cells from the hydrogel. Cells encapsulated in 0.75% agarose +20% trehalose showed comparable post-thaw viability to the DMSO control (***Figure 5.3***), indicating NK cells are well protected during the freeze/thaw process. On the other hand, 1% alginate + 20% trehalose showed less effectiveness in the protection of NK cells during freeze/thaw (***Table 5.1***). For both agarose and alginate, significant viability drop and compromised cytotoxicity were observed after cells were extracted from hydrogel after thawing (***Table 5.1***), which might be due to (1) the detrimental effects of the extraction process and (2) the increased vulnerability of cells due to cryopreservation-induced stresses.

Chapter 7: Explorative Study and Future Work

7.1 Explorative Study

7.2.1 Explorative study on cryopreservation of primary NK cells using agarose hydrogel with trehalose

Primary NK cells, in contrast to the established NK-92 cell line, are derived from human donors' peripheral blood or tissues, closely resemble the characteristics of native immune cells. While NK-92 cells can be grown easily in larger quantities, primary NK cells offer the advantage of genetic diversity, allowing for potential compatibility with a broader range of patients.[235] They also possess a wider repertoire of natural killer cell receptors, which can enhance their ability to recognize and target tumor cells.[102, 104] Given their important role in immune-mediated therapies, we conducted preliminary studies to evaluate the cryopreservation of primary NK cells using agarose hydrogel encapsulation.

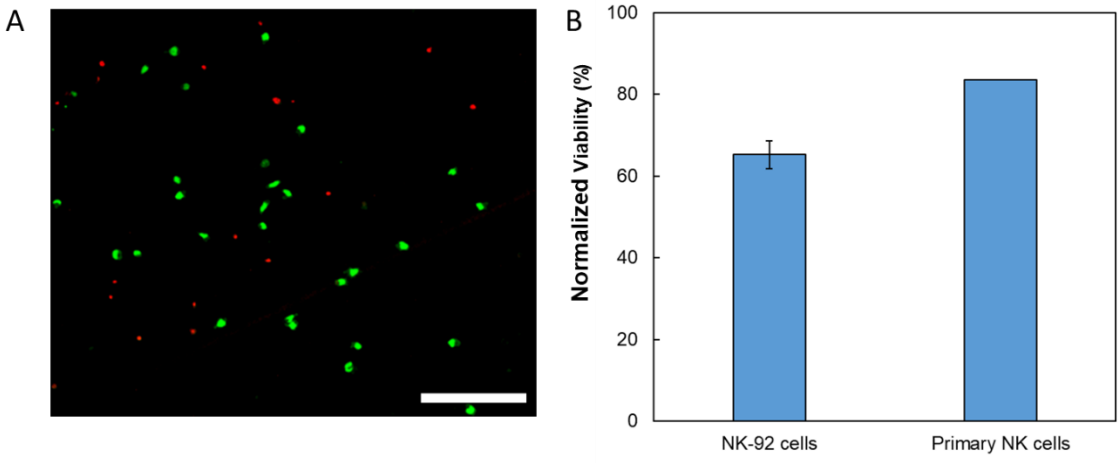

Figure 7.1 (A) Live/dead fluorescence image of freshly expanded primary NK cells. (2) Post-thaw viability (normalized to fresh control) of NK-92 cells (n=3) and primary NK cells (n=1) frozen/thawed in 0.75% agarose + 20% trehalose (before cell extraction). (Scale bar: 200μm)

The primary NK cells were frozen/thawed following the same cooling/warming protocol as for NK-92 cells, as described in Chapter 5. And the viability of primary NK cells was measured before freezing and after thawing. It was found that freshly expanded primary NK cells (***Figure 7.1A***) display lower viability (approximately 72%) compared to fresh NK-92 cells (typically 80% to 90%). This difference may be attributed to the primary NK cells' requirement for specific culture conditions and growth factors, as well as their higher sensitivity to environmental stresses. However, after encapsulation and freeze/thaw in 0.75% agarose + 20% trehalose, the normalized post-thaw viability of primary NK cells is approximately 83% (***Figure 7.1B***), significantly higher than that of NK-92 cells (65.2 ± 3.4%). This observation is interesting because primary NK cells are theoretically more susceptible to the stresses during cryopreservation (such as osmotic changes, ice crystal formation, and temperature fluctuations) compared to the established NK-92 cell line. Given that primary NK cells exhibit genetic diversity due to individual variations among donors (which can affect their behavior and response to cryopreservation), conducting additional viability and cytotoxicity assays with multiple replicates is warranted to gain a better understanding of the encapsulation effect on cryopreservation outcomes of primary NK cells.

7.2 Future Work

7.2.1 Mitigating cryopreservation-induced stresses on NK cells

In Chapter 4, we provided a comprehensive explanation of the cryoprotection mechanisms offered by agarose encapsulation with trehalose during cryopreservation. These mechanisms include minimizing the volume of the ice phase, forming ice with a less ordered structure, inhibiting ice recrystallization during the warming process, and preventing cryoinjury associated with eutectic crystallization/melting. However, since the use of cell membrane-permeable CPAs was avoided, the inhibition of intracellular ice may not be as effective as DMSO, this might be a reason for the decreased post-thaw viability of encapsulated NK-92 cells compared to the DMSO control. Besides that, our analysis of the protective mechanisms offered by hydrogel encapsulation during freeze/thaw primarily focused on the physicochemical aspects. Some studies, however, have shown the stresses associated with cryopreservation also have detrimental effects on cells through various cellular physiology and biochemistry mechanisms.[229, 236-238] These stresses can cleavage DNA molecules [239, 240], trigger mitochondrial damage [241-243], and initiate cellular necrosis and apoptosis [229, 230, 236, 237, 241]. Therefore, efforts should be directed toward minimizing cryopreservation-induced stress on NK cells, which could further improve their post-thaw survival and functionality.

a. Induction of ice nucleation to minimize intracellular ice formation (IIF)

Inducing ice nucleation at a higher subzero temperature in the extracellular space has been demonstrated to enhance post-thaw survival for a variety of cell types.[244,

[245] In our experiments, simultaneous ice nucleation for hydrogel samples containing 20% trehalose typically occurs within the temperature range of -20°C to -25°C during cooling. Therefore, inducing extracellular ice nucleation at a higher temperature (e.g. -5°C) could allow for continued cell dehydration during cooling and reduces the possibility of IIF at lower temperatures. Additionally, it has been reported that ice nucleation could induce a strong highly cooperative fluid–gel phase transition of the cell membrane,[58] and the extent of this freezing-induced phase transition decreases as the ice nucleation temperature decreases.[58] By inducing ice nucleation at a higher subzero temperature, the greater magnitude of the cell membrane phase transition facilitates the uptake of membrane-impermeable trehalose from the extracellular medium, which could further reduce the occurrence of IIF.

Except for the inhibition of IIF, inducing ice nucleation at a specific temperature offers another advantage by minimizing variations in results from sample to sample, run to run. This approach has been widely used in the cryopreservation of cell therapy products, ensuring more consistent outcomes and reproducibility.[224]

b. Incorporating specific inhibitors into the cryopreservation process

Incorporating inhibitors into the cryopreservation process represents another promising approach for enhancing the viability and functionality of NK cells post-thaw. Specifically, Rho-associated protein kinase (ROCK) inhibitors[73], caspase inhibitors[229, 230, 236], and oxidative stress inhibitors[229, 230, 243], have shown potential

in mitigating the detrimental effects which could be induced by cryopreservation. These inhibitors can target and inhibit crucial pathways involved in necroptosis or apoptosis[230], cytoskeletal damage[229, 230], and oxidative stress[1, 9], therefore preserving cellular integrity and promoting cell survival after thawing. In addition, the inclusion of inhibitors may also modulate the cellular response to environmental stimuli during the cell extraction process following thawing, further improving the overall survival and functionality of the extracted cells.

7.2.2 Optimization of the cell encapsulation and extraction process

a. Encapsulation of NK cells using microencapsulation

Encapsulating NK cells in hydrogel microbeads (e.g. using a microfluidic device), can reduce the size of the hydrogel and facilitate the cell extraction process. In our experiments involving NK cells frozen/thawed in the agarose-trehalose hydrogel, the sample volume can be as large as 100-200 µL, therefore the homogenization step is required to break down the large hydrogel into smaller pieces before incubating the hydrogel with agarase. However, by encapsulating the NK cells within agarose microbeads, the homogenization step is no longer necessary, minimizing the risk of mechanical damage to the NK cells and also avoiding cell loss in this step. Moreover, the small size may allow for lower requirements in terms of agarase enzyme concentration, incubation temperature, and incubation time. Consequently, the extraction of NK cells from agarose hydrogel becomes less detrimental.

Similarly, encapsulation of NK-92 cells in alginate microbeads could significantly reduce the digestion time and EDTA concentration. Our preliminary data showed that decreasing the size of alginate hydrogel beads from 20 µL to 10 µL can minimize the digestion time from approximately 50 minutes to 20 minutes in a 100 mM EDTA solution. Therefore, if NK cells are encapsulated in a smaller size of alginate beads, it is possible to extract cells within a few minutes at a lower EDTA concentration, further minimizing the adverse effects on the cells.

However, to ensure effective protection during cryopreservation, the size of microbeads used for encapsulating NK cells should not be too small. Microbeads with diameters below 200 µm have been observed to be much more susceptible to damage caused by ice formation during slow or controlled-rate freezing.[246] This is attributed to the increased surface-to-volume ratios of smaller beads, which enhance the possibility of direct contact between the encapsulated cells in the beads and the growing ice crystals outside the beads during cryopreservation.[29]

b. Explore other types of agarose or combinations of agarase with other enzymes

In this study, the use of low-gelling temperature agarose (which undergoes gelation around 20°C compared to the standard agarose with gelation around 37°C) provides us with more flexibility for cell encapsulation. The lower gelling temperature of agarose is achieved by decreasing the level of hydrogen bonding via methylation of the hydroxyl side groups.[247] However, the methylated backbone may inhibit enzymatic digestion. Although we could extract most cells via agarase

enzymatic digestion, the need to use a high concentration of the agarase and long incubation time might contribute to decreased cell viability. Therefore, either using a higher temperature gelation agarose (less methylation) or an enzyme or biocompatible chemical that functions on a methylated backbone might be beneficial to reduce the amount of time and concentration of enzyme to minimize the adverse effect on cells, and therefore increase viable cell recovery after cell extraction.

References

(1) Cell And Gene Therapy Clinical Trials Market Size, Share & Trends Analysis Report By Phase (Phase I, II, III, IV), By Indication (Oncology, CNS), By Region (Asia Pacific, North America), And Segment Forecasts, 2022 - 2030; GVR-4-68039-409-7; Grand View Research, 2021. https://www.grandviewresearch.com/industry-analysis/cell-gene-therapy-clinical-trials-market.
(2) Gao, D.; Critser, J. K. Mechanisms of cryoinjury in living cells. ILAR J **2000**, 41 (4), 187-196. DOI: 10.1093/ilar.41.4.187.
(3) Pegg, D. E. Principles of cryopreservation. Methods Mol Biol **2015**, 1257, 3-19. DOI: 10.1007/978-1-4939-2193-5_1.
(4) Eroglu, A.; Russo, M. J.; Bieganski, R.; Fowler, A.; Cheley, S.; Bayley, H.; Toner, M. Intracellular trehalose improves the survival of cryopreserved mammalian cells. Nat Biotechnol **2000**, 18 (2), 163-167. DOI: 10.1038/72608.
(5) Mazur, P. Equilibrium, quasi-equilibrium, and nonequilibrium freezing of mammalian embryos. Cell Biophys **1990**, 17 (1), 53-92.
(6) Haddock, R.; Lin-Gibson, S.; Lumelsky, N.; McFarland, R.; Roy, K.; Saha, K.; Zhang, J.; Zylberberg, C. Manufacturing cell therapies: the paradigm shift in health care of this century. NAM Perspectives **2017**.
(7) Cao, E.; Chen, Y.; Cui, Z.; Foster, P. R. Effect of freezing and thawing rates on denaturation of proteins in aqueous solutions. Biotechnology and bioengineering **2003**, 82 (6), 684-690.
(8) Mazur, P. The role of intracellular freezing in the death of cells cooled at supraoptimal rates. Cryobiology **1977**, 14 (3), 251-272.
(9) Mazur, P.; Leibo, S. P.; Chu, E. H. A two-factor hypothesis of freezing injury. Evidence from Chinese hamster tissue-culture cells. Exp Cell Res **1972**, 71 (2), 345-355.
(10) Rall, W. F.; Polge, C. Effect of warming rate on mouse embryos frozen and thawed in glycerol. J Reprod Fertil **1984**, 70 (1), 285-292.
(11) Robert H.Miller, P. Survival of frozen-thawed human red cells as a function of cooling and warming velocities. Cryobiology **1976**, 13 (4), 404-414.
(12) Karlsson, J. O. M. A theoretical model of intracellular devitrification. Cryobiology **2001**, 42 (3), 154-169.
(13) MacFarlane, D. R.; Forsyth, M. Devitrification and recrystallization of glass forming aqueous solutions. In The biophysics of organ cryopreservation, Springer, 1987; pp 237-263.
(14) Fahy, G. M. Biological effects of vitrification and devitrification. In The biophysics of organ cryopreservation, Springer, 1987; pp 265-297.
(15) Douglas R. MacFarlane, M. F. Devitrification and Recrystallization of Glass Forming Aqueous Solutions. The Biophysics of Organ Cryopreservation **1986**, 147, 237-263.
(16) Wood, D. C.; Wirth, N. V.; Weber, F. S.; Palmquist, M. A. Mechanism considerations of dimethyl sulfoxide (DMSO)-lenticular changes in rabbits. J Pharmacol Exp Ther **1971**, 177 (3), 528-535.

(17) Donaldson, C.; Armitage, W. J.; Denning-Kendall, P. A.; Nicol, A. J.; Bradley, B. A.; Hows, J. M. Optimal cryopreservation of human umbilical cord blood. Bone Marrow Transplant **1996**, 18 (4), 725-731.
(18) Liseth, K.; Foss Abrahamsen, J.; Bjørsvik, S.; Grøttebø, K.; Bruserud, Ø. The viability of cryopreserved PBPC depends on the DMSO concentration and the concentration of nucleated cells in the graft. Cytotherapy **2005**, 7 (4), 328-333.
(19) Rowley, S. D.; Anderson, G. L. Effect of DMSO exposure without cryopreservation on hematopoietic progenitor cells. Bone Marrow Transplant **1993**, 11 (5), 389-393.
(20) Dominguez, E.; Lowdell, M. W.; Perez-Cruz, I.; Madrigal, A.; Cohen, S. B. Natural killer cell function is altered by freezing in DMSO. Portland Press Ltd.: 1997.
(21) Ock, S. A.; Rho, G. J. Effect of Dimethyl Sulfoxide (DMSO) on Cryopreservation of Porcine Mesenchymal Stem Cells (pMSCs). Cell Transplantation **2011**, 20 (8), 1231-1239. DOI: 10.3727/096368910x552835.
(22) Sumida, K.; Igarashi, Y.; Toritsuka, N.; Matsushita, T.; Abe-Tomizawa, K.; Aoki, M.; Urushidani, T.; Yamada, H.; Ohno, Y. Effects of DMSO on gene expression in human and rat hepatocytes. Hum Exp Toxicol **2011**, 30 (10), 1701-1709. DOI: 10.1177/0960327111399325.
(23) Pal, R.; Mamidi, M. K.; Das, A. K.; Bhonde, R. Diverse effects of dimethyl sulfoxide (DMSO) on the differentiation potential of human embryonic stem cells. Arch Toxicol **2012**, 86 (4), 651-661. DOI: 10.1007/s00204-011-0782-2.
(24) Davis, J. M.; Rowley, S. D.; Braine, H. G.; Piantadosi, S.; Santos, G. W. Clinical toxicity of cryopreserved bone marrow graft infusion. Blood **1990**, 75 (3), 781-786.
(25) Zenhäusern, R.; Tobler, A.; Leoncini, L.; Hess, O.; Ferrari, P. Fatal cardiac arrhythmia after infusion of dimethyl sulfoxide-cryopreserved hematopoietic stem cells in a patient with severe primary cardiac amyloidosis and end-stage renal failure. Annals of hematology **2000**, 79 (9), 523-526.
(26) Benekli, M.; Anderson, B.; Wentling, D.; Bernstein, S.; Czuczman, M.; McCarthy, P. Severe respiratory depression after dimethylsulphoxide-containing autologous stem cell infusion in a patient with AL amyloidosis. Bone marrow transplantation **2000**, 25 (12), 1299.
(27) Pravdyuk, A. I.; Petrenko, Y. A.; Fuller, B. J.; Petrenko, A. Y. Cryopreservation of alginate encapsulated mesenchymal stromal cells. Cryobiology **2013**, 66 (3), 215-222. DOI: 10.1016/j.cryobiol.2013.02.002.
(28) Chen, B.; Wright, B.; Sahoo, R.; Connon, C. J. A novel alternative to cryopreservation for the short-term storage of stem cells for use in cell therapy using alginate encapsulation. Tissue Eng Part C Methods **2013**, 19 (7), 568-576. DOI: 10.1089/ten.TEC.2012.0489.
(29) Zhao, G.; Liu, X.; Zhu, K.; He, X. Hydrogel Encapsulation Facilitates Rapid‐Cooling Cryopreservation of Stem Cell‐Laden Core–Shell Microcapsules as Cell–Biomaterial Constructs. Advanced healthcare materials **2017**, 6 (23), 1700988.
(30) Cao, K.; Shen, L.; Guo, X.; Wang, K.; Hu, X.; Ouyang, X.; Zhao, G. Hydrogel microfiber encapsulation enhances cryopreservation of human red blood cells with low concentrations of glycerol. Biopreservation and Biobanking **2020**, 18 (3), 228-234.

(31) Huang, H.; Choi, J. K.; Rao, W.; Zhao, S.; Agarwal, P.; Zhao, G.; He, X. Alginate hydrogel microencapsulation inhibits devitrification and enables large-volume low-CPA cell vitrification. Advanced functional materials **2015**, 25 (44), 6839-6850.
(32) Yao, J.; Shen, L.; Chen, Z.; Zhang, B.; Zhao, G. Hydrogel Microencapsulation Enhances Cryopreservation of Red Blood Cells with Trehalose. ACS Biomaterials Science & Engineering **2022**, 8 (5), 2066-2075.
(33) Sputtek, A. Cryopreservation of red blood cells and platelets. In Cryopreservation and freeze-drying protocols, Springer, 2007; pp 283-301.
(34) Ford, J. Red blood cell morphology. International journal of laboratory hematology **2013**, 35 (3), 351-357.
(35) Zhang, C.; Zhou, Y.; Zhang, L.; Wu, L.; Chen, Y.; Xie, D.; Chen, W. Hydrogel Cryopreservation System: An Effective Method for Cell Storage. Int J Mol Sci **2018**, 19 (11). DOI: 10.3390/ijms19113330 From NLM.
(36) Mao, A. S.; Özkale, B.; Shah, N. J.; Vining, K. H.; Descombes, T.; Zhang, L.; Tringides, C. M.; Wong, S. W.; Shin, J. W.; Scadden, D. T.; et al. Programmable microencapsulation for enhanced mesenchymal stem cell persistence and immunomodulation. Proc Natl Acad Sci U S A **2019**, 116 (31), 15392-15397. DOI: 10.1073/pnas.1819415116.
(37) Harris, C. L.; Toner, M.; Hubel, A.; Cravalho, E. G.; Yarmush, M. L.; Tompkins, R. G. Cryopreservation of isolated hepatocytes: intracellular ice formation under various chemical and physical conditions. Cryobiology **1991**, 28 (5), 436-444.
(38) Fahy, G. M.; MacFarlane, D. R.; Angell, C. A.; Meryman, H. T. Vitrification as an approach to cryopreservation. Cryobiology **1984**, 21 (4), 407-426. DOI: 10.1016/0011-2240(84)90079-8.
(39) Meryman, H. T. Cryopreservation of living cells: principles and practice. Transfusion **2007**, 47 (5), 935-945. DOI: 10.1111/j.1537-2995.2007.01212.x.
(40) Fahy, G. M.; Wowk, B. Principles of cryopreservation by vitrification. Methods Mol Biol **2015**, 1257, 21-82. DOI: 10.1007/978-1-4939-2193-5_2.
(41) Wusteman, M. C.; Pegg, D. E.; Robinson, M. P.; Wang, L. H.; Fitch, P. Vitrification media: toxicity, permeability, and dielectric properties. Cryobiology **2002**, 44 (1), 24-37. DOI: 10.1016/S0011-2240(02)00002-0.
(42) Ledda, S.; Leoni, G.; Bogliolo, L.; Naitana, S. Oocyte cryopreservation and ovarian tissue banking. Theriogenology **2001**, 55 (6), 1359-1371. DOI: 10.1016/s0093-691x(01)00487-3.
(43) Bhattacharya, S. Cryoprotectants and Their Usage in Cryopreservation Process. In Cryopreservation Biotechnology in Biomedical and Biological Sciences, IntechOpen, 2018.
(44) Karow Jr, A. Cryopreservation: pharmacological considerations. In Organ preservation for transplantation, Little, Brown Boston, Massachusetts, 1974; pp 86-107.
(45) Chaytor, J. L.; Tokarew, J. M.; Wu, L. K.; Leclère, M.; Tam, R. Y.; Capicciotti, C. J.; Guolla, L.; von Moos, E.; Findlay, C. S.; Allan, D. S.; et al. Inhibiting ice recrystallization and optimization of cell viability after cryopreservation. Glycobiology **2012**, 22 (1), 123-133. DOI: 10.1093/glycob/cwr115.

(46) Huang, H.; Zhao, G.; Zhang, Y.; Xu, J.; Toth, T. L.; He, X. Predehydration and Ice Seeding in the Presence of Trehalose Enable Cell Cryopreservation. ACS Biomater Sci Eng **2017**, 3 (8), 1758-1768. DOI: 10.1021/acsbiomaterials.7b00201.
(47) Meryman, H. T.; Williams, R. J.; Douglas, M. S. Freezing injury from "solution effects" and its prevention by natural or artificial cryoprotection. Cryobiology **1977**, 14 (3), 287-302. DOI: 10.1016/0011-2240(77)90177-8.
(48) LOVELOCK, J. E.; BISHOP, M. W. Prevention of freezing damage to living cells by dimethyl sulphoxide. Nature **1959**, 183 (4672), 1394-1395. DOI: 10.1038/1831394a0.
(49) Gurtovenko, A. A.; Anwar, J. Modulating the structure and properties of cell membranes: the molecular mechanism of action of dimethyl sulfoxide. J Phys Chem B **2007**, 111 (35), 10453-10460. DOI: 10.1021/jp073113e.
(50) Westh, P. Preferential interaction of dimethyl sulfoxide and phosphatidyl choline membranes. Biochim Biophys Acta **2004**, 1664 (2), 217-223. DOI: 10.1016/j.bbamem.2004.06.001.
(51) Worsham, D. N.; Reems, J. A.; Szczepiorkowski, Z. M.; McKenna, D. H.; Leemhuis, T.; Mathew, A. J.; Cancelas, J. A.; Group, B. E. f. S. T. C. Clinical methods of cryopreservation for donor lymphocyte infusions vary in their ability to preserve functional T‐cell subpopulations. Transfusion **2017**, 57 (6), 1555-1565.
(52) Ford, T.; Wenden, C.; Mbekeani, A.; Dally, L.; Cox, J. H.; Morin, M.; Winstone, N.; Hill, A. V.; Gilmour, J.; Ewer, K. J. Cryopreservation-related loss of antigen-specific IFNγ producing CD4+ T-cells can skew immunogenicity data in vaccine trials: Lessons from a malaria vaccine trial substudy. Vaccine **2017**, 35 (15), 1898-1906.
(53) Holthaus, L.; Lamp, D.; Gavrisan, A.; Sharma, V.; Ziegler, A.-G.; Jastroch, M.; Bonifacio, E. CD4+ T cell activation, function, and metabolism are inhibited by low concentrations of DMSO. Journal of immunological methods **2018**, 463, 54-60.
(54) Pu, L. L.; Cui, X.; Fink, B. F.; Cibull, M. L.; Gao, D. Cryopreservation of adipose tissues: The role of trehalose. Aesthetic surgery journal **2005**, 25 (2), 126-131.
(55) Crowe, J. H.; Crowe, L. M.; Chapman, D. Preservation of membranes in anhydrobiotic organisms: the role of trehalose. Science **1984**, 223 (4637), 701-703. DOI: 10.1126/science.223.4637.701 From NLM.
(56) Beattie, G. M.; Crowe, J. H.; Lopez, A. D.; Cirulli, V.; Ricordi, C.; Hayek, A. Trehalose: a cryoprotectant that enhances recovery and preserves function of human pancreatic islets after long-term storage. Diabetes **1997**, 46 (3), 519-523.
(57) Eroglu, A.; Toner, M.; Toth, T. L. Beneficial effect of microinjected trehalose on the cryosurvival of human oocytes. Fertil Steril **2002**, 77 (1), 152-158. DOI: 10.1016/s0015-0282(01)02959-4.
(58) Zhang, M.; Oldenhof, H.; Sieme, H.; Wolkers, W. F. Freezing-induced uptake of trehalose into mammalian cells facilitates cryopreservation. Biochimica Et Biophysica Acta-Biomembranes **2016**, 1858 (6), 1400-1409. DOI: 10.1016/j.bbamem.2016.03.020.
(59) Buchanan, S. S.; Gross, S. A.; Acker, J. P.; Toner, M.; Carpenter, J. F.; Pyatt, D. W. Cryopreservation of stem cells using trehalose: evaluation of the method using a human hematopoietic cell line. Stem cells and development **2004**, 13 (3), 295-305.

(60) Wolkers, W. F.; Walker, N. J.; Tablin, F.; Crowe, J. H. Human platelets loaded with trehalose survive freeze-drying. Cryobiology **2001**, 42 (2), 79-87.
(61) Russo, M. J.; Bayley, H.; Toner, M. Reversible permeabilization of plasma membranes with an engineered switchable pore. Nature biotechnology **1997**, 15 (3), 278-282.
(62) MAZUR, P. KINETICS OF WATER LOSS FROM CELLS AT SUBZERO TEMPERATURES AND THE LIKELIHOOD OF INTRACELLULAR FREEZING. J Gen Physiol **1963**, 47, 347-369. DOI: 10.1085/jgp.47.2.347.
(63) Flowers, T. J.; Munns, R.; Colmer, T. D. Sodium chloride toxicity and the cellular basis of salt tolerance in halophytes. Annals of botany **2015**, 115 (3), 419-431.
(64) Stott, S. L.; Karlsson, J. O. M. Visualization of intracellular ice formation using high-speed video cryomicroscopy. Cryobiology **2009**, 58 (1), 84-95. DOI: 10.1016/j.cryobiol.2008.11.003.
(65) Diller, K. R. Intracellular freezing: effect of extracellular supercooling. Cryobiology **1975**, 12 (5), 480-485.
(66) Drebushchak, V.; Ogienko, A.; Yunoshev, A. Metastable eutectic melting in the NaCl-H2O system. Thermochimica Acta **2017**, 647, 94-100.
(67) Kristiansen, J. Leakage of a trapped fluorescent marker from liposomes: effects of eutectic crystallization of NaCl and internal freezing. Cryobiology **1992**, 29 (5), 575-584.
(68) Bumsoo Han, J. C. B. Direct cell injury associated with eutectic crystallization during freezing. Cryobiology **2004**, 46 (1), 8-21.
(69) Bumsoo Han, J. C. B. Enhancement of cell and tissue destruction in cryosurgery by use of eutectic freezing. International Society for Optics and Photonics **2003**, 4954, 106-114.
(70) Regand, A.; Goff, H. D. Effect of biopolymers on structure and ice recrystallization in dynamically frozen ice cream model systems. J Dairy Sci **2002**, 85 (11), 2722-2732. DOI: 10.3168/jds.S0022-0302(02)74359-2.
(71) Martino, M. N.; Zaritzky, N. Ice recrystallization in a model system and in frozen muscle tissue. Cryobiology **1989**, 26 (2), 138-148.
(72) REY, L. R. Thermal analysis of eutectics in freezing solutions. Ann N Y Acad Sci **1960**, 85, 510-534. DOI: 10.1111/j.1749-6632.1960.tb49979.x.
(73) Yao, X.; Matosevic, S. Cryopreservation of NK and T cells without DMSO for adoptive cell-based immunotherapy. BioDrugs **2021**, 35 (5), 529-545.
(74) Nicodemus, G. D.; Bryant, S. J. Cell encapsulation in biodegradable hydrogels for tissue engineering applications. Tissue Eng Part B Rev **2008**, 14 (2), 149-165. DOI: 10.1089/ten.teb.2007.0332.
(75) Orive, G.; Santos, E.; Poncelet, D.; Hernández, R. M.; Pedraz, J. L.; Wahlberg, L. U.; De Vos, P.; Emerich, D. Cell encapsulation: technical and clinical advances. Trends Pharmacol Sci **2015**, 36 (8), 537-546. DOI: 10.1016/j.tips.2015.05.003.
(76) Uludag, H.; De Vos, P.; Tresco, P. A. Technology of mammalian cell encapsulation. Adv Drug Deliv Rev **2000**, 42 (1-2), 29-64. DOI: 10.1016/s0169-409x(00)00053-3.

(77) Strand, B. L.; Coron, A. E.; Skjak-Braek, G. Current and Future Perspectives on Alginate Encapsulated Pancreatic Islet. Stem Cells Transl Med **2017**, 6 (4), 1053-1058. DOI: 10.1002/sctm.16-0116.
(78) Schmidt, J. J.; Rowley, J.; Kong, H. J. Hydrogels used for cell-based drug delivery. J Biomed Mater Res A **2008**, 87 (4), 1113-1122. DOI: 10.1002/jbm.a.32287.
(79) Lim, G. J.; Lee, S. J.; Atala, A. Cell-Based Drug Delivery. In Principles of Regenerative Medicine, Elsevier Inc., 2008; pp 954-966.
(80) Pierigè, F.; Serafini, S.; Rossi, L.; Magnani, M. Cell-based drug delivery. Adv Drug Deliv Rev **2008**, 60 (2), 286-295. DOI: 10.1016/j.addr.2007.08.029.
(81) Correia, C. R.; Reis, R. L.; Mano, J. F. Design Principles and Multifunctionality in Cell Encapsulation Systems for Tissue Regeneration. Adv Healthc Mater **2018**, 7 (19), e1701444. DOI: 10.1002/adhm.201701444.
(82) Ahmed, E. M. Hydrogel: Preparation, characterization, and applications: A review. Journal of advanced research **2015**, 6 (2), 105-121.
(83) Parhi, R. Cross-Linked Hydrogel for Pharmaceutical Applications: A Review. Adv Pharm Bull **2017**, 7 (4), 515-530. DOI: 10.15171/apb.2017.064.
(84) Akhtar, M. F.; Hanif, M.; Ranjha, N. M. Methods of synthesis of hydrogels … A review. Saudi Pharm J **2016**, 24 (5), 554-559. DOI: 10.1016/j.jsps.2015.03.022.
(85) Nagatomo, H.; Yao, T.; Araki, Y.; Mizutani, E.; Wakayama, T. Agarose capsules as new tools for protecting denuded mouse oocytes/embryos during handling and freezing-thawing and supporting embryonic development in vivo. Scientific Reports **2017**, 7 (1), 1-9.
(86) Gryshkov, O.; Pogozhykh, D.; Hofmann, N.; Pogozhykh, O.; Mueller, T.; Glasmacher, B. Encapsulating non-human primate multipotent stromal cells in alginate via high voltage for cell-based therapies and cryopreservation. PloS one **2014**, 9 (9), e107911.
(87) Cagol, N.; Bonani, W.; Maniglio, D.; Migliaresi, C.; Motta, A. Effect of Cryopreservation on Cell-Laden Hydrogels: Comparison of Different Cryoprotectants. Tissue Engineering Part C: Methods **2018**, 24 (1), 20-31. DOI: 10.1089/ten.tec.2017.0258.
(88) Gurruchaga, H.; del Burgo, L. S.; Orive, G.; Hernandez, R.; Ciriza, J.; Pedraz, J. Low molecular-weight hyaluronan as a cryoprotectant for the storage of microencapsulated cells. International journal of pharmaceutics **2018**, 548 (1), 206-216.
(89) Teasdale, B.; Sieber, V.; Riches, D.; Nanchahal, J. Cryopreservation of cultured dermal fibroblast impregnated collagen gels. Burns **1993**, 19 (5), 406-410.
(90) Miyamoto, Y.; Enosawa, S.; Takeuchi, T.; Takezawa, T. Cryopreservation in situ of cell monolayers on collagen vitrigel membrane culture substrata: ready-to-use preparation of primary hepatocytes and ES cells. Cell transplantation **2009**, 18 (5-6), 619-626.
(91) Lee, J. Y.; Koo, Y.; Kim, G. Innovative Cryopreservation Process Using a Modified Core/Shell Cell-Printing with a Microfluidic System for Cell-Laden Scaffolds. ACS applied materials & interfaces **2018**, 10 (11), 9257-9268.
(92) Vrana, N.; O'Grady, A.; Kay, E.; Cahill, P.; McGuinness, G. Cell encapsulation within PVA-based hydrogels via freeze-thawing: a one-step scaffold formation

and cell storage technique. Journal of tissue engineering and regenerative medicine **2009**, 3 (7), 567-572.
(93) Kumari, J.; Kumar, A. Development of polymer based cryogel matrix for transportation and storage of mammalian cells. Sci Rep **2017**, 7, 41551. DOI: 10.1038/srep41551.
(94) Cheng, Y.; Yu, Y.; Zhang, Y.; Zhao, G.; Zhao, Y. Cold‐Responsive Nanocapsules Enable the Sole‐Cryoprotectant‐Trehalose Cryopreservation of β Cell–Laden Hydrogels for Diabetes Treatment. Small **2019**, 15 (50), 1904290.
(95) Porter, D. L.; Kalos, M.; Zheng, Z.; Levine, B.; June, C. Chimeric antigen receptor therapy for B-cell malignancies. Journal of Cancer **2011**, 2, 331.
(96) Rodgers, D. T.; Mazagova, M.; Hampton, E. N.; Cao, Y.; Ramadoss, N. S.; Hardy, I. R.; Schulman, A.; Du, J.; Wang, F.; Singer, O. Switch-mediated activation and retargeting of CAR-T cells for B-cell malignancies. Proceedings of the National Academy of Sciences **2016**, 113 (4), E459-E468.
(97) Smyth, M. J.; Cretney, E.; Kelly, J. M.; Westwood, J. A.; Street, S. E.; Yagita, H.; Takeda, K.; Van Dommelen, S. L.; Degli-Esposti, M. A.; Hayakawa, Y. Activation of NK cell cytotoxicity. Molecular immunology **2005**, 42 (4), 501-510.
(98) Zamai, L.; Ponti, C.; Mirandola, P.; Gobbi, G.; Papa, S.; Galeotti, L.; Cocco, L.; Vitale, M. NK cells and cancer. The Journal of Immunology **2007**, 178 (7), 4011-4016.
(99) Crome, S. Q.; Lang, P. A.; Lang, K. S.; Ohashi, P. S. Natural killer cells regulate diverse T cell responses. Trends in immunology **2013**, 34 (7), 342-349.
(100) Olson, J. A.; Leveson-Gower, D. B.; Gill, S.; Baker, J.; Beilhack, A.; Negrin, R. S. NK cells mediate reduction of GVHD by inhibiting activated, alloreactive T cells while retaining GVT effects. Blood, The Journal of the American Society of Hematology **2010**, 115 (21), 4293-4301.
(101) Lundqvist, A.; Philip McCoy, J.; Samsel, L.; Childs, R. Reduction of GVHD and enhanced antitumor effects after adoptive infusion of alloreactive Ly49-mismatched NK cells from MHC-matched donors. Blood **2007**, 109 (8), 3603-3606.
(102) Siegler, E. L.; Zhu, Y.; Wang, P.; Yang, L. Off-the-shelf CAR-NK cells for cancer immunotherapy. Cell stem cell **2018**, 23 (2), 160-161.
(103) Vivier, E.; Tomasello, E.; Baratin, M.; Walzer, T.; Ugolini, S. Functions of natural killer cells. Nature immunology **2008**, 9 (5), 503-510.
(104) Klingemann, H.; Boissel, L.; Toneguzzo, F. Natural killer cells for immunotherapy–advantages of the NK-92 cell line over blood NK cells. Frontiers in immunology **2016**, 7, 91.
(105) Klingemann, H. Natural killer cell-based immunotherapeutic strategies. Cytotherapy **2005**, 7 (1), 16-22.
(106) Suck, G.; Odendahl, M.; Nowakowska, P.; Seidl, C.; Wels, W. S.; Klingemann, H. G.; Tonn, T. NK-92: an 'off-the-shelf therapeutic'for adoptive natural killer cell-based cancer immunotherapy. Cancer immunology, immunotherapy **2016**, 65, 485-492.
(107) Zhang, J.; Zheng, H.; Diao, Y. Natural killer cells and current applications of chimeric antigen receptor-modified NK-92 cells in tumor immunotherapy. International journal of molecular sciences **2019**, 20 (2), 317.

(108) Reusch, U.; Ellwanger, K.; Fucek, I.; Müller, T.; Schniegler-Mattox, U.; Koch, J.; Tesar, M. Cryopreservation of natural killer cells pre-complexed with innate cell engagers. Antibodies **2022**, 11 (1), 12.
(109) Pasley, S.; Zylberberg, C.; Matosevic, S. Natural killer-92 cells maintain cytotoxic activity after long-term cryopreservation in novel DMSO-free media. Immunology Letters **2017**, 192, 35-41.
(110) Mark, C.; Czerwinski, T.; Roessner, S.; Mainka, A.; Hörsch, F.; Heublein, L.; Winterl, A.; Sanokowski, S.; Richter, S.; Bauer, N. Cryopreservation impairs cytotoxicity and migration of NK cells in 3-D tissue: Implications for cancer immunotherapy. bioRxiv **2019**, 812172.
(111) Mata, M. M.; Mahmood, F.; Sowell, R. T.; Baum, L. L. Effects of cryopreservation on effector cells for antibody dependent cell-mediated cytotoxicity (ADCC) and natural killer (NK) cell activity in 51Cr-release and CD107a assays. Journal of immunological methods **2014**, 406, 1-9.
(112) Miller, J. S.; Rooney, C. M.; Curtsinger, J.; McElmurry, R.; McCullar, V.; Verneris, M. R.; Lapteva, N.; McKenna, D.; Wagner, J. E.; Blazar, B. R. Expansion and homing of adoptively transferred human natural killer cells in immunodeficient mice varies with product preparation and in vivo cytokine administration: implications for clinical therapy. Biology of Blood and Marrow Transplantation **2014**, 20 (8), 1252-1257.
(113) El Assal, R.; Abou‐Elkacem, L.; Tocchio, A.; Pasley, S.; Matosevic, S.; Kaplan, D. L.; Zylberberg, C.; Demirci, U. Bioinspired preservation of natural killer cells for cancer immunotherapy. Advanced Science **2019**, 6 (6), 1802045.
(114) Stroncek, D. F.; Xing, L.; Chau, Q.; Zia, N.; McKelvy, A.; Pracht, L.; Sabatino, M.; Jin, P. Stability of Cryopreserved Leukocytes Prepared For Donor Leukocyte Infusions. Transfusion **2011**, 51 (12), 2647.
(115) Rosenberg, S. A.; Restifo, N. P.; Yang, J. C.; Morgan, R. A.; Dudley, M. E. Adoptive cell transfer: a clinical path to effective cancer immunotherapy. Nat Rev Cancer **2008**, 8 (4), 299-308. DOI: 10.1038/nrc2355.
(116) Karlsson, J. O. M.; Toner, M. Cryopreservation. In Principles of Tissue Engineering (Second Edition), Elsevier, 2000; pp 293-307.
(117) Mazur, P.; Cole, K. W. Roles of unfrozen fraction, salt concentration, and changes in cell volume in the survival of frozen human erythrocytes. Cryobiology **1989**, 26 (1), 1-29.
(118) Djuwantono, T.; Wirakusumah, F. F.; Achmad, T. H.; Sandra, F.; Halim, D.; Faried, A. A comparison of cryopreservation methods: Slow-cooling vs. rapid-cooling based on cell viability, oxidative stress, apoptosis, and CD34+ enumeration of human umbilical cord blood mononucleated cells. BMC Res Notes **2011**, 4, 371. DOI: 10.1186/1756-0500-4-371.
(119) Mazur, P. Freezing of living cells: mechanisms and implications. Am J Physiol **1984**, 247 (3 Pt 1), C125-142. DOI: 10.1152/ajpcell.1984.247.3.C125.
(120) Karlsson, J. O. M., Cravalho, E. G., & Toner, M. . Intracellular ice formation: Causes and consequences. Cryo-Letters **1993**, 14 (6).
(121) Toner, M. Nucleation of ice crystals inside biological cells. Advances in low-temperature biology **1993**, 2, 1-51.

(122) Elliott, G. D.; Wang, S. P.; Fuller, B. J. Cryoprotectants: A review of the actions and applications of cryoprotective solutes that modulate cell recovery from ultra-low temperatures. Cryobiology **2017**, 76, 74-91. DOI: 10.1016/j.cryobiol.2017.04.004.
(123) Stiff, P. J.; Murgo, A. J.; Zaroulis, C. G.; DeRisi, M. F.; Clarkson, B. D. Unfractionated human marrow cell cryopreservation using dimethylsulfoxide and hydroxyethyl starch. Cryobiology **1983**, 20 (1), 17-24.
(124) Fahy, G. M. The relevance of cryoprotectant "toxicity" to cryobiology. Cryobiology **1986**, 23 (1), 1-13.
(125) Tsutomu Arakawa, J. F. C., Yoshiko A.Kita, John H.Crowe. The basis for toxicity of certain cryoprotectants: A hypothesis. Cryobiology **1990**, 27 (4), 401-415.
(126) Petrenko, Y. A.; Jones, D. R. E.; Petrenko, A. Y. Cryopreservation of human fetal liver hematopoietic stem/progenitor cells using sucrose as an additive to the cryoprotective medium. Cryobiology **2008**, 57 (3), 195-200.
(127) Pegg, D. E.; Jacobsen, I. A.; Diaper, M. P.; Foreman, J. The effect of cooling and warming rate on cortical cell function of glycerolized rabbit kidneys. Cryobiology **1984**, 21 (5), 529-535.
(128) Robinson, M. P.; Pegg, D. E. Rapid electromagnetic warming of cells and tissues. IEEE Trans Biomed Eng **1999**, 46 (12), 1413-1425.
(129) Seki, S.; Mazur, P. The dominance of warming rate over cooling rate in the survival of mouse oocytes subjected to a vitrification procedure. Cryobiology **2009**, 59 (1), 75-82. DOI: 10.1016/j.cryobiol.2009.04.012.
(130) Parmegiani, L.; Tatone, C.; Cognigni, G. E.; Bernardi, S.; Troilo, E.; Arnone, A.; Maccarini, A. M.; Di Emidio, G.; Vitti, M.; Filicori, M. Rapid warming increases survival of slow-frozen sibling oocytes: a step towards a single warming procedure irrespective of the freezing protocol? Reprod Biomed Online **2014**, 28 (5), 614-623. DOI: 10.1016/j.rbmo.2014.01.015.
(131) Takahashi, T.; Hirsh, A. Calorimetric studies of the state of water in deeply frozen human monocytes. Biophys J **1985**, 47 (3), 373-380. DOI: 10.1016/S0006-3495(85)83928-X.
(132) Lee, D.-K.; Kwon, B. S.; Ramamoorthy, A. Freezing point depression of water in phospholipid membranes: a solid-state NMR study. Langmuir **2008**, 24 (23), 13598-13604.
(133) Kent, B.; Hauß, T.; Demé, B.; Cristiglio, V.; Darwish, T.; Hunt, T.; Bryant, G.; Garvey, C. J. Direct comparison of disaccharide interaction with lipid membranes at reduced hydrations. Langmuir **2015**, 31 (33), 9134-9141.
(134) Krasteva, N.; Vollhardt, D.; Brezesinski, G.; Möhwald, H. Effect of sugars and dimethyl sulfoxide on the structure and phase behavior of DPPC monolayers. Langmuir **2001**, 17 (4), 1209-1214.
(135) Wolkers, W. F.; Balasubramanian, S. K.; Ongstad, E. L.; Zec, H. C.; Bischof, J. C. Effects of freezing on membranes and proteins in LNCaP prostate tumor cells. Biochim Biophys Acta **2007**, 1768 (3), 728-736. DOI: 10.1016/j.bbamem.2006.12.007.

(136) Wolkers, W. F.; Oldenhof, H. In situ FTIR studies on mammalian cells. Spectroscopy-an International Journal **2010**, 24 (5), 525-534. DOI: 10.3233/Spe-2010-0474.
(137) Giugliarelli, A.; Sassi, P.; Urbanelli, L.; Paolantoni, M.; Caponi, S.; Ricci, M.; Emiliani, C.; Fioretto, D.; Morresi, A. Cryopreservation of cells: FT-IR monitoring of lipid membrane at freeze–thaw cycles. Biophysical chemistry **2016**, 208, 34-39.
(138) Ragoonanan, V.; Wiedmann, T.; Aksan, A. Characterization of the effect of NaCl and trehalose on the thermotropic hysteresis of DOPC lipids during freeze/thaw. J Phys Chem B **2010**, 114 (50), 16752-16758. DOI: 10.1021/jp103960r.
(139) Barth, A. Infrared spectroscopy of proteins. Biochimica et Biophysica Acta (BBA)-Bioenergetics **2007**, 1767 (9), 1073-1101.
(140) Gallagher, W. FTIR analysis of protein structure. Course manual Chem **2009**, 455.
(141) Jena, S.; Horn, J.; Suryanarayanan, R.; Friess, W.; Aksan, A. Effects of Excipient Interactions on the State of the Freeze-Concentrate and Protein Stability. Pharm Res **2017**, 34 (2), 462-478. DOI: 10.1007/s11095-016-2078-y.
(142) Reategui, E.; Aksan, A. Effects of the low-temperature transitions of confined water on the structures of isolated and cytoplasmic proteins. J Phys Chem B **2009**, 113 (39), 13048-13060. DOI: 10.1021/jp903294q.
(143) Rowley, S.; Anderson, G. Effect of DMSO exposure without cryopreservation on hematopoietic progenitor cells. Bone marrow transplantation **1993**, 11 (5), 389-393.
(144) Abrahamsen, J. F.; Rusten, L.; Bakken, A. M.; Bruserud, Ø. Better preservation of early hematopoietic progenitor cells when human peripheral blood progenitor cells are cryopreserved with 5 percent dimethylsulfoxide instead of 10 percent dimethylsulfoxide. Transfusion **2004**, 44 (5), 785-789.
(145) Karlsson, J. O. M.; Toner, M. Long-term storage of tissues by cryopreservation: Critical issues. Biomaterials **1996**, 17 (3), 243-256. DOI: 10.1016/0142-9612(96)85562-1.
(146) Uygun-Sarıbay, M.; Ergun, E.; Kalaycı, Y.; Köseoğlu, T. The secondary structure of proteins in liquid, frozen, and dried egg-white samples: Effect of gamma irradiation treatment. International Journal of Food Properties **2017**, 20 (sup2), 1195-1203.
(147) Hull, M. C.; Cambrea, L. R.; Hovis, J. S. Infrared spectroscopy of fluid lipid bilayers. Anal Chem **2005**, 77 (18), 6096-6099. DOI: 10.1021/ac050990c.
(148) Wolfangel, P.; Müller, K. Chain order in lipid bilayers: FTIR and solid state NMR studies on bilayer membranes from 1, 2-dimyristoyl-sn-glycero-3-phosphoglucose. The Journal of Physical Chemistry B **2003**, 107 (36), 9918-9928.
(149) Chen, C.; Tripp, C. P. An infrared spectroscopic based method to measure membrane permeance in liposomes. Biochim Biophys Acta **2008**, 1778 (10), 2266-2272. DOI: 10.1016/j.bbamem.2008.05.010.
(150) Szalontai, B.; Nishiyama, Y.; Gombos, Z.; Murata, N. Membrane dynamics as seen by Fourier transform infrared spectroscopy in a cyanobacterium, Synechocystis PCC 6803 - The effects of lipid unsaturation and the protein-to-lipid

ratio. Biochimica Et Biophysica Acta-Biomembranes **2000**, 1509 (1-2), 409-419. DOI: Doi 10.1016/S0005-2736(00)00323-0.
(151) Mereghetti, P.; Corsetto, P. A.; Cremona, A.; Rizzo, A. M.; Doglia, S. M.; Ami, D. A Fourier transform infrared spectroscopy study of cell membrane domain modifications induced by docosahexaenoic acid. Biochimica Et Biophysica Acta-General Subjects **2014**, 1840 (10), 3115-3122. DOI: 10.1016/j.bbagen.2014.07.003.
(152) Wellner, N.; Belton, P. S.; Tatham, A. S. Fourier transform IR spectroscopic study of hydration-induced structure changes in the solid state of omega-gliadins. Biochem J **1996**, 319 (Pt 3), 741-747.
(153) Mukherjee, S.; Chowdhury, P.; Gai, F. Infrared study of the effect of hydration on the amide I band and aggregation properties of helical peptides. J Phys Chem B **2007**, 111 (17), 4596-4602. DOI: 10.1021/jp0689060.
(154) Vanstokkum, I. H. M.; Linsdell, H.; Hadden, J. M.; Haris, P. I.; Chapman, D.; Bloemendal, M. Temperature-Induced Changes in Protein Structures Studied by Fourier-Transform Infrared-Spectroscopy and Global Analysis. Biochemistry **1995**, 34 (33), 10508-10518. DOI: DOI 10.1021/bi00033a024.
(155) Pechkova, E.; Innocenzi, P.; Malfatti, L.; Kidchob, T.; Gaspa, L.; Nicolini, C. Thermal stability of lysozyme Langmuir-Schaefer films by FTIR spectroscopy. Langmuir **2007**, 23 (3), 1147-1151. DOI: 10.1021/la061970o.
(156) Demirdöven, N.; Cheatum, C. M.; Chung, H. S.; Khalil, M.; Knoester, J.; Tokmakoff, A. Two-dimensional infrared spectroscopy of antiparallel β-sheet secondary structure. Journal of the American Chemical Society **2004**, 126 (25), 7981-7990.
(157) Kong, J.; Yu, S. Fourier transform infrared spectroscopic analysis of protein secondary structures. Acta Biochim Biophys Sin (Shanghai) **2007**, 39 (8), 549-559.
(158) Dong, A.; Huang, P.; Caughey, W. S. Protein secondary structures in water from second-derivative amide I infrared spectra. Biochemistry **1990**, 29 (13), 3303-3308.
(159) Shivu, B.; Seshadri, S.; Li, J.; Oberg, K. A.; Uversky, V. N.; Fink, A. L. Distinct β-sheet structure in protein aggregates determined by ATR–FTIR spectroscopy. Biochemistry **2013**, 52 (31), 5176-5183.
(160) Han, B.; Bischof, J. C. Enhancement of cell and tissue destruction in cryosurgery by use of eutectic freezing. 2003, International Society for Optics and Photonics: Vol. 4954, pp 106-114.
(161) Han, B.; Bischof, J. C. Direct cell injury associated with eutectic crystallization during freezing. Cryobiology **2004**, 48 (1), 8-21.
(162) Rasmussen, D. H.; MacKenzie, A. P. Phase Diagram for the System Water-Dimethylsulphoxide. Nature **1968**, 220, 1315-1317.
(163) MAZUR, P. Studies on rapidly frozen suspensions of yeast cells by differential thermal analysis and conductometry. Biophys J **1963**, 3, 323-353.
(164) Mazur, P. Kinetics of water loss from cells at subzero temperatures and the likelihood of intracellular freezing. J. Gen. Physiol. **1963**, 47, 347-369.
(165) Sundaramurthi, P.; Shalaev, E.; Suryanarayanan, R. “pH Swing” in Frozen Solutions—Consequence of Sequential Crystallization of Buffer Components. The

Journal of Physical Chemistry Letters **2009**, 1 (1), 265-268. DOI: 10.1021/jz900164q.
(166) Aita, K.; Irie, H.; Tanuma, Y.; Toida, S.; Okuma, Y.; Mori, S.; Shiga, J. Apoptosis in murine lymphoid organs following intraperitoneal administration of dimethyl sulfoxide (DMSO). Exp Mol Pathol **2005**, 79 (3), 265-271. DOI: 10.1016/j.yexmp.2005.07.001.
(167) Saeko, F.; Mitoshi, A.; Michio, Y.; Toshio, S.; Kyoko, K.; Masayuki, H.; Seishi, K.; Jones, S. L. Cryopreservation of human lymphocytes for assessment of lymphocyte subsets and natural killer cytotoxicity. J. Immunol. Methods **1986**, 90 (2), 265-273.
(168) Voshol, H.; Dullens, H. F.; Den Otter, W.; Vliegenthart, J. F. Human natural killer cells: a convenient purification procedure and the influence of cryopreservation on cytotoxic activity. J. Immunol. Methods **1993**, 165 (1), 21-30.
(169) Duske, H.; Sputtek, A.; Binder, T.; Kröger, N.; Schrepfer, S.; Eiermann, T. Assessment of physiologic natural killer cell cytotoxicity in vitro. Hum. Immunol. **2011**, 72 (11), 1007-1012.
(170) Lapteva, N.; Szmania, S. M.; van Rhee, F.; Rooney, C. M. Clinical grade purification and expansion of natural killer cells. Critical Reviews™ in Oncogenesis **2014**, 19 (1-2).
(171) Domogala, A.; Madrigal, J. A.; Saudemont, A. Cryopreservation has no effect on function of natural killer cells differentiated in vitro from umbilical cord blood CD34+ cells. Cytotherapy **2016**, 18 (6), 754-759.
(172) Min, B.; Choi, H.; Her, J. H.; Jung, M. Y.; Kim, H.-J.; Jung, M.-y.; Lee, E.-K.; Cho, S. Y.; Hwang, Y. K.; Shin, E.-C. Optimization of large-scale expansion and cryopreservation of human natural killer cells for anti-tumor therapy. Immune network **2018**, 18 (4).
(173) Jochems, C. E. A.; van der Valk, J. B. F.; Stafleu, F. R.; Baumans, V. The Use of Fetal Bovine Serum: Ethical or Scientific Problem? Alternatives to Laboratory Animals **2002**, 30 (2), 219-227. DOI: 10.1177/026119290203000208 (acccessed 2022/10/20).
(174) Jochems, C. E.; van der Valk, J. B.; Stafleu, F. R.; Baumans, V. The use of fetal bovine serum: ethical or scientific problem? Altern Lab Anim **2002**, 30 (2), 219-227. DOI: 10.1177/026119290203000208 From NLM.
(175) Huang, H.; Choi, J. K.; Rao, W.; Zhao, S.; Agarwal, P.; Zhao, G.; He, X. Alginate Hydrogel Microencapsulation Inhibits Devitrification and Enables Large-Volume Low-CPA Cell Vitrification. Advanced Functional Materials **2015**, 25 (44), 6839-6850. DOI: https://doi.org/10.1002/adfm.201503047.
(176) Gurruchaga, H.; Saenz del Burgo, L.; Hernandez, R. M.; Orive, G.; Selden, C.; Fuller, B.; Ciriza, J.; Pedraz, J. L. Advances in the slow freezing cryopreservation of microencapsulated cells. Journal of Controlled Release **2018**, 281, 119-138. DOI: https://doi.org/10.1016/j.jconrel.2018.05.016.
(177) Huang, H.; Choi, J. K.; Rao, W.; Zhao, S.; Agarwal, P.; Zhao, G.; He, X. Alginate Hydrogel Microencapsulation Inhibits Devitrification and Enables Large-Volume Low-CPA Cell Vitrification. Adv Funct Mater **2015**, 25 (44), 6939-6850. DOI: 10.1002/adfm.201503047 From NLM.

(178) Yang, T.; Zhang, Q.; Xie, L.; Zhang, R.; Qian, R.; Tian, Y.; Chen, G.; Tian, W. hDPSC-laden GelMA microspheres fabricated using electrostatic microdroplet method for endodontic regeneration. Materials Science and Engineering: C **2021**, 121, 111850. DOI: https://doi.org/10.1016/j.msec.2020.111850.
(179) Espona-Noguera, A.; Ciriza, J.; Cañibano-Hernández, A.; Fernandez, L.; Ochoa, I.; Saenz del Burgo, L.; Pedraz, J. L. Tunable injectable alginate-based hydrogel for cell therapy in Type 1 Diabetes Mellitus. International Journal of Biological Macromolecules **2018**, 107, 1261-1269. DOI: https://doi.org/10.1016/j.ijbiomac.2017.09.103.
(180) Gonzalez-Pujana, A.; Rementeria, A.; Blanco, F. J.; Igartua, M.; Pedraz, J. L.; Santos-Vizcaino, E.; Hernandez, R. M. The role of osmolarity adjusting agents in the regulation of encapsulated cell behavior to provide a safer and more predictable delivery of therapeutics. Drug Deliv. **2017**, 24 (1), 1654-1666. DOI: 10.1080/10717544.2017.1391894.
(181) Rao, A.; Gebauer, D.; Cölfen, H. Modulating Nucleation by Kosmotropes and Chaotropes: Testing the Waters. Crystals **2017**, 7 (10), 302.
(182) Aboagla, E. M.; Terada, T. Trehalose-enhanced fluidity of the goat sperm membrane and its protection during freezing. Biol Reprod **2003**, 69 (4), 1245-1250. DOI: 10.1095/biolreprod.103.017889.
(183) Wang, M.; Karlsson, J. O. M.; Aksan, A. FTIR Analysis of Molecular Changes Associated with Warming Injury in Cryopreserved Leukocytes. Langmuir **2019**, 35 (23), 7552-7559. DOI: 10.1021/acs.langmuir.8b02982.
(184) Fu, X. T.; Kim, S. M. Agarase: review of major sources, categories, purification method, enzyme characteristics and applications. Mar Drugs **2010**, 8 (1), 200-218. DOI: 10.3390/md8010200.
(185) Wang, Z.; Pakoulev, A.; Pang, Y.; Dlott, D. D. Vibrational substructure in the OH stretching transition of water and HOD. The Journal of Physical Chemistry A **2004**, 108 (42), 9054-9063.
(186) Malsam, J.; Aksan, A. Hydrogen Bonding and Kinetic/Thermodynamic Transitions of Aqueous Trehalose Solutions at Cryogenic Temperatures. The Journal of Physical Chemistry B **2009**, 113 (19), 6792-6799. DOI: 10.1021/jp8099434.
(187) Kačuráková, M.; Mathlouthi, M. FTIR and laser-Raman spectra of oligosaccharides in water: characterization of the glycosidic bond. Carbohydrate research **1996**, 284 (2), 145-157.
(188) Wolkers, W. F.; Oliver, A. E.; Tablin, F.; Crowe, J. H. A Fourier-transform infrared spectroscopy study of sugar glasses. Carbohydrate research **2004**, 339 (6), 1077-1085.
(189) Rennie, G. K.; Clifford, J. Melting of ice in porous solids. Journal of the Chemical Society, Faraday Transactions 1: Physical Chemistry in Condensed Phases **1977**, 73, 680-689.
(190) ITO, K. Freeze drying of pharmaceuticals. Eutectic temperature and collapse temperature of solute matrix upon freeze drying of three-component systems. Chemical and Pharmaceutical Bulletin **1971**, 19 (6), 1095-1102.

(191) Thorat, A. A.; Suryanarayanan, R. Characterization of Phosphate Buffered Saline (PBS) in Frozen State and after Freeze-Drying. Pharm Res **2019**, 36 (7), 98. DOI: 10.1007/s11095-019-2619-2.
(192) Kratochvílová, I.; Golan, M.; Pomeisl, K.; Richter, J.; Sedláková, S.; Šebera, J.; Mičová, J.; Falk, M.; Falková, I.; Řeha, D. Theoretical and experimental study of the antifreeze protein AFP752, trehalose and dimethyl sulfoxide cryoprotection mechanism: correlation with cryopreserved cell viability. RSC advances **2017**, 7 (1), 352-360.
(193) Whelan, A. P.; Regand, A.; Vega, C.; Kerry, J. P.; Goff, H. D. Effect of trehalose on the glass transition and ice crystal growth in ice cream. International journal of food science & technology **2008**, 43 (3), 510-516.
(194) Goff, H.; Verespej, E.; Jermann, D. Glass transitions in frozen sucrose solutions are influenced by solute inclusions within ice crystals. Thermochimica acta **2003**, 399 (1-2), 43-55.
(195) Roos, Y.; Karel, M. Phase transitions of mixtures of amorphous polysaccharides and sugars. Biotechnology progress **1991**, 7 (1), 49-53.
(196) Wang, G.; Haymet, A. Trehalose and other sugar solutions at low temperature: Modulated differential scanning calorimetry (MDSC). The Journal of Physical Chemistry B **1998**, 102 (27), 5341-5347.
(197) Zhang, W.; Yang, G.; Zhang, A.; Xu, L. X.; He, X. Preferential vitrification of water in small alginate microcapsules significantly augments cell cryopreservation by vitrification. Biomed. Microdevices **2010**, 12 (1), 89-96. DOI: 10.1007/s10544-009-9363-z.
(198) Pernodet, N.; Maaloum, M.; Tinland, B. Pore size of agarose gels by atomic force microscopy. Electrophoresis **1997**, 18 (1), 55-58.
(199) Narayanan, J.; Xiong, J.-Y.; Liu, X.-Y. Determination of agarose gel pore size: Absorbance measurements vis a vis other techniques. In Journal of Physics: Conference Series, 2006; IOP Publishing: Vol. 28, p 83.
(200) Zelent, B.; Vanderkooi, J. Infrared spectroscopy used to study ice formation: The effect of trehalose, maltose, and glucose on melting. Analytical biochemistry **2009**, 390 (2), 215-217.
(201) Avila, G.; Fernández, J.; Tejeda, G.; Montero, S. The Raman spectra and cross-sections of H2O, D2O, and HDO in the OH/OD stretching regions. Journal of Molecular Spectroscopy **2004**, 228 (1), 38-65.
(202) Abalmassov, V.; Surovtsev, N. Frequencies of Stretching and Bending OH (OD) Vibrations in KDP (DKDP) Crystals, According to the Temperature Dependence of Their Raman Spectrum. Bulletin of the Russian Academy of Sciences: Physics **2018**, 82 (3), 294-298.
(203) Branca, C.; Magazu, S.; Maisano, G.; Migliardo, P. α, α-Trehalose− water solutions. 3. Vibrational dynamics studies by inelastic light scattering. The Journal of Physical Chemistry B **1999**, 103 (8), 1347-1353.
(204) Branca, C.; Magazù, S.; Maisano, G.; Migliardo, P.; Villari, V.; Sokolov, A. The fragile character and structure-breaker role of,-trehalose: viscosity and Raman scattering findings. Journal of Physics: Condensed Matter **1999**, 11 (19), 3823.
(205) Freda, M.; Piluso, A.; Santucci, A.; Sassi, P. Transmittance Fourier transform infrared spectra of liquid water in the whole mid-infrared region: temperature

dependence and structural analysis. Applied spectroscopy **2005**, 59 (9), 1155-1159.
(206) Mitlin, S.; Leung, K. Film Growth of Ice by Vapor Deposition at 128− 185 K Studied by Fourier Transform Infrared Reflection− Absorption Spectroscopy: Evolution of the OH Stretch and the Dangling Bond with Film Thickness. The Journal of Physical Chemistry B **2002**, 106 (24), 6234-6247.
(207) Ragoonanan, V.; Aksan, A. Heterogeneity in desiccated solutions: implications for biostabilization. Biophysical journal **2008**, 94 (6), 2212-2227.
(208) Jena, S.; Suryanarayanan, R.; Aksan, A. Mutual Influence of Mannitol and Trehalose on Crystallization Behavior in Frozen Solutions. Pharm Res **2016**, 33 (6), 1413-1425. DOI: 10.1007/s11095-016-1883-7.
(209) Mathlouthi, M. Food packaging and preservation; Springer Science & Business Media, 1994.
(210) Sundaramurthi, P.; Suryanarayanan, R. Trehalose Crystallization During Freeze-Drying: Implications On Lyoprotection. Journal of Physical Chemistry Letters **2010**, 1 (2), 510-514. DOI: 10.1021/jz900338m.
(211) Sundaramurthi, P.; Patapoff, T. W.; Suryanarayanan, R. Crystallization of trehalose in frozen solutions and its phase behavior during drying. Pharmaceutical research **2010**, 27 (11), 2374-2383.
(212) Bashor, C. J.; Hilton, I. B.; Bandukwala, H.; Smith, D. M.; Veiseh, O. Engineering the next generation of cell-based therapeutics. Nature Reviews Drug Discovery **2022**, 21 (9), 655-675. DOI: 10.1038/s41573-022-00476-6.
(213) Yu, H.; Pan, J.; Guo, Z.; Yang, C.; Mao, L. CART cell therapy for prostate cancer: status and promise. Onco Targets Ther **2019**, 12, 391-395. DOI: 10.2147/OTT.S185556.
(214) Levine, B. L.; Miskin, J.; Wonnacott, K.; Keir, C. Global Manufacturing of CAR T Cell Therapy. Mol Ther Methods Clin Dev **2017**, 4, 92-101. DOI: 10.1016/j.omtm.2016.12.006.
(215) Miller, J. S.; Rooney, C. M.; Curtsinger, J.; McElmurry, R.; McCullar, V.; Verneris, M. R.; Lapteva, N.; McKenna, D.; Wagner, J. E.; Blazar, B. R.; et al. Expansion and homing of adoptively transferred human natural killer cells in immunodeficient mice varies with product preparation and in vivo cytokine administration: implications for clinical therapy. Biol Blood Marrow Transplant **2014**, 20 (8), 1252-1257. DOI: 10.1016/j.bbmt.2014.05.004 From NLM.
(216) Lugthart, G.; van Ostaijen-ten Dam, M. M.; van Tol, M. J. D.; Lankester, A. C.; Schilham, M. W. CD56dimCD16− NK cell phenotype can be induced by cryopreservation. Blood **2015**, 125 (11), 1842-1843. DOI: 10.1182/blood-2014-11-610311 (acccessed 12/16/2022).
(217) Berg, M.; Lundqvist, A.; McCoy Jr, P.; Samsel, L.; Fan, Y.; Tawab, A.; Childs, R. Clinical-grade ex vivo-expanded human natural killer cells up-regulate activating receptors and death receptor ligands and have enhanced cytolytic activity against tumor cells. Cytotherapy **2009**, 11 (3), 341-355.
(218) Guillaumet-Adkins, A.; Rodríguez-Esteban, G.; Mereu, E.; Mendez-Lago, M.; Jaitin, D. A.; Villanueva, A.; Vidal, A.; Martinez-Marti, A.; Felip, E.; Vivancos, A.; et al. Single-cell transcriptome conservation in cryopreserved cells and tissues. Genome Biology **2017**, 18 (1), 45. DOI: 10.1186/s13059-017-1171-9.

(219) Krjutškov, K.; Katayama, S.; Saare, M.; Vera-Rodriguez, M.; Lubenets, D.; Samuel, K.; Laisk-Podar, T.; Teder, H.; Einarsdottir, E.; Salumets, A.; et al. Single-cell transcriptome analysis of endometrial tissue. Human Reproduction **2016**, 31 (4), 844-853. DOI: 10.1093/humrep/dew008 (acccessed 12/16/2022).
(220) Zheng, G. X. Y.; Terry, J. M.; Belgrader, P.; Ryvkin, P.; Bent, Z. W.; Wilson, R.; Ziraldo, S. B.; Wheeler, T. D.; McDermott, G. P.; Zhu, J.; et al. Massively parallel digital transcriptional profiling of single cells. Nature Communications **2017**, 8 (1), 14049. DOI: 10.1038/ncomms14049.
(221) Çalışkan, M.; Pritchard, J. K.; Ober, C.; Gilad, Y. The Effect of Freeze-Thaw Cycles on Gene Expression Levels in Lymphoblastoid Cell Lines. PLOS ONE **2014**, 9 (9), e107166. DOI: 10.1371/journal.pone.0107166.
(222) Oyer, J. L.; Croom-Perez, T. J.; Dieffenthaller, T. A.; Robles-Carillo, L. D.; Gitto, S. B.; Altomare, D. A.; Copik, A. J. Cryopreserved PM21-Particle-Expanded Natural Killer Cells Maintain Cytotoxicity and Effector Functions In Vitro and In Vivo. Frontiers in Immunology **2022**, 13, Original Research. DOI: 10.3389/fimmu.2022.861681.
(223) Mata, M. M.; Mahmood, F.; Sowell, R. T.; Baum, L. L. Effects of cryopreservation on effector cells for antibody dependent cell-mediated cytotoxicity (ADCC) and natural killer (NK) cell activity in (51)Cr-release and CD107a assays. J. Immunol. Methods **2014**, 406, 1-9. DOI: 10.1016/j.jim.2014.01.017 From NLM.
(224) Hubel, A. Preservation of cells: a practical manual; John Wiley & Sons, 2018.
(225) Jesus, A. R.; Meneses, L.; Duarte, A. R. C.; Paiva, A. Natural deep eutectic systems—A new era of cryopreservation. In Advances in Botanical Research, Vol. 97; Elsevier, 2021; pp 385-409.
(226) Malpique, R.; Osório, L. M.; Ferreira, D. S.; Ehrhart, F.; Brito, C.; Zimmermann, H.; Alves, P. M. Alginate encapsulation as a novel strategy for the cryopreservation of neurospheres. Tissue Eng Part C Methods **2010**, 16 (5), 965-977. DOI: 10.1089/ten.TEC.2009.0660.
(227) Chiavazzo, E.; Fasano, M.; Asinari, P.; Decuzzi, P. Scaling behaviour for the water transport in nanoconfined geometries. Nature communications **2014**, 5 (1), 1-11.
(228) Serghei, A.; Tress, M.; Kremer, F. Confinement effects on the relaxation time distribution of the dynamic glass transition in ultrathin polymer films. Macromolecules **2006**, 39 (26), 9385-9387.
(229) Baust, J. M.; Vogel, M. J.; Van Buskirk, R.; Baust, J. G. A molecular basis of cryopreservation failure and its modulation to improve cell survival. Cell transplantation **2001**, 10 (7), 561-571.
(230) Bissoyi, A.; Nayak, B.; Pramanik, K.; Sarangi, S. K. Targeting cryopreservation-induced cell death: a review. Biopreservation and biobanking **2014**, 12 (1), 23-34.
(231) Baust, J. M.; Snyder, K. K.; Van Buskirk, R. G.; Baust, J. G. Assessment of the impact of post-thaw stress pathway modulation on cell recovery following cryopreservation in a hematopoietic progenitor cell model. Cells **2022**, 11 (2), 278.
(232) Fujisaki, H.; Kakuda, H.; Shimasaki, N.; Imai, C.; Ma, J.; Lockey, T.; Eldridge, P.; Leung, W. H.; Campana, D. Expansion of highly cytotoxic human natural killer

cells for cancer cell therapy. Cancer Res **2009**, 69 (9), 4010-4017. DOI: 10.1158/0008-5472.CAN-08-3712.
(233) Luhm, J.; Brand, J. M.; Koritke, P.; Höppner, M.; Kirchner, H.; Frohn, C. Large-scale generation of natural killer lymphocytes for clinical application. J Hematother Stem Cell Res **2002**, 11 (4), 651-657. DOI: 10.1089/15258160260194794.
(234) Nishimura, M.; Mitsunaga, S.; Akaza, T.; Mitomi, Y.; Tadokoro, K.; Juji, T. Protection against natural killer cells by interferon-gamma treatment of K562 cells cannot be explained by augmented major histocompatibility complex class I expression. Immunology **1994**, 83 (1), 75.
(235) Minetto, P.; Guolo, F.; Pesce, S.; Greppi, M.; Obino, V.; Ferretti, E.; Sivori, S.; Genova, C.; Lemoli, R. M.; Marcenaro, E. Harnessing NK Cells for Cancer Treatment. Front Immunol **2019**, 10, 2836. DOI: 10.3389/fimmu.2019.02836.
(236) Baust, J. M.; Van Buskirk, R.; Baust, J. G. Cell viability improves following inhibition of cryopreservation-induced apoptosis. In Vitro Cellular & Developmental Biology-Animal **2000**, 36 (4), 262-270.
(237) Baust, J. M.; Van Buskirk, R. G.; Baust, J. G. Cryopreservation of an engineered skin equivalent: the apoptosis paradigm. In ASME International Mechanical Engineering Congress and Exposition, 1999; American Society of Mechanical Engineers: Vol. 16431, pp 71-76.
(238) Riesco, M. F.; Félix, F.; Matias, D.; Joaquim, S.; Suquet, M.; Cabrita, E. Comparative study on cellular and molecular responses in oyster sperm revealed different susceptibilities to cryopreservation. Aquaculture **2019**, 498, 223-229.
(239) Thomson, L. K.; Fleming, S. D.; Aitken, R. J.; De Iuliis, G. N.; Zieschang, J.-A.; Clark, A. M. Cryopreservation-induced human sperm DNA damage is predominantly mediated by oxidative stress rather than apoptosis. Human Reproduction **2009**, 24 (9), 2061-2070.
(240) Kopeika, J.; Zhang, T.; Rawson, D. M.; Elgar, G. Effect of cryopreservation on mitochondrial DNA of zebrafish (Danio rerio) blastomere cells. Mutation Research/Fundamental and Molecular Mechanisms of Mutagenesis **2005**, 570 (1), 49-61.
(241) Ferrusola, C. O.; Fernández, L. G.; Sandoval, C. S.; García, B. M.; Martínez, H. R.; Tapia, J.; Peña, F. Inhibition of the mitochondrial permeability transition pore reduces “apoptosis like” changes during cryopreservation of stallion spermatozoa. Theriogenology **2010**, 74 (3), 458-465.
(242) Garrido, C.; Galluzzi, L.; Brunet, M.; Puig, P.; Didelot, C.; Kroemer, G. Mechanisms of cytochrome c release from mitochondria. Cell Death & Differentiation **2006**, 13 (9), 1423-1433.
(243) Gualtieri, R.; Kalthur, G.; Barbato, V.; Di Nardo, M.; Adiga, S. K.; Talevi, R. Mitochondrial dysfunction and oxidative stress caused by cryopreservation in reproductive cells. Antioxidants **2021**, 10 (3), 337.
(244) Murray, K. A.; Gao, Y.; Griffiths, C. A.; Kinney, N. L.; Guo, Q.; Gibson, M. I.; Whale, T. F. Chemically Induced Extracellular Ice Nucleation Reduces Intracellular Ice Formation Enabling 2D and 3D Cellular Cryopreservation. JACS Au **2023**, 3 (5), 1314-1320.

(245) Morris, G. J.; Acton, E. Controlled ice nucleation in cryopreservation–a review. Cryobiology **2013**, 66 (2), 85-92.
(246) Murua, A.; Orive, G.; Hernandez, R. M.; Pedraz, J. L. Cryopreservation based on freezing protocols for the long-term storage of microencapsulated myoblasts. Biomaterials **2009**, 30 (20), 3495-3501.
(247) Arnott, S.; Fulmer, A.; Scott, W.; Dea, I.; Moorhouse, R.; Rees, D. The agarose double helix and its function in agarose gel structure. Journal of molecular biology **1974**, 90 (2), 269-284.